AFRL-SR-BL-TR-98-

REPORT DOCUMENTATION PAGE

0634

1. AGENCY USE ONLY (Leave blank)	2. REPORT DATE September 1998	3. REPORT TYPE AND DATES COVERED Final Technical Report, 9/1/96-8/31/98

4. TITLE AND SUBTITLE Spectroscopic and Kinetic Studies Using Ultra-Sensitive Absorption and Room Temperature Diode Lasers	5. FUNDING NUMBERS F49620-96-C-0010 2303/FS 61102F
6. AUTHOR(S) Steven J. Davis and William J. Kessler	

7. PERFORMING ORGANIZATION NAME(S) AND ADDRESS(ES) Physical Sciences Inc. 20 New England Business Center Andover, MA 01810	8. PERFORMING ORGANIZATION REPORT NUMBER PSI-1247/TR-1578
9. SPONSORING/MONITORING AGENCY NAME(S) AND ADDRESS(ES) AFOSR/NL Directorate of Chemistry and Life Sciences 110 Duncan Avenue, Suite B115 Bolling AFB, DC 20332-6448	10. SPONSORING/MONITORING AGENCY REPORT NUMBER

11. SUPPLEMENTARY NOTES

12a. DISTRIBUTION/AVAILABILITY STATEMENT "Distribution Statement A. Approved for public release; distribution unlimited."	12b. DISTRIBUTION CODE

13.   ABSTRACT (Maximum 200 words)

A program to apply diode lasers and ultra-sensitive absorption techniques to a variety of important Air Force problems is described. In this program, new gas phase sensors were developed for several applications including: diagnostics for advanced chemical oxygen iodine lasers (COIL), gas phase sensors for atmospheric studies and environmental monitoring, process manufacturing, and development of control strategies based on outputs from the sensors. In this report we present experimental measurements of collisional broadening coefficients of selected transitions in molecular oxygen and water vapor. We make comparisons to earlier measurements and to models for line broadening. We also discuss the production of optical amplification in molecular iodine pumped by a low power visible wavelength diode laser. Finally we present data from characterizations of diode lasers appropriate for development into sensitive diagnostics for the NCl/I* laser system.

14. SUBJECT TERMS		15. NUMBER OF PAGES 145
		16. PRICE CODE

17. SECURITY CLASSIFICATION OF REPORT Unclassified	18. SECURITY CLASSIFICATION OF THIS PAGE Unclassified	19. SECURITY CLASSIFICATION OF ABSTRACT Unclassified	20. LIMITATION OF ABSTRACT Unlimited

NSN 7540-01-280-5500

Standard Form 298 (Rev. 2-89)
Prescribed by ANSI Sta. Z39-18
298-102

DTIC QUALITY INSPECTED

TABLE OF CONTENTS

TABLE OF CONTENTS (Continued)

LIST OF FIGURES

LIST OF FIGURES (Continued)

LIST OF TABLES

1. OBJECTIVES

The objective of this project is to apply miniature diode lasers and ultra sensitive absorption techniques to basic spectroscopic and kinetic problems relevant to Air Force missions. Measurement of fundamental properties and the development of gas phase sensors for several applications are important objectives.

2. STATUS OF EFFORT (FINAL)

During this contract (basic program and 50% of first option) we accomplished the following:

- Determined the absorption linestrength and its temperature dependence and self-broadening coefficient for the H_2O absorption line at 1.3925 microns.

- Measured collisional broadening coefficients for the 1.39253 μm water vapor line for numerous collision partners including: H_2O, CO_2, N_2, O_2, He, Ar, and NH_3.

- Measured collisional broadening coefficients and pressure shifts for the $O_2(b^1\Sigma <-X^3\Sigma)$ system in O_2 for several bath gases: O_2, Cl_2, He, Ne, Ar, CO_2, N_2, and H_2O. Comparisons to theoretical treatments were completed.

- Designed and completed an experiment to demonstrate small signal gain in molecular iodine pumped by a low-power diode laser.

- Designed method to measure small signal gain, temperature, and other kinetics in the NCl/I chemical laser. Preliminary diode laser characterizations completed.

- Continued close interaction with the Phillips Laboratory personnel to help interpret data recorded by the diode laser based sensors.

- Transferred diode laser sensor technology to other chemical oxygen iodine laser (COIL) programs in the U.S., Germany, and Israel through Air Force sponsored program.

- Completed manuscripts for several papers; two already published.

3. ACCOMPLISHMENTS/NEW FINDINGS

In the following progress summary, we discuss the results obtained in this program.

3.1   INTRODUCTION

With the advent of the Air Force Airborne Laser (ABL), the efficiency of the COIL laser has become critically important since this parameter translates directly into payload weight. As the efficiency of the device is increased, the weight/laser output power can be reduced. One of the important drivers for the efficiency of COIL is the fraction of the oxygen that is produced in the excited singlet delta state.

The overall COIL kinetics are well documented and we only present the essential features here. In brief the system is described by Eqs. (1) through (3).

$$I + O_2\left({}^1\Delta\right) \underset{k_r}{\overset{k_f}{\rightleftarrows}} I^* + O_2\left({}^1\Sigma\right) \tag{1}$$

$$O_2\left({}^1\Delta\right) + O_2\left({}^1\Delta\right) \rightarrow O_2\left({}^1\Sigma\right) + O_2\left({}^3\Sigma\right) \tag{2}$$

$$I^* + h\nu \rightarrow I + 2h\nu \tag{3}$$
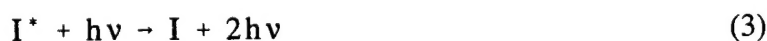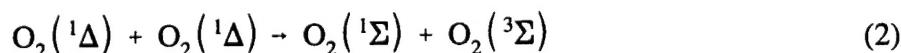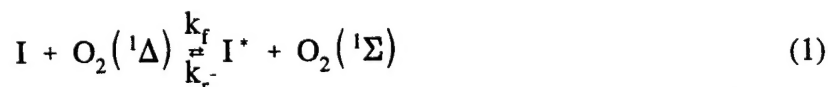
The equilibrium condition for inversion of the atomic iodine in COIL is given by Eq. (4).

$$K_{eq} = \frac{k_f}{k_r} = 0.75 \exp\left(402/T\right) \tag{4}$$

Consequently, at room temperature, the atomic iodine lasant species can be inverted with about 18% of the iodine inverted; the fraction of the oxygen required to invert the iodine is less at

3

lower temperatures. This means that any additional singlet delta oxygen can be used to derive output power from the COIL device.

Clearly, a sensitive diagnostic for singlet oxygen would be a valuable tool for detailed kinetic studies on COIL. Recently, we developed an ultra sensitive monitor for the fraction of the oxygen that is in the ground electronic state based upon diode laser absorption measurements of the oxygen produced in the COIL chemical generator.[1,2] The excited oxygen in COIL is produced by the reaction of Cl_2 and hydrogen peroxide. This reaction has an inherent efficiency of nearly unity for singlet oxygen production, but since COIL generators involve liquid chemistry, a fraction of the excited oxygen is quenched prior to evolving into the gas phase output of the chemical generator. Consequently, the singlet oxygen yield from COIL generators is usually described in terms of the gas phase fraction $Y = [O_2(^1\Delta)]/\{[O_2(^1\Delta)] + [O_2(^3\Sigma)]\}$. Since the total oxygen flow rate is equal to the Cl_2 flowrate into the generator, a measurement of the ground state oxygen concentration can be combined with a measurement of the Cl_2 flowrate to determine the generator yield.

From the equilibrium condition (Eq. (4)) one can discern that the power available for laser output is strongly dependent upon the temperature in the flow. Indeed, the temperature is one of the most important, yet least understood parameters in COIL devices. There are several possible methods for determining the flow temperature. These include a simple thermocouple, but the fact that the flow contains metastable oxygen leads to errors in thermocouple measurements due to deactivation of the excited oxygen on the thermocouples. In addition, thermocouple measurements are notoriously inaccurate in rarified gas flows such as in COIL. Other potential methods include measurement of the rotational temperature of species in the flow such as the rotational manifold of oxygen. Van Benthem and Davis[3] demonstrated a variant of this approach by monitoring the rotationally resolved emission on the O_2 (b -> X) system produced in chemical oxygen generators used in COIL. While potentially useful, one must be assured that the rotational manifold is at the translational flow temperature, and this may not be true at typical low pressure COIL conditions.

4

We have taken the more fundamental approach by suggesting that temperature can be determined from an accurate deconvolution of the Doppler profile from measured absorption lineshapes species within COIL For example, one could use water vapor or oxygen in the plenum and the cavity or atomic iodine in the cavity.[4] Keating and coworkers recently described such cavity measurements using this approach on atomic iodine in the cavity.[5]

While the temperature in the active gain region of COIL is important, the temperature in the plenum near the generation of the singlet oxygen is also crucial for interpretation of the performance and possible improvements in the performance of COIL devices. Consequently, we have determined some broadening parameters for oxygen collisions with several gases relevant to COIL and we have also measured the absolute value and temperature dependence of the absorption coefficient for the strong water absorption line at 1392.5 nm that is used to monitor water vapor by diode laser absorption.

We next describe the water vapor measurements followed by the oxygen results. Next we describe the diode laser pumped iodine gain experiments. Finally we present progress in the development of absorption diagnostics for the NCl/laser.

3.2   WATER VAPOR MEASUREMENTS

3.2.1   Introduction

Water vapor is one of the most important species in COIL since it can influence the rate of dissociation of molecular iodine and quench excited atomic iodine. Consequently, an accurate monitor for water vapor is crucial for optimizing and controlling COIL devices. Recently, we have developed a water vapor diagnostic based upon diode laser absorption on the strong transition near 1392 nm. This is an overtone/combination band that had previously been entered in the HITRAN database. We have made detailed measurements of the absolute value of the absorption coefficient of this transition and determined its temperature dependence over the range 250 to 300 K. The temperature dependence is required in order to anchor this transition as a

5

quantitative monitor for water vapor in COIL, and the self-broadening coefficient is valuable for potential use of this transition as a temperature monitor in both the plenum and gain region of COIL.

Measurements of broadening coefficients in water vapor are also important for numerous other applications. The spectroscopic and radiative properties of water vapor are of current interest for a number of reasons. From a fundamental perspective, the strength of the transitions can be used as sensitive tests of theoretical wavefunctions. Accurate measurements of collisional broadening coefficients provide data that can be used to better understand interaction potentials.[6,7] Numerous practical applications also require accurate knowledge of these properties. Water vapor optical transitions have also been exploited to develop sensitive diagnostics for the concentration of water vapor in a variety of media. Knowledge of the water vapor concentration is often crucial for atmospheric sounding studies. Other important applications include combustion diagnostics and materials processing. For example, high rates of water vapor evolution during the manufacture of exotic materials such as carbon-carbon composites can be deleterious to the production of high quality materials.[8] Trace amounts of water in common semiconductor processing gases such as HCl, NH_3, and Hbr is known to cause corrosion in the semiconductor processing chamber and the gas delivery systems. It has also been suggested that reduction of water vapor will enhance final products such as blue LEDs.[8]

Near infrared diode lasers are excellent candidates as diagnostics for many of these applications. Silver and Hovde[9] and Allen et al.[10] have developed a airborne hygrometers based on near IR diode laser absorption. Allen and Kessler[11] and Nagali et al.[12] have each described diode laser techniques for simultaneous water vapor concentration and temperature for combustion applications. Recent papers by Wu and coworkers[8] and Inman and McAndrew[13] discuss the application of diode laser spectrometers to trace moisture detection in process gas flows. Davis and coworkers have also described water vapor detection for low pressure, supersonic flow chemical laser applications.[1,2]

Accurate calculation of water vapor concentration from absorption measurements depends upon reliable values for the inherent linestrengths of the transitions being probed. In addition, for some applications such as the measurement of temperature from the Doppler linewidth component of the absorption lineshape requires accurate values for the broadening coefficients of the constituent bath gases. There have been several experimental measurements of the linestrengths and collisional broadening coefficients for numerous absorption lines in water vapor. Toth[14] has published an extensive compendium of line positions and strengths covering the range 5750 to 7965 cm^{-1} derived from measurements made with a high resolution Fourier transform spectrometer. A survey of experimental results for broadening of water vapor line has also been published by Gamache, Hartmann, and Rosenmann.[15] Recent results using diode laser absorption techniques have also been reported. Hanson and coworkers published results of measurements of linestrenths and collisional broadening for water transitions in the 1.4 micron region.[16] Very recent measurements of linestrengths and self-broadening coefficients in the 1.3 micron region have been reported by Upschulte and Allen.[17]

Numerous theoretical treatments have produced predicted values both self-broadening and collisional broadening by other collision partners covering numerous transitions in water vapor.

In this report we describe extensive measurements of collisional broadening of a single transition in water vapor at 1.39253 microns. This line is due to the $3_{03} <- 2_{02}$ rotational line in the $v_3 + v_2$ vibrational band. In numerous water vapor investigations we have found that this strong line is relatively isolated and is ideal for sensitive water vapor measurements. Surprisingly there is relatively little published information concerning collisional broadening of this line. We also report measurements of the linestrength at room temperature and the temperature dependence of the line over a limited temperature range: 250 to 300 K.

3.2.2 Experiment

Near IR Water Vapor Spectroscopy

The diode laser absorption measurements were based upon the strong absorption line at 1.39253 μm line. The absorbance, A, is described by the Beer Lambert law:

$$A = \ln\{I_0(\nu)/I_t(\nu)\} = NS(T)g(\nu)l \tag{5}$$

where

I$_t$(ν) and I$_t$(ν) are the transmitted and incident intensities of the diode laser beam

N is the water vapor number density

l is the absorption pathlength

S(T) is the temperature dependent absorption linestrength, and

g(ν) is the line shape factor.

Note that the lineshape factor is normalized when integrated over all frequencies and also contains all the linebroadening information. In general, at low pressures (less than 1 Torr) g(ν) is a Gaussian and at high pressures (atmospheric pressure) g(ν) is Lorentzian. At intermediate pressures, the profile is usually described by a convolution of a Gaussian and a Lorentzian known as the Voigt profile. For all the results reported here we used a Voigt lineshape to describe g(ν).

We analyzed the recorded absorption lineshapes using a Voigt profile fitting routine. The Voigt function is a convolution of a Gaussian and a Lorentzian. The Gaussian function describes Doppler broadening of a spectral line and dominates the lineshape when collisional broadening is negligible. In contrast, at high pressures where collisional broadening governs the lineshape, a Lorentzian profile is an adequate description. At intermediate conditions, the Voigt profile is often used to describe the absorption profile. The Voigt function is given by equation

$$g(\nu - \nu_0) = 2(\ln 2/\pi)^{1/2} \, \Delta\nu_D^{-1} \, V(y,a) \tag{6}$$

where

$V(y,a)$ is the Voigt function

$a = (\ln 2)^{1/2} \Delta\nu_c/\Delta\nu_D$

$y = 2(\ln 2)^{1/2} (\nu-\nu_o)/\Delta\nu_D.$

In the above, $\Delta\nu_D$ is the Doppler width and $\Delta\nu_c$ is the collision width. The collision width is given by $\Delta\nu_c = 2\Sigma_i \gamma_i P_i$ where P_i is the partial pressure of collision partner, i, and γ_i is the collision broadening parameter.

Although there are several closed form approximations for the Voigt function, there is no closed form analytical treatment. We used a commercial software package, Peakfit (Jandel, Inc.) to fit the observed lineshapes to the Voigt function. Since all of our broadening measurements were obtained a room temperature, we fixed the Doppler component of the Voigt function to that appropriate for the 1.39253 µm line in H_2O ($\Delta\nu_D = 635$ MHz FWHM). The fitting routine then produced the best fit for the Lorentzian component of the absorption line. The Lorentzian linewidth is linearly related to the bath gas number density with the slope equal to the broadening coefficient.

We quote our broadening coefficients as FWHM /Torr. Note that this is 2γ as defined above using the conventional Voigt parameter definitions.

In these experiments we recorded the absorbance in a measured pathlength, l, while the diode laser frequency was scanned over the entire absorption line. For measurements of the broadening coefficients, bath gas was added and its partial pressure was measured with a capacitance manometer. For the linestrength measurements the line integrated absorbance was recorded as a function of the water vapor concentration in the cell. The temperature dependence of S(T) was measured by cooling the sample cell.

The apparatus, shown in Figure 1, consisted of an absorption cell, gas handling system, and the diode laser spectrometer system. The absorption cell was 50 cm in length and was a
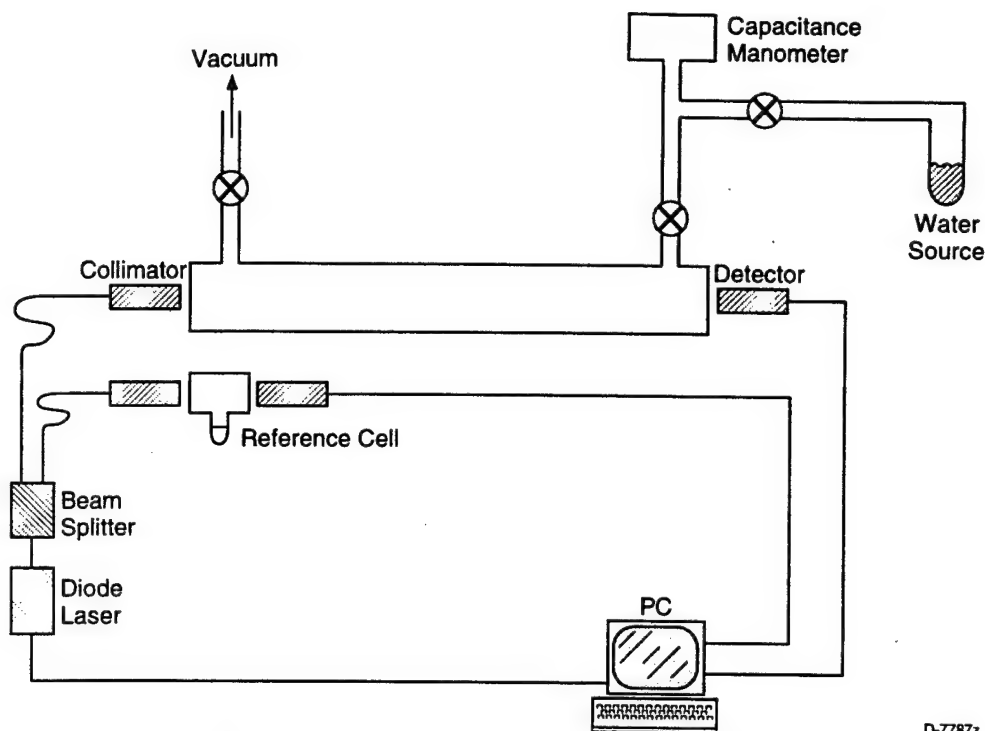
Figure 1. Block diagram of water vapor measurement apparatus.

jacketed stainless steel cell. The inner cell contained the water vapor sample and the water vapor pressure and bath gas pressure in the cell was measured using an MKS Baratron capacitance manometer. Outside the inner cell was a volume that contained a thermal controlling fluid. Finally, a 2 in. thick coating of thermal insulation surrounded the outer jacket. The temperature of the cell was controlled by circulating the fluid through a chiller and then through the cell jacket. Several thermocouples were used to continuously monitor the temperature. We used methanol as the fluid and could vary the temperature from -60 to 20°C.

For these measurements we used a PSI Waterscan model 1001 diode laser spectrometer. This instrument contained a distributed feedback (DFB) diode laser that produced about 2 mW of single longitudinal mode output. The diode laser was powered by an ILX 3722 Diode Laser Controller. We wrote custom software using a National Instruments CVI LabWindows environment. A Pentium class PC controlled the diode laser frequency scans and lineshapes were stored for subsequent analysis. With this configuration we could scan the water vapor absorption line at rates up to 250 Hz, but for most runs we scanned the diode laser at a rate of 25 Hz.

A single mode, 1x3 fiber splitter provided diode laser outputs for the water vapor sample cell and for a permanently sealed reference cell that contained 22 Torr of water vapor at room temperature. Both of these fiber legs were connected to collimators that produced 2 mm diameter beams that were used to probe the sample and reference cells. The reference cell also contained a sidearm that could be inserted in ice water to reduce the water vapor pressure in the reference cell to about 5 Torr. The reference cell was used to assure that the central frequency of the diode laser did not drift. The third output from the fiber splitter was sent directly to an InGaAs detector that provided a real time reference of the diode laser power as the laser was scanned.

As indicated in Figure 1, the signal beam and calibration beams were detected with 3 mm diameter InGaAs detectors. The outputs of all three InGaAs detectors were amplified using transimpedence amplifiers that provided a voltage output. These three outputs were connected to a National Instruments A/D board that was an integral part of the data acquisition and analysis PC.

In these measurements The absorptions were relatively strong (typically greater than 1%). Thus, we used a simple dual beam absorption technique as indicated in Figure 1. After digitization the sample channel data were divided by the reference channel data. This provided traces that were normalized with respect to the diode laser power. By taking the natural log of the ratio of these two digitized channels, data files of absorbance versus frequency were obtained. Since the absorptions were so strong, residual etalons were not a significant source of uncertainty.

The frequency scan rate (MHz/mA) of the diode laser was calibrated with a Burleigh confocal Fabry Perot spectrum analyzer that served as the frequency calibration source. The absolute frequency of the diode laser was measured with a Burleigh WV-20 Wavemeter. Numerous calibrations of the diode laser scan rates were completed over a wide range of diode laser scan frequencies. These calibrations are crucial for accurate conversion of diode laser current to frequency.

11

In Figure 2 we show an absorbance spectrum for the water line taken at room temperature (296 K) with a pressure of 1 Torr in the sample cell. A fit of the data to a Voigt profile and the residuals are also shown. For the data reported the maximum residual was always less than 1%. Data similar to that shown in Figure 2 were recorded for several pressures of each bath gas. An example of the collisional broadening with CO_2 as the bath gas is shown in Figure 3. Two traces are shown: one shows an absorption trace for neat water (1 Torr) and the second trace shows the effects of adding 200 Torr of CO_2. A small red shift of the peak absorption is also apparent. We do not report any pressure shift results here.

In order to determine the collisional broadening coefficients, we fixed the Doppler width to be 635 MHz which corresponds to the room temperature value. The fitting routine then produced the Lorentzian component of the lineshape. The Lorentzian width was then plotted as a function of the added bath gas pressure to determine the pressure broadening coefficient. We report values as FWHM (MHz)/Torr. We note that the diode laser linewidth was only 35 MHz as measured with the spectrum analyzer described above.
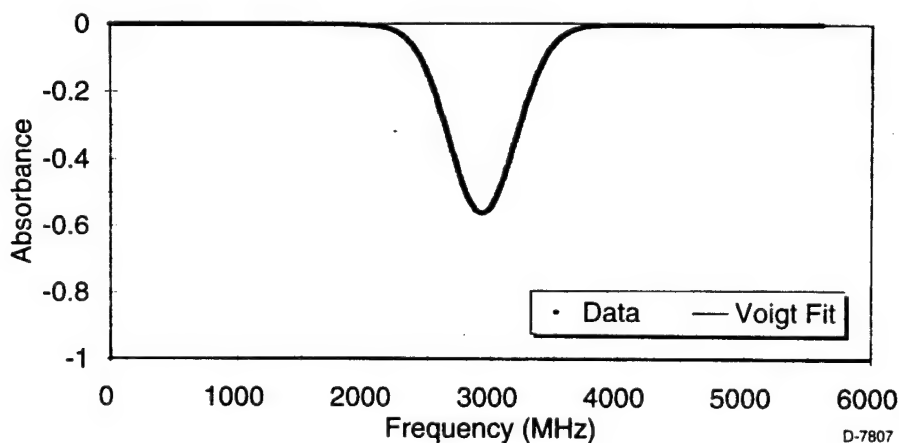
Figure 2. Water vapor absorption profile and Voigt fit to data.
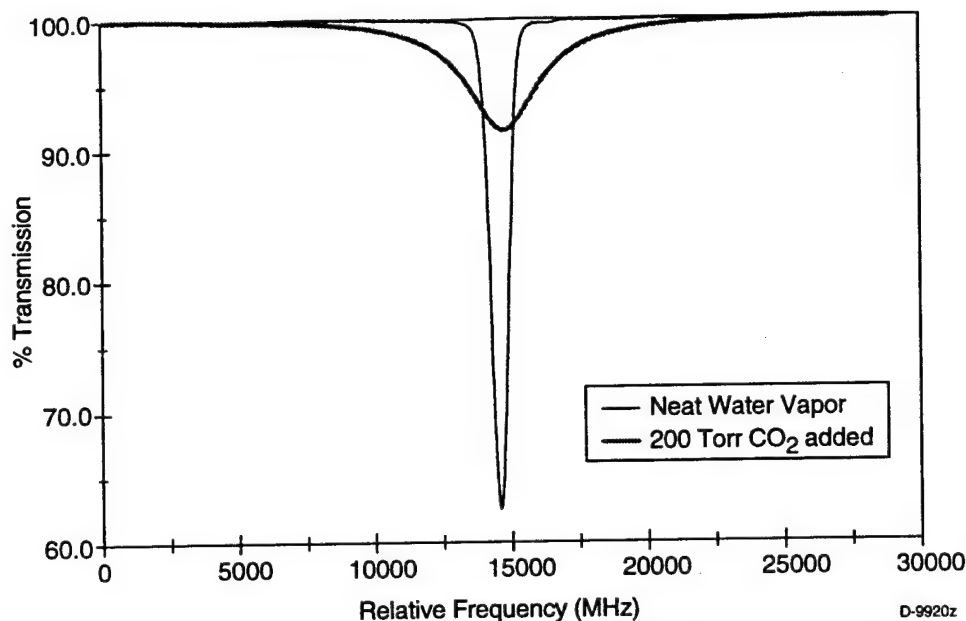
Figure 3. Spectra showing collisional broadening of H_2O 1.3925 μm line by 200 Torr of CO_2.

3.2.3 Results

In Figure 4 we show a plot of the collisional FWHM as a function of CO_2 pressure. These data reduce to a value of $2\gamma=14.75$ MHz/Torr. A similar plot for self broadening by water vapor is shown in Figure 5. The self-broadening data produced a broadening coefficient of 31.28 MHz/Torr. A summary for all bath gases studied is provided in Table 1. We quote a 1σ uncertainty of 5% due to our estimations in uncertainties in the pressure measurement and in the diode laser frequency calibrations. These independent uncertainties were added in quadrature.

3.2.4 Discussion

It is relevant to examine the trends in the collisional broadening data and make comparisons both to other previous measurements and to theoretical predictions. There have been numerous measurements of collisional broadening on water lines. The original work was motivated by atmospheric research and concentrated on water broadening by air. However, due the importance of radiative transport in combustion phenomena, there has been considerable

13
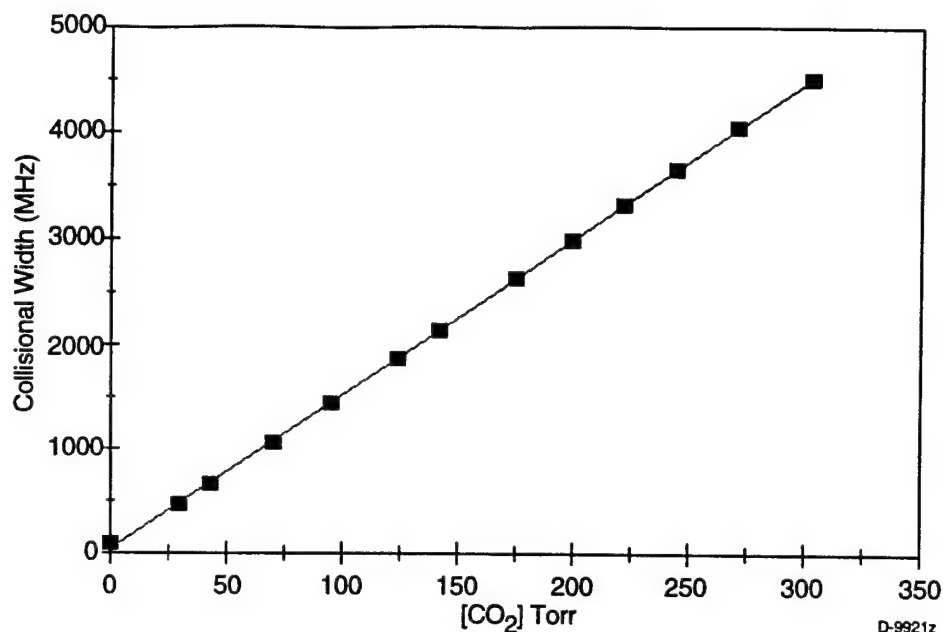
Figure 4. Collision FWHM for water vapor line as a function of CO_2 pressure.
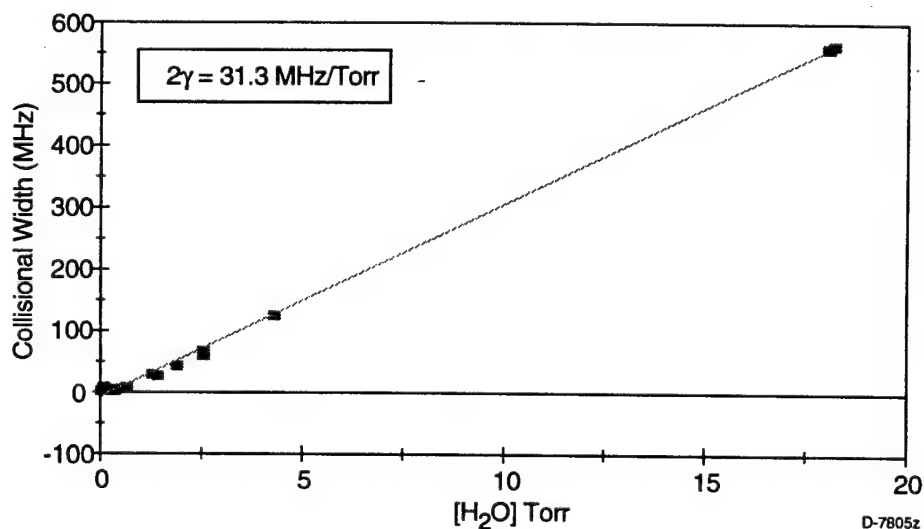
Figure 5. Collision FWHM for water vapor line with H_2O as collision partner.

recent work on self broadening. The most relevant recent measurements were completed by Langlois, Birbeck, and Hanson[17] and by Upschulte and Allen.[18] Both groups used diode laser absorption spectroscopy similar to the present work. Langlois et al. studied 12 absorption lines near 1.4 μm, and reported a room temperature self-broadening coefficients in the range:

Table 1. Collisional Broadening Coefficients for Water Vapor Measured in This Work

Collision Partner	Broadening Coefficient (28) (MHz/Torr)
H_2O	31.28
CO_2	14.75
NH_3	23.8
He	1.75
Ar	3.68
O_2	4.82
N_2	8.83
Air	7.64

$28.42 < 2\gamma < 41.05$ in units of MHz/Torr. Upschulte and Allen investigated the temperature dependence of several lines in the 1.3 μm region and report values ranging from 13.57 to 32.68 MHz/Torr. These experiments differed in that Upschulte and Allen studies some transitions that originated from much higher rotational levels than in either Langlois' or our work. The broadening coefficients from these higher levels were considerably lower. Gainfrani et al.[19] report a self-broadening coefficient of 56.4 MHz/Torr for a water line at 1.39217 μm at 439 K. This is larger than any other literature value. More work is needed to resolve this discrepancy.

The most relevant theoretical predictions for comparison are from Delaye, Hartmann, an Taine.[18,20] They used a model originally developed by Robert and Bonamy[6] to calculate collisional broadening coefficients for line broadening by H_2O, N_2, O_2, and CO_2. We can make direct comparisons to there results since they applied the model to the water vapor line that we investigated. In Table 2 we present a comparison of our results to the prediction of Delaye et al. The agreement is quite good and provides support for the adequacy of these theoretical descriptions.

Table 2. Comparisons to Recent Theoretical Predictions

Collision Partner	2γ (MHz/Torr) Predictions of Reference [18]	2γ (MHz/Torr) This Work
CO_2	13.38	14.75
H_2O	38.62	31.28
N_2	8.42	8.83
O_2	5.29	4.82

3.3   MEASUREMENT OF LINESTRENGTH, S(T)

Measurement of S(T)

The most recently published room temperature (300 K) value for S(T) is 1.4×10^{-20} cm^2 molecule^{-1} cm^{-1}. We have made direct measurements of S(T=300) using two approaches. First we measured peak absorption $(1- I/I_0)$ at line center as a function of the water vapor concentration. We also measured the integrated absorbance over the entire lineshape as a function of the water vapor pressure. The data obtained from the line center measurements are shown in Figure 6. Note that these data are not linear since we plotted absorption, not absorbance versus the water vapor pressure. The solid line is the predicted absorption using a value of S(T=296) = 1.24×10^{-20} cm^2 molecule^{-1} cm^{-1}.

At room temperature, our quoted value for $S_{7181\,cm-1}$ is 1.24×10^{-20} (cm^{-1}/molecule-cm^{-2}). We will contribute the results to the HITRAN database. The temperature dependence for S(T) is predicted to follow the functional form:

$$S(T) = S(296) \cdot \frac{Q_{rot}(296)}{Q_{rot}(T)} \cdot \exp\left[\frac{E''}{k} \cdot \left(\frac{1}{296} - \frac{1}{T}\right)\right] \qquad (7)$$

where Q_{rot} is the rotational partition function and E'' is the energy of the ground level which is 136.7 cm^{-1} for the 7181.172 cm^{-1} line.

16
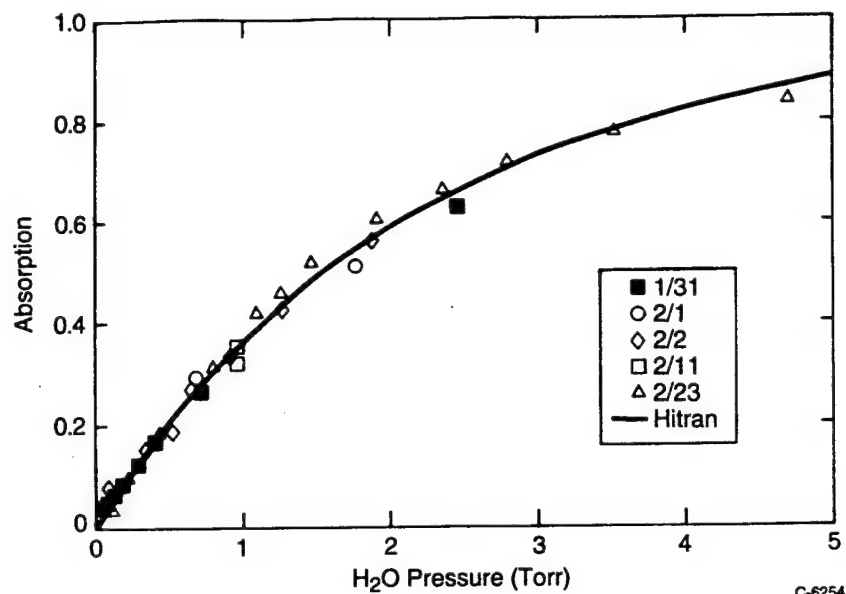
Figure 6. Absorption data for 1.3925 micron diode laser line. Symbols represent different experimental runs. Solid curve from HITRAN (adjusted; see text).

For these measurements we saturated the inside of the temperature controlled cell described above and shown in Figure 7. We varied the temperature of the inside of the cell using the cooling fluid. At each temperature we allowed the water vapor pressure to come to equilibrium and measured the temperature from thermocouples. Vapor pressure curves were
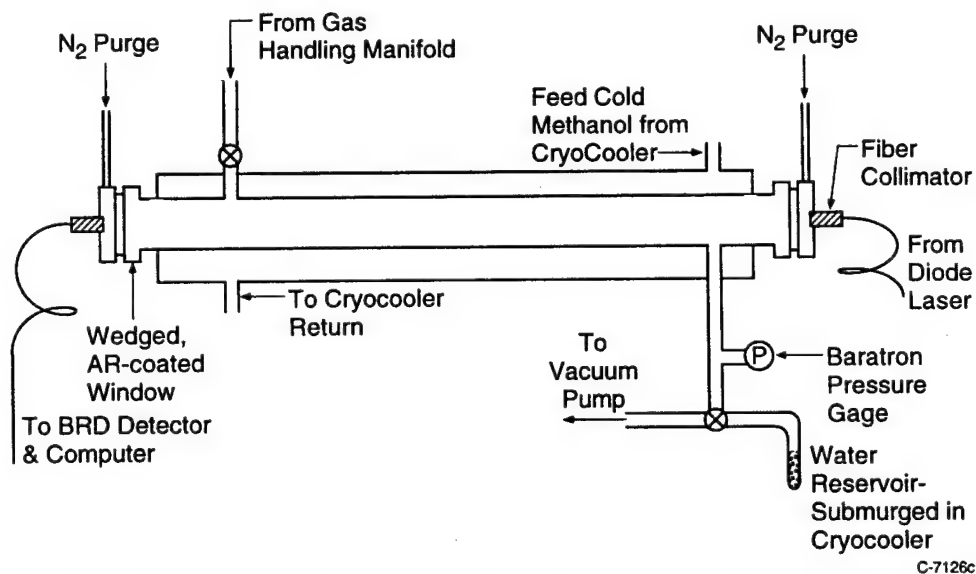
Figure 7. Apparatus for measurement of the temperature dependence of S(T)

17

determine the water vapor pressure at each temperature. We varied the temperature over a range of -60 to 23 C. The water vapor absorbance was integrated over the entire line to produce the linestrength, S(T), at each temperature. The results of these measurements are shown in Figure 8 along with a comparison to the predictions using Eq. (7) above.
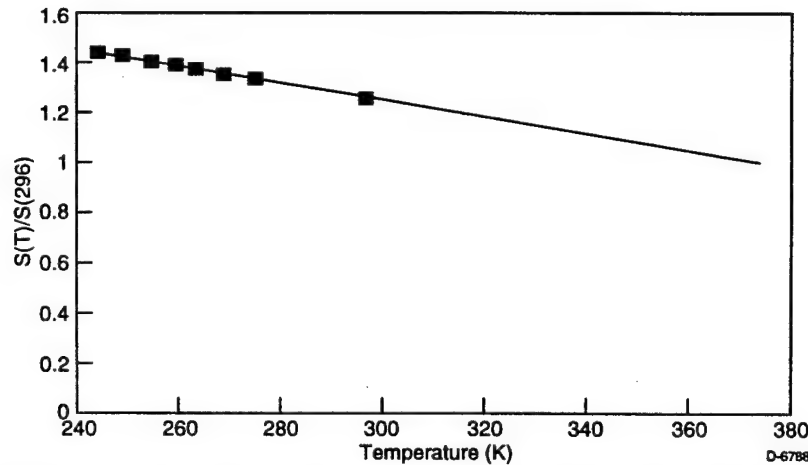
Figure 8. Measured temperature dependence of S(T) (dots) and predictions of Eq. (7) (solid line).

3.4   MEASUREMENT OF BROADENING AND PRESSURE SHIFTS IN OXYGEN

The COIL oxygen diagnostic infers the concentration of molecular oxygen from sensitive absorption measurements on the (b ← X) band using a tunable diode laser that operates near 762 nm. The diode laser tunes over a complete rovibronic line and the oxygen concentration N_{O_2} is calculated using Eq. (8),

$$N_{O_2} = \frac{1}{S_T \ell} \int_\omega \ln\left(\frac{I_{0,\nu}}{I_\nu}\right) d\nu \qquad (8)$$

where

S_T is the absorption linestrength

ℓ is the absorption pathlength

and $I_{0,\nu}$ and I_ν are the initial and transmitted light intensities.

18

Note that since we scan the diode laser over the entire absorption feature, the integrated absorption is independent of the pressure since the integral under any absorption line is constant for constant number density of absorbers. The peak absorption is reduced as the pressure is increased, but the line broadens and the integral remains constant. Likewise, as the temperature increases, the Doppler width increases, but the integral under the absorption line remains constant. The absorption linestrength (S) does have a temperature dependence due to the Boltzmann population distribution within the absorbing state. However, we have selected lines that have a minimum temperature dependence for typical COIL conditions.

The actual shape of the absorption curve is described by the lineshape function, $g(\omega)$. At low pressures where collisional broadening can be neglected $g(\omega)$ is described by a Gaussian function. At high pressures where collisional broadening dominates Doppler broadening, $g(\omega)$ is a Lorentzian. In these two limits, fitting the data is relatively straightforward. However, under many conditions, both Doppler and collisional broadening are significant and the lineshape is described by a Voigt profile. This convolution of a Gaussian and a Lorentzian is much more difficult to fit and does not have a closed form analytic solution. Consequently, we use a non-linear iterative numerical procedure. We have developed some routines at PSI, but selected a commercial package called Peakfit for these experiments (also used by PL personnel). Peakfit allows data files to be selected and fit to the Voigt function and produces values of both the Gaussian width and Lorenztian width.

The $b^1\Sigma_g^+ <- X^3\Sigma_g^-$ system in O_2 is spin forbidden, and the radiative lifetime of the b state is approximately 12 ms. Using the notation for Hund's case b, the quantum numbers J and N describe the rotational levels in the b and X states. N is the rotational angular momentum quantum number, and J represents the sum of the rotational and spin angular momenta (J= N+S). Thus the b state (S=0) has $J'=N'$ only. Symmetry considerations also require only even values for N'. In the X state, S=1, so J'' can take the values: $N''-1$, N'', and $N''+1$. Only odd values for J'' are allowed. Absorptions on this band system take place in four branches. In this paper we use the following notation for these branches: $\Delta N(N'')\Delta J(,J'')$: $P(N'')P(J'')$, $P(N'')Q(J'')$,

R(N″)Q(J″), and R(N″)R(J″). In Figure 9 we show this system from the HITRAN data base.
Also indicated are some of the branches that we probed in this experiment.
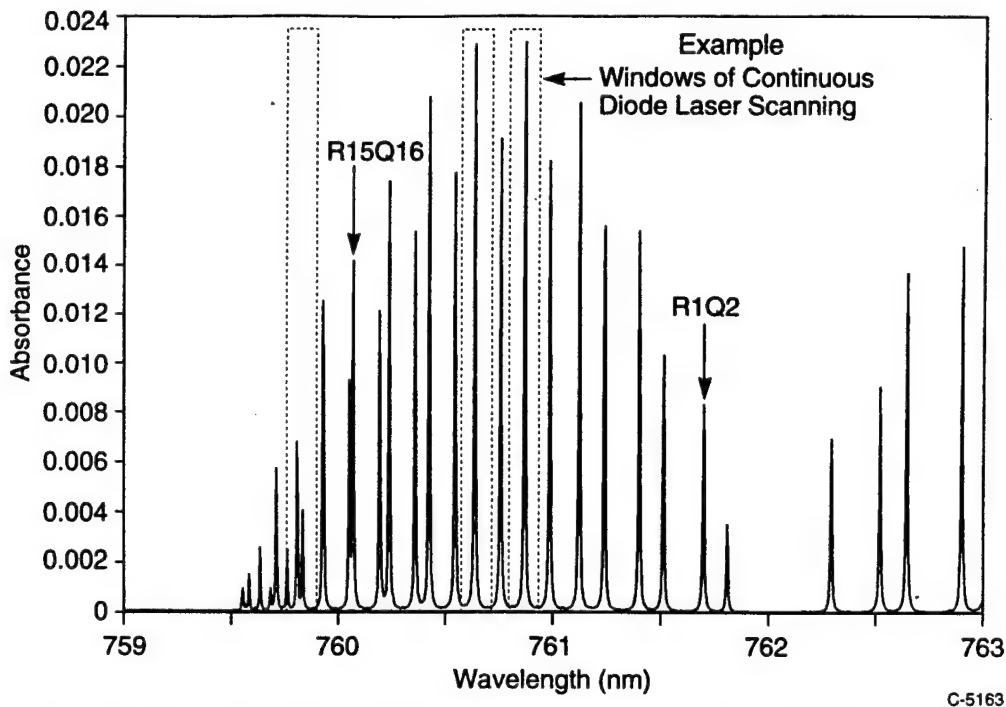
Figure 9. Portion of the O_2 (b <- X) absorption spectrum from HITRAN database.

3.4.1 Description of Experiment

The experiments were performed at PSI using the apparatus described in Figure 10.
An optically isolated diode laser (SDL) was coupled to a single mode fiber optic that in turn
was split into six fibers as indicated in Figure 10. The diode laser was powered by an ILX
current controller and an ILX temperature controller. The diode laser produced single
longitudinal mode output and was tunable over several nanometers. In practice, the diode laser
was temperature-tuned to a desired line. Scanning over the desired line was accomplished using
a Hewlett-Packard ramp generator as an input to the diode laser current controller. With this
setup, we were able to scan the diode laser over the selected line at a 100 Hz rate, and this
allowed extensive signal averaging to be completed.

20
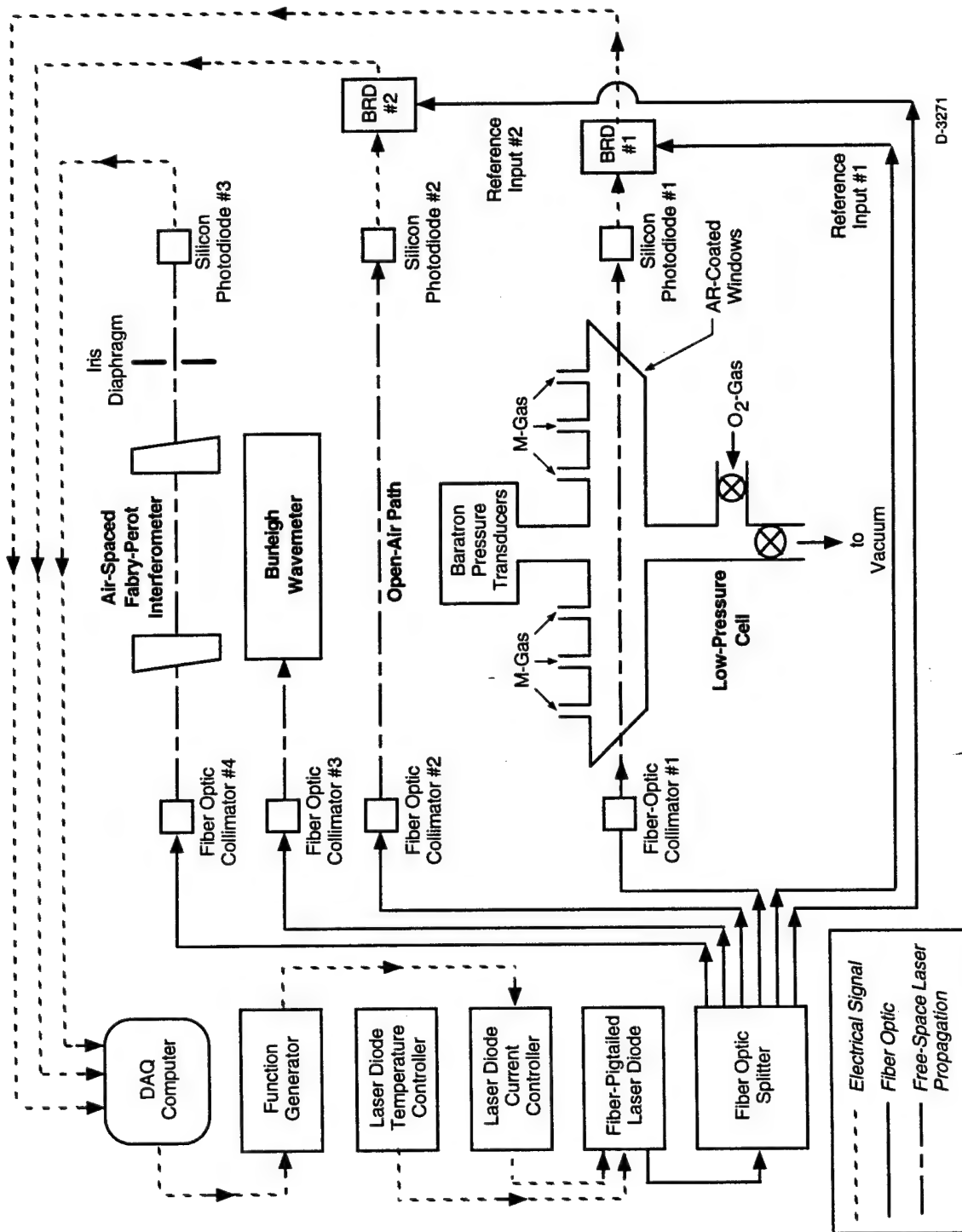
Figure 10. Block diagram of apparatus used in O_2 line broadening measurements.

21

Detection of the optical signals was by a series of Si photodiodes that were contained in two balanced ratiometric detectors (BRD). The BRD allows efficient cancellation of excess laser noise that exists on both the reference and signal legs in any absorption measurement. The six outputs from the fiber splitter were each used for a specific purpose. Two of the outputs were fiber connected to the reference inputs of the balanced ratiometric detectors (BRD) that were used to make the small absorption measurements. Typical maximum absorptions in the 2 m cell were on the order of 10^{-4} to 10^{-2}.

One of the BRDs was used to measure absorptions in the low pressure sample cell, and the other was used to determine absorptions in an open air reference cell. Two other fibers were connected to beam launch collimators: one beam was sent through the sample cell, and one passed through the open air reference cell. The fifth fiber was coupled to a Burleigh WV 20 wavemeter to measure the diode laser wavelength, and the remaining fiber was used to input a small fraction of the diode laser output into a Burleigh model 140 Fabry-Perot interferometer, used to determine the frequency of the diode laser.

The six data channels were recorded simultaneously on a PC using software developed by PSI. Lineshapes could be viewed in real time, but all data reduction was completed off-line subsequent to the experiments. The pressure in the sample cell was measured using a series of MKS Baratrons that covered the pressure range 1 to 750 Torr. The sample cell was connected to a stainless steel vacuum line and gas handling system that was pumped by an Alcatel 4-in. diffusion pump. The entire system could be pumped to pressures of a few times 10^{-5} Torr. This was adequate since all measurements used gas pressures of at least several Torr.

All experiments except those involving H_2O as a collision partner were completed as follows. Using the wavemeter, the diode laser was tuned to one of several lines in the O_2 (b ← X) system. Figure 9 is from the HITRAN data base and shows this absorption spectrum. Once the diode laser was temperature tuned to the selected line, the laser was current tuned so that an entire line could be scanned at a 100 Hz rate. Absorption traces were recorded simultaneously

from both the sample cell and the open air reference cell. In addition, the laser light transmitted through the Fabry-Perot interferometer was recorded to continuously monitor the scan rate of the diode laser.

A measured amount of oxygen was added to the sample cell and spectra were again recorded. Next, the selected bath gas was added to the sample cell in measured increments and the absorption spectra for both the sample cell and open-air path were recorded for each pressure in the sample cell. Note that the spectrum in the open-air path was constant. It however provided a reference oxygen absorption spectrum to which we could compare both the linewidth and shift of the absorption line measured in the sample cell where conditions were varied.

In Figure 11 we show an example of recorded data. The broad feature is the absorption line from the P13 P13 line in the open air path (760 Torr). The narrow feature was simultaneously recorded in the sample cell with at pressure of 30 Torr pure oxygen. The effects of both broadening and shift to longer wavelengths as the pressure is increased is readily apparent. Sets of data similar to this were recorded at many pressures for each bath gas.
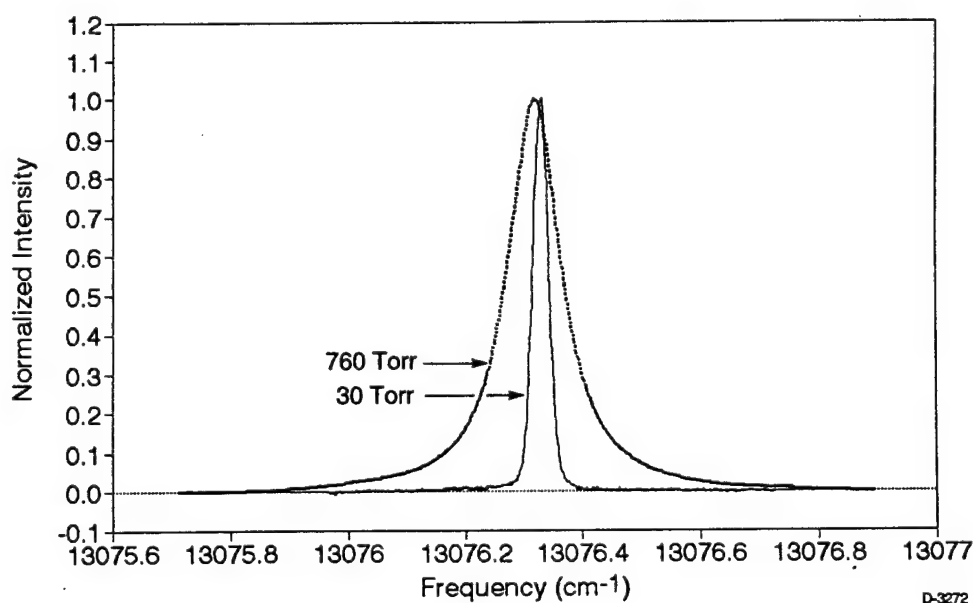

Figure 11. Example of recorded spectra for P13, P13 line absorption spectra recorded simultaneously at two pressures. The dark line is for 760 Torr and the light line was recorded at 30 Torr.

23

For water vapor an alternate procedure was used because we could only use water vapor up to about 17 Torr in our room temperature cell. For these measurements, a measured water vapor pressure was added to the previously evacuated sample cell. Then a small amount of O_2 (10 to 30 Torr) was added to the water vapor in the cell. Absorption measurements were then performed, the cell was evacuated, and this procedure was repeated for several water vapor pressures.

As indicated above, data were reduced off line using a software package called Peakfit. This routine fits recorded data to a Voigt lineshape and provides not only the fit but also all the Voigt parameters from which one can determine the Lorentzian and Gaussian components. For these experiments we fixed the Gaussian component to be the value of the Doppler width at 294 K since all experiments were performed at room temperature. This significantly increased the accuracy of the data reduction. Otherwise the non linear fitting routine would iterate both the Gaussian and Lorentzian widths to provide the best fit. However, it is inaccurate to allow such an unrestrained fit since the Gaussian portion of the linewidth is known since the temperature in the cell is fixed.

3.4.2   Results

A sample of an absorption scan and fit to the data is presented in Figure 12. The fit is the thin solid line. We present this data to illustrate some of the difficulties that arise when performing fits for such small absorptions, typically less than 1% peak absorption. The quality of the fit in the wings of the line is poorer than in the center. While this may not seem to be a significant discrepancy, the wings of the line are most sensitive to the pressure broadening mechanism. Systematic effects such as etalons from optical elements in the optical train can also cause these variations. We take great care to reduce these effects to a minimum.

In Figure 13 we plot the width of P17Q16 absorption line as a function of the oxygen pressure in the sample cell. The linearity of the plot indicates that there are no significant systematic errors. From these data we calculate a self-broadening coefficient of $2\gamma = 3.42$ MHz/
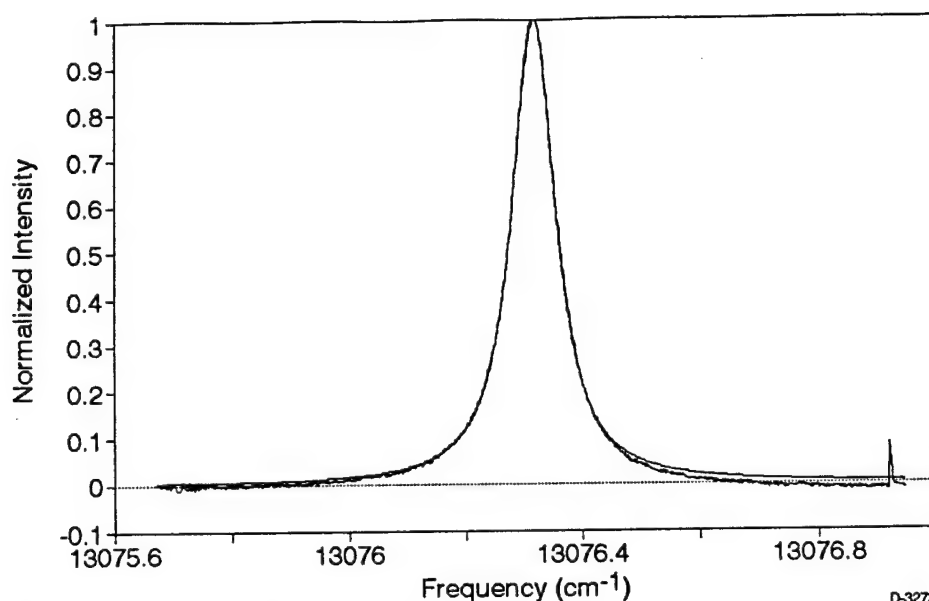
Figure 12. Absorption trace of O_2 P17 Q16 line at a pressure of 703 Torr.
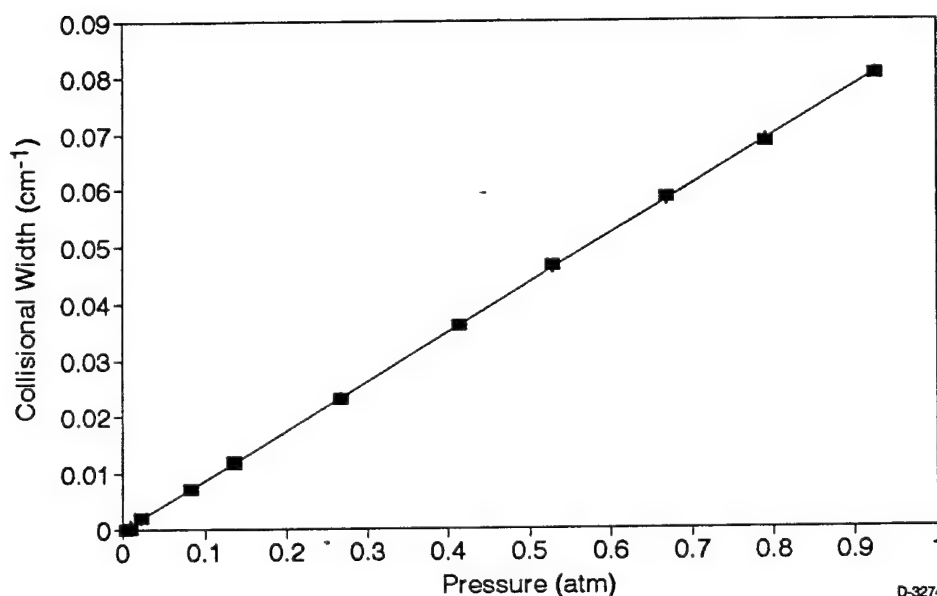
Figure 13. Plot of linewidth of O_2 P17 Q16 line of (b ← X) system as a function of oxygen pressure.

Torr. In Figure 14 we show the measured shift in the center of the absorption line as a function of O_2 pressure. The shift is negative (red shifted) and for the P17, Q17 transition has a value of 0.32 MHz/Torr. Note that the ratio of the broadening to shift is greater than an order of magnitude.
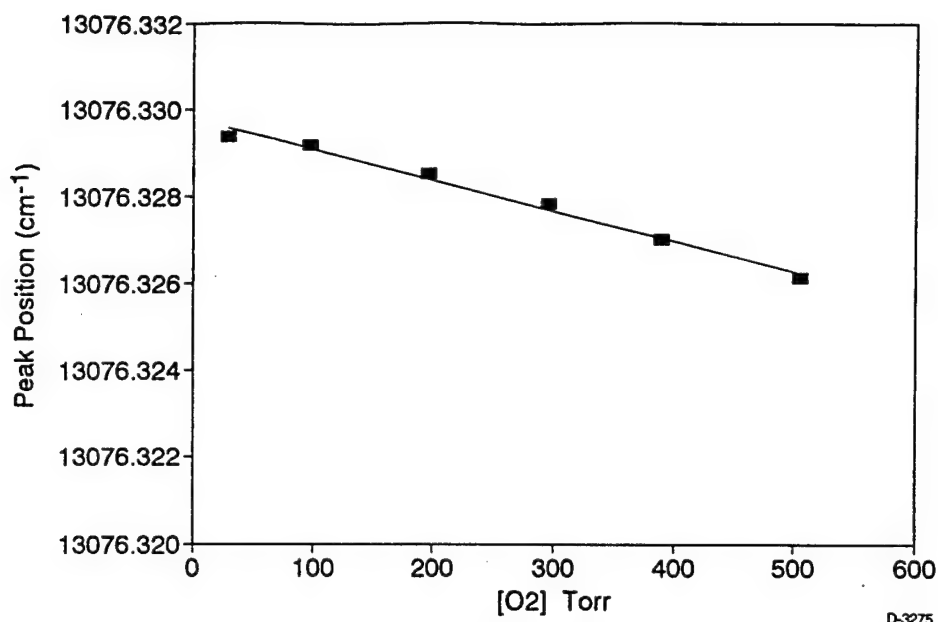
25

Figure 14. Data showing collisional shift of center of P17 Q16 absorption line due to oxygen collisions.

In Figures 15 and 16 we show similar data for the P5 P5 transition but with argon as the bath gas. The values for the broadening and shift parameters are 3.67 MHz/Torr and -0.31 MHz/ Torr respectively. Other bath gases examined in this detailed studies are: helium, neon, nitrogen,
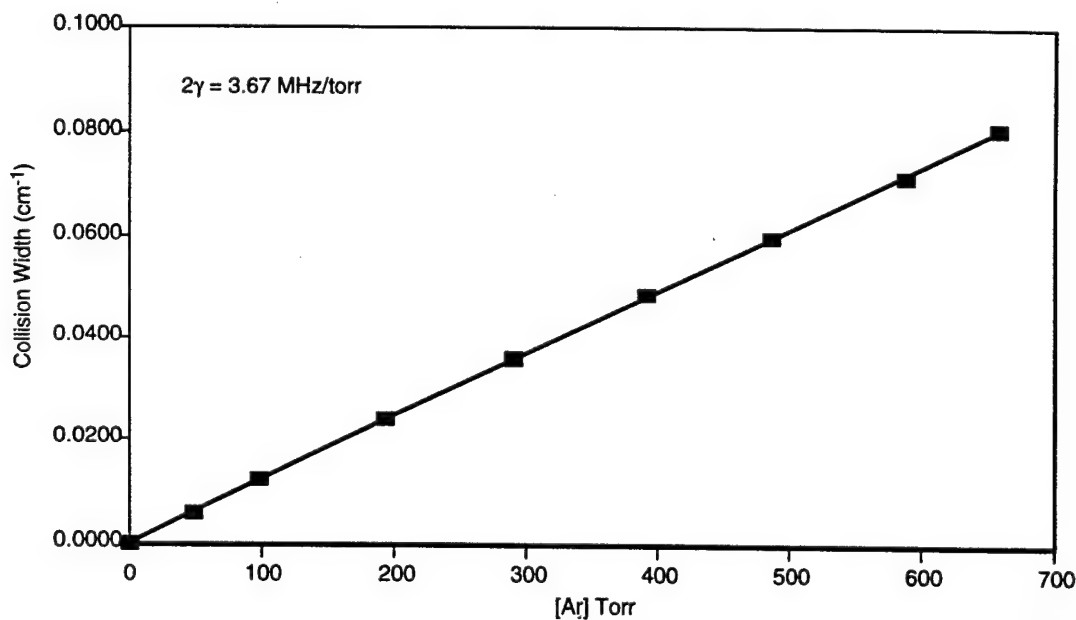
Figure 15. Plot of O_2 self-broadening on the P5 P5 transition.

26
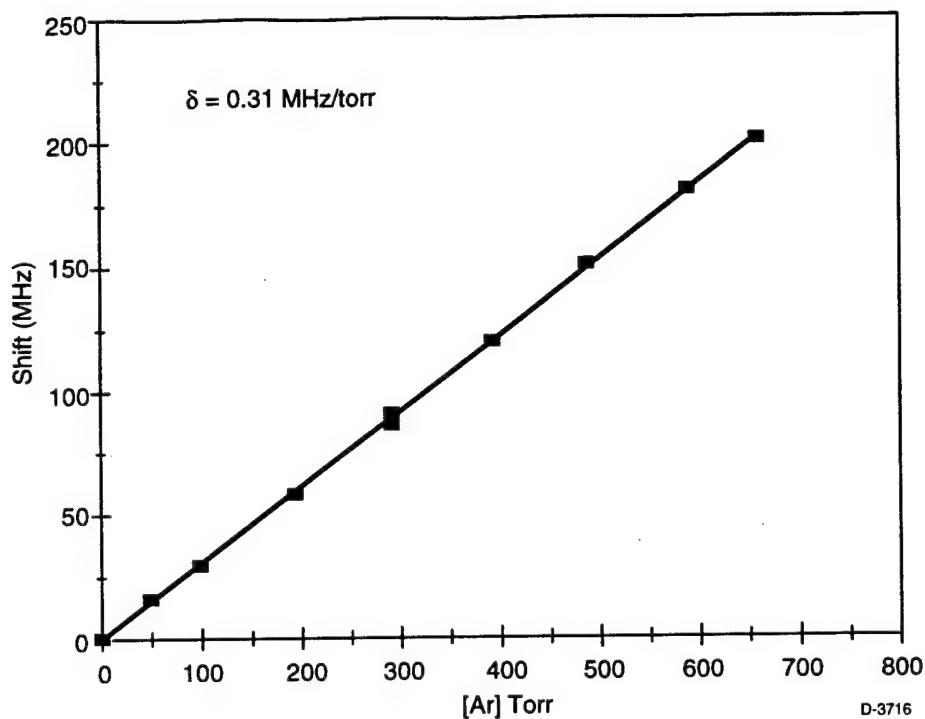
Figure 16. Collisional shift data for P5 P5 line due to oxygen collisions.

carbon dioxide, chlorine, and water vapor. Helium, chlorine, and water vapor are present in COIL and the results are particularly relevant to the operation of COIL.

The line broadening results are summarized in Table 3.

In Figure 17 we show the measured broadening coefficient as a function of the rotational level of the oxygen. We find a weak dependence of the broadening coefficient upon J, and this is consistent with the prior dye laser measurements of Ritter and Wilkerson.[21]

We can extract the cross-section for line broadening from the measurements. This provides a more fundamental parameter with respect to the collision. For these initial comparisons we use the theory originally developed by Lorentz.[22]

27

Table 3. Broadening Coefficient of O_2 (b ← X) by Several Gases

Bath Gas	Oxygen Transition	Broadening Coefficient (MHz/Torr)	Line Shift Coefficient (MHz/Torr)
Oxygen	P5 P5	4.2	0.21
Oxygen	P19 P19	3.3	0.23
Helium	P5 P5	3.1	0.04
Neon	P5 P5	3.2	0.12
Argon	P5 P5	3.7	0.31
Nitrogen	P5 P5	4.1	0.29
Carbon Dioxide	P5 P5	4.7	0.17
Chlorine	P5 P5	5.2	0.34
Water Vapor	P9 Q8	5.0	—
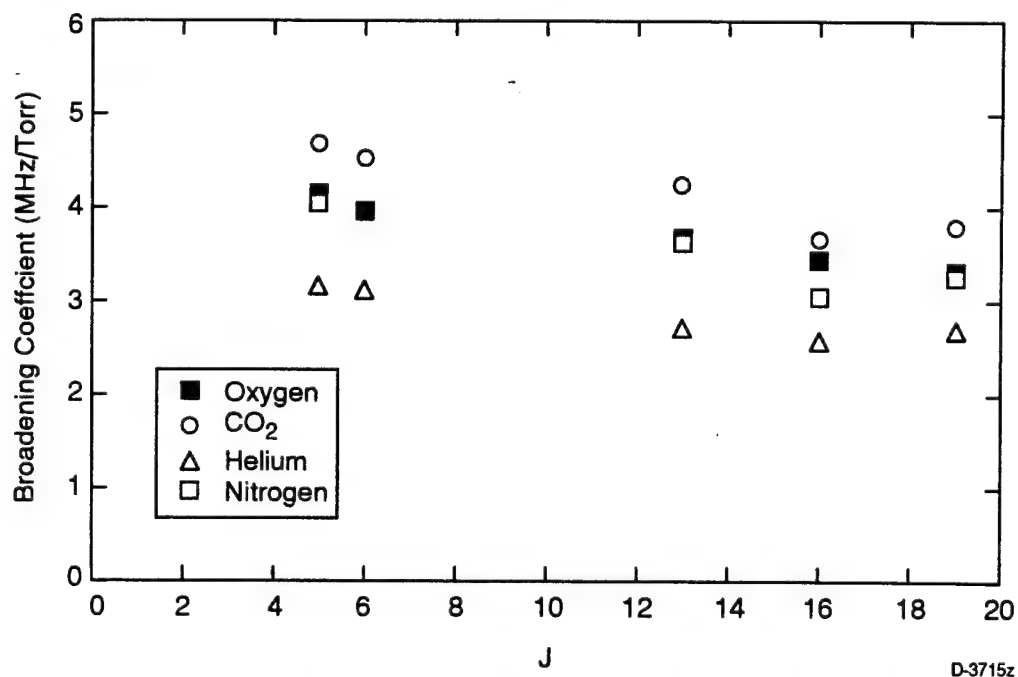
Figure 17. Rotational level dependence of broadening coefficient for four bath gases.

28

The cross-section, σ_c, is determined from the line broadening coefficient, k_c, via Eq. (9):

$$\sigma_c = \frac{k_c}{2\bar{v}} \tag{9}$$

where $\bar{v}$ = relative velocity between the oxygen molecule and the collision partner. Note that $\bar{v}$ is given by Eq. (9):

$$\bar{v} = \left[8\ kT\ \left(M_1 + M_2 / \pi M_1 M_2 \right) \right]^{1/2} \tag{10}$$

where M_1 and M_2 are the respective masses of O_2 and the collision partner.

Equation (9) implies that the collisional broadening coefficient should scale as $\left(\dfrac{1}{\mu} \right)^{1/2}$,

where μ is the reduced mass. In Figure 18 we present a plot of σ_c versus $\left(\dfrac{1}{\mu} \right)^{1/2}$ and observe
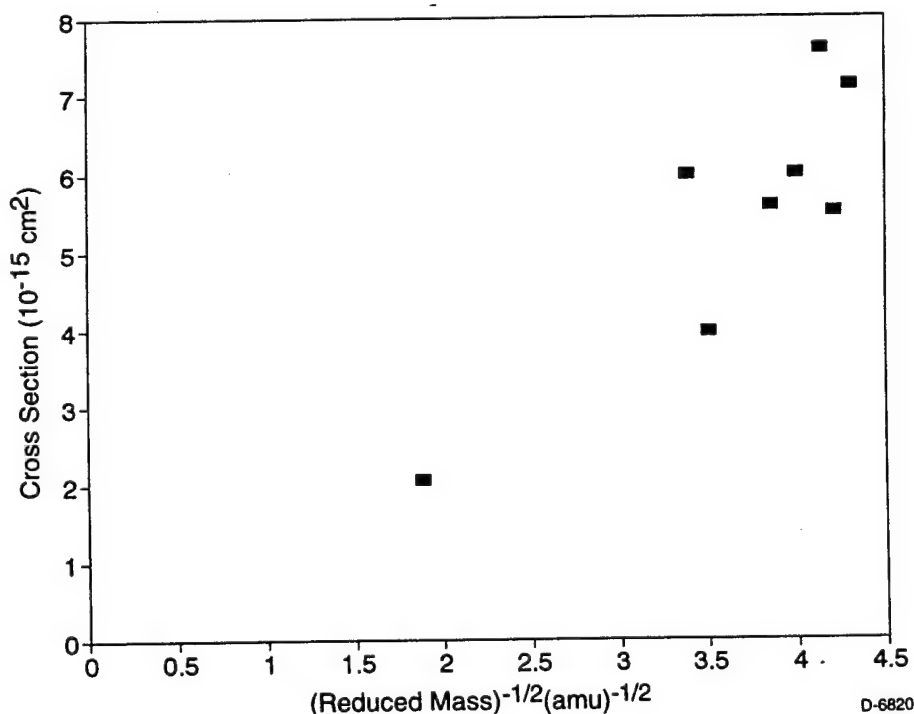
Figure 18. Measured O_2 broadening coefficient versus (reduced mass)$^{-1/2}$ of collision partners

29

that the cross-sections follow the trend in general. In addition, the linebroadening coefficients are considerably larger than the hard sphere values.

There are numerous other more sophisticated analytical treatments that have been developed for line broadening and frequency shifts due to collisions such as the Weisskopf theory[23] and the adiabatic impact theory.[24] Weisskopf's treatment allowed line broadening in the absence of electronic quenching, a more realistic model. The adiabatic model considers even smaller phase changes (softer collisions) and predicts that the frequency shifts will be several times smaller than the line broadening values. Our data for O_2 and the several other collision partners display this behavior. We are presently making more detailed comparisons with predictions of modern collision theory. We feel that the high precision of our data supports these comparisons, and may lead to important insights into the interaction potentials.

We have also compared our results to other previous measurements that used a CW dye laser, a grating spectrometer, and a Fourier transform spectrometer[25], as presented in Table 4.

Table 4. Comparisons to Previous Measurements

Transition	Bath Gas	Broadening Coefficient (MHz/Torr)	Frequency Shift (MHz/Torr)	Reference
P5 P5	Oxygen	4.2	0.21	This work
P19 P19	Oxygen	3.3	0.23	This work
P5 P5	Oxygen	4.20 ± 0.06	—	Ritter and Wilkerson, J. Mol. Spectr. (1987)[21]
P19 P19	Oxygen	3.39 ± 0.04	—	
Rotationally Averaged (N = 5 to 19)	Oxygen	—	0.23	This work
Rotationally Averaged (N = 0 to 24)	Oxygen	—	0.16 .	Phillips and Hamilton, J. Mol. Spectr. (1995)[25]

For COIL applications, the most important broadening coefficient is probably self-broadening. For example, if an oxygen generator were running at 70 Torr and 40 Torr were O_2, the data from Table 3 imply a collisional width of approximately 150 MHz. This is approximately 18% of the Doppler width at 300 K and would need to be accounted for in any temperature determinations using lineshape measurements.

3.5   NCl DIAGNOSTIC DEVELOPMENT

We used the support remaining in our abbreviated program to begin development of sensitive diagnostics for the NCl/I* laser system. Two experiments were performed. The first was in conjunction with Dr. Michael Heaven of Emory University. The second experiment characterized a candidate diode laser for wavelength suitability as a NCl absorption probe and was performed at PSI.

3.5.1   Experiments at Emory

For the Emory University experiments, we provided a Balanced Ratiometric Detector for a series of measurements that were designed to measure absorption spectra in on the NCl (b <- X) system near 665 nm. A Coherent model 699-21 ring dye laser was tuned to the region of 664 nm. The output beam was split so that approximately 60% of the light impinged upon the reference detector of the BRD and the remaining 40% traversed a 100 cm sample cell for seven passes giving a total transit of 700 cm. Upon emerging from the sample cell the dye laser beam transited a 25 cm iodine cell and then was captured by the Si, BRD sample detector. The output of the BRD was monitored on a LeCroy Digital Scope. The iodine cell provided absorption markers at known wavelengths as the ring dye laser was scanned.

Two methods were attempted to produce NCl ground state. First a mixture of N_2 and Cl_2 was passed through a high power rf discharge. In a second arrangement we used a 100 W micro-wave discharge (Evenson Cavity) in attempts to produce a measurable concentration of NCl(X). Neither approach produced a detectable signal of NCl via absorption. In addition, emission spec-

31

tra of the discharge products obtained with a 0.5 m spectrometer revealed only emission from the $N_2(B \rightarrow A)$ system. Although the BRD was able to detect the iodine absorption spectral features, no NCl absorption was detected. Clearly, this simple discharge technique that had been used in prior measurements of NCl microwave absorption spectra was inadequate as a source for optical absorption. These experiments are continuing at Emory using a photolytic source for NCl(X).

3.5.2 Experiments at PSI

At PSI we have a long pathlength, fast flow reactor that is configured to test chemical laser concepts to make high sensitivity diode absorption or gain measurements. This device is shown as a block diagram in Figure 19. A staged mixing configuration allows iodine to be mixed with the primary flow. In Figures 20 and 21 we show photographs of the device. Figure 20 shows the device with no flow and Figure 21 shows the chemiluminescence that results from mixing molecular iodine with singlet delta oxygen.
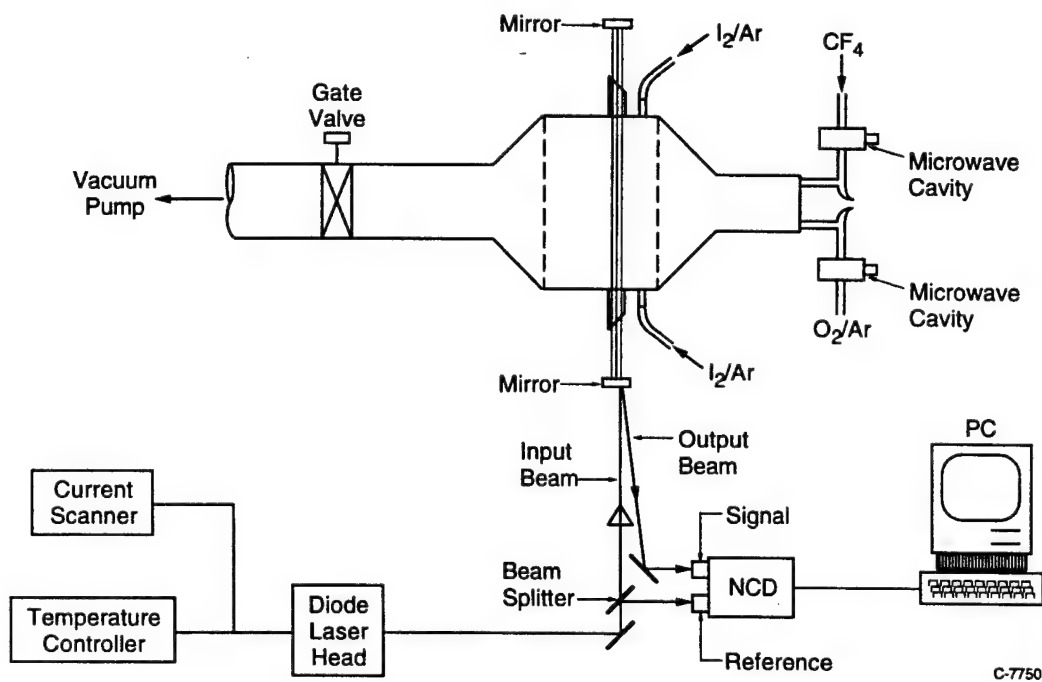
Figure 19. Block diagram of fast flow, long path reactor.

32
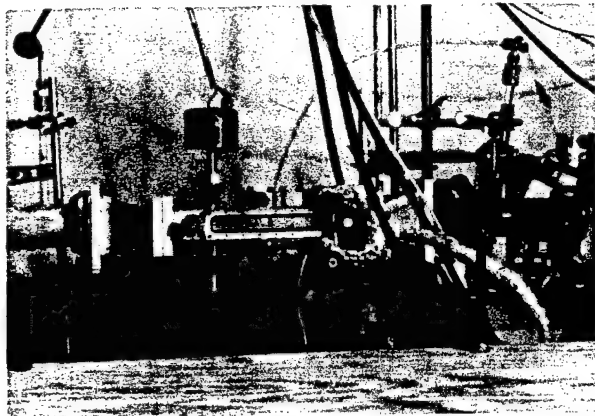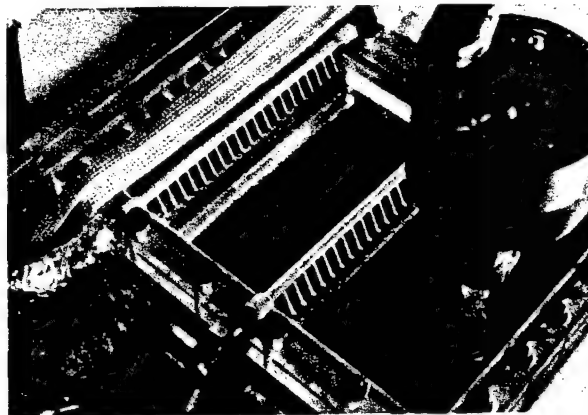
Figure 20. Photographs showing mixing region of fast flow reactor.
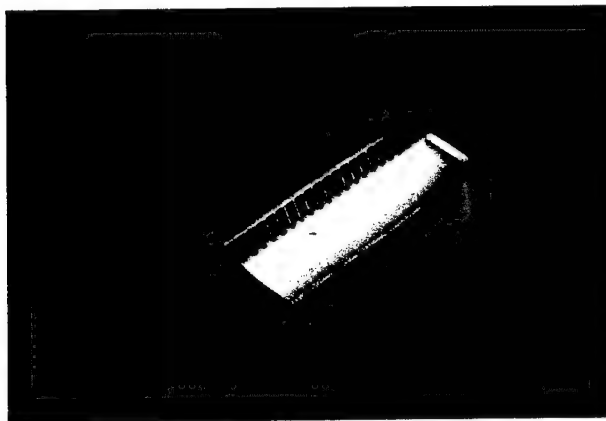
Figure 21. Photograph of reactor operating with $I_2 + O_2^*$ flow.

This device is also compatible with compact multipass cells and we have constructed cells around the device that allows over 3 m of active pathlength for sensitive absorption or gain measurements. We have measured absorption in rovibronic transitions in the IF(B <-X) system as low as a few ppm.

In our original proposal to AFOSR we had proposed to perform spectroscopic and kinetic measurements on the NCl/I laser system using this unique flow reactor and our proven ultra-sensitive diode laser techniques. The lack of funds for the second half of the proposed effort

33

prevented us from completing these studies. In an effort to advance the technology as far as possible with our limited funds, we have performed important characterizations on a diode laser that is suitable for development into a sensitive diagnostic.

We characterized the tuning range of a specially selected, Fabry Perot cavity diode laser that operates in the 660 to 670 nm range. The diode laser was mounted in an ILX 4412 laser mount and was controlled with an ILX current and temperature controller. The output of the diode laser was directed into a Burleigh WV 20 wavemeter and the frequency and wavelength of the diode laser was measured as a function of current and temperature. The tuning characteristics for the diode laser are shown in Figure 22.
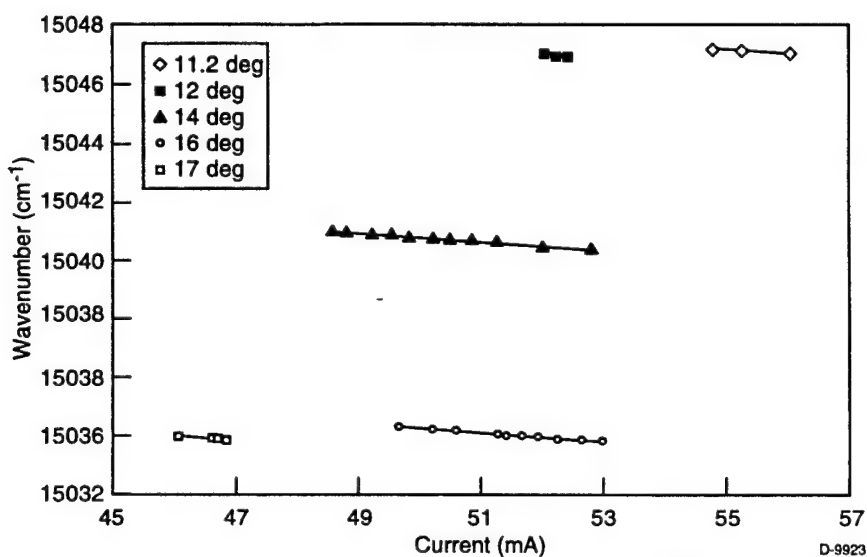
Figure 22. Temperature and current tuning curves for 660 nm diode laser.

In order to evaluate whether the diode laser would be appropriate as an NCl (b <- X) absorption probe, we have plotted the line positions (from Ref. 26) and expected relative intensities for branches in the (0,0) band (Figure 23). Measured tuning of the diode laser is also shown in Figure 23. Clearly, this diode could be used to probe strong rovibronic lines in NCl.

We can estimate our expected sensitivity for NCl(b <- X) absorption from our prior measurements in the analogous system in O_2. We have been able to measure number densities of

34
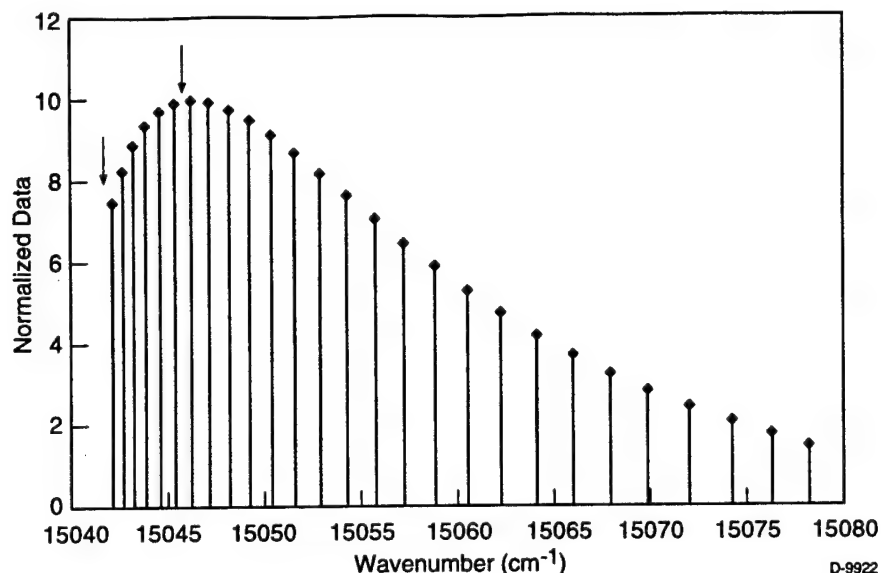
Figure 23.   Positions of NCl (b ← X) lines in (0,0) band. Arrows show regions accessible by diode laser.

less than 1×10^{15} /cm^3 in a 5 cm long cell using a multipass configuration and our BRD detectors. The radiative rate for the NCl(b -> X) system is 2 ms. In contrast the radiative lifetime of the analogous system in O_2 is 12 s. Thus the inherent absorption for this system in NCl is 6×10^3 times stronger than in O_2. Thus we expect that we will be able to measure NCl(X) concentrations of less than 2×10^{11} cm^{-3}. In addition sensitive kinetic studies could also be performed using this approach.

3.6   DIODE LASER PUMPED IODINE OPTICAL AMPLIFIER

These results are summarized in the Appendix 3.

4. SUMMARY

In this program we have provided nearly 20 detailed collisional broadening coefficients for optical transitions in both molecular oxygen and water vapor. These transitions are often used in atmospheric science, laboratory research, combustion studies, and in COIL diagnostics. In addition these transitions are prime candidates for process control development for several important applications. The broadening coefficients provide important data for interpretation of absorption measurements and also are valuable for comparison to the latest theoretical models.

In this program we have also continued to transition the diode laser technology developed under AFOSR support into several important commercial and Government applications as itemized below.

The diode laser pumped iodine results, summarized in the Appendix, provide the first confirmation of a diode pumped gas phase laser. This may lead to advanced, compact, mid-IR diode pumped gas phase lasers for several important Air Force applications.

5. REFERENCES

1. M. G. Allen, K. L. Carleton, S. J. Davis, W. J. Kessler, and K. R. McManus, AIAA 25th Plasmadynamics and Lasers Conference, Colorado Springs, CO (June 1994).

2. S. J. Davis, M. G. Allen, W. J. Kessler, and K. R. McManus, M. F. Miller, and P. A. Mulhall, Paper 2702-18 SPIE Conference on Gas and Chemical Lasers, San Jose, CA (Jan 1996).

3. S. J. Davis, W. J. Kessler, M. Bachmann, and P. A. Mulhall, Paper 3268-80, SPIE Conference on Gas and Chemical Lasers and Intense Beam Applications, San Jose, CA (Jan 1998).

4. S. J. Davis and M. VanBenthem, Laser Digest, AFWL, Kirtland AFB (1993).

5. P. B. Keating, C.A. Helms, B. T. Anderson, T. L. Rittenhouse, K. A. Truesdell, and G. D. Hager, Paper 3268-28, SPIE Conference on Gas and Chemical Lasers and Intense Beam Applications, San Jose, CA (Jan 1998).

6. B. Labini, J. Bonamy, and D. Robert, *J. Chem. Phys.* **87**, 2781 (1987).

7. William S. Benedict and Lewis D. Kaplan, *JQRST* **4**, 453 (1964).

8. Shang-Qian Wu, Jun-IchI Morishita, Hiroshi Masusaki, ahd Tetsuya Kimishima, *Analytical Chem.* **70**, 3315 (1998).

9. J. A. Silver and D. C. Hovde, Rev. Sci. Instrum. <u>65</u>, 1691 (1994).

10. D.M. Sonnenfroh, W.J. Kessler, J.C. McGill, B.L. Upschulte, and M.G. Allen, Appl. Phys. **B** (in press).

11. Mark G. Allen and William J. Kessler, *AIAA Journal* **34**, 483 (1996).

12. V. Nagali, S.I. Chou, D.S. Baer, and R.K. Hanson, AIAA Paper 96-2225 (1996).

13. R. S. Inman and J. F. McAndrew, Anal. Chem. <u>66</u>, 2471 (1994).

14. Robert A. Toth, *Applied Optics* **33**, 4851 (1994).

15 R.R. Gamache, J.M. Hartmann, and L. Rosenmann, *JQRST* **52**, 481 (1994).

16 S. Langlois, T.P. Birbeck, and R.K. Hanson, J *Mole. Spectr.* **163**, 27 (1994).

17.   Bernard L. Upschulte and Mark G. Allen, *JQRST* **59**, 653 (1998).

18   Corrine Delaye, Jean-Michael Hartmann, and Jean Taine, *Applied Optics* **28**, 5080 (1989).

19.   Livio Gainfrani, Mathias Gabrysch, Chiara Corsi, and Paolo Natale, *Applied Optics* **36**, 9481 (1997).

20.   B. Labani, J. Bonamy, D. Robert, J.M. Hartmann, and J. Taine, *J. Chem. Phys.* **84**, 4256 (1986).

21.   K.J. Ritter and T.D. Wilkerson, "High Resolution Spectroscopy of the Oxygen A Band," *J. Molec. Spectr.* **121**, 1 (1987).

22.   H.A. Lorentz, P*roc. Acad. Sci. Amst.* **8**, 591 (1906).

23.   V. Weisskopf, *Phys. Z.* **34**, 1 (1933).

24.   V. Lindholm, *Ark. Mat. Astr. Phys.* **28B** (1941).

25.   Alexander J. Phillips and Peter S. Hamilton, *J. Mole. Spectros.* **174**, 587 (1995).

26.   R. Colin and W. E. Jones, Candian Journ. Phys. 45, 301 (1967) .

6. PERSONNEL SUPPORTED

Senior Research Personnel: Dr. Steven J. Davis, Mr. William J. Kessler,
Dr. Bernard Upschulte

Junior Research Personnel: Mr. Phil Mulhall

7. PUBLICATIONS AND PRESENTATIONS

"Optically Pumped Overtone HF Laser," S.J. Davis, W.J. Kessler, H. Miller, and G. Hager. - Appendix 1

"Optically Pumped HCl Vibrational Laser," H. Miller, G. Hager, S.J. Davis, and W. J. Kessler (Manuscript accepted by J. Appl. Phys, to be published October 1, 1998.) - Appendix 2

"Diode Laser Pumped Molecular Iodine Optical Amplifier," S. J. Davis and K. W. Holtzclaw. (Submitted to J. Appl. Phys) - Appendix 3

"Rotational Energy Transfer in ICL(B); Collisions with ICl," S. J. Davis and K. W. Holtzclaw (Manuscript complete for submission to J. Chem. Phys.) - Appendix 4

"Collisional Broadening of the 1.39253 μm line in Water Vapor" (Manuscript completed for submission to J. Appl. Phys.)

"Collisional Broadening and Pressure Shifts in the b <- X system of O_2," W. J. Kessler, M. Bachmann, and S. J. Davis (Manuscript completed for submission the J. Mole. Spectr.)

Rotational Energy Transfer in ICl (B); Collisions with He and Xe," S. J. Davis and K. W. Holtzclaw. (Manuscript complete for submission to J. Chem. Phys)

8. INTERACTIONS/TRANSITIONS

A.   Participation/Presentation at Meetings, Conferences, Seminars

We have presented several papers at professional meetings and invited seminars:

1.   "Collisional Broadening of the (0,0) Band in Molecular Oxygen," S.J. Davis, A.J.R. Hunter, M.F. Miller, and W.J. Kessler, paper presented to the OSA Annual Meeting, Rochester, NY (October 1996).

2.   "Novel Diagnostics Using Tunable Lasers," S.J. Davis, Invited Seminar to Physics Department, Middlebury College, Middlebury, VT.

3.   "Collisional Broadening for Oxygen and Water Vapor Lines Relevant to COIL Diagnostics," S.J. Davis, Matthew Bachmann, and William J. Kessler, SPIE Lasers '98 Paper, San Jose, CA (January 1998).

4.   "Ultra Sensitive Absorption and Gain Measurements for Chemical Lasers," S.J. Davis and W.J. Kessler, Lasers '98, SPIE; San Jose, CA (January 1996).

B.   Consultive and Advisory Functions to Other Laboratories

Continual dialogue with Phillips Laboratory personnel (Dr. Gordon Hager, Dr. Charles Helms, Mr. Brian Anderson) on applications of COIL diagnostics and potential improvements in operation of advanced COIL devices. Presented seminar to Phillips Laboratory and Rocketdyne on temperature diagnostics.

C.   Technology Transitions

Diode laser diagnostic built by PSI and delivered to Phillips Lab are now in routine use on several COIL devices. These devices are being used to extract data crucial to understanding the conditions in COIL and will lead to designs of improved COIL devices. Parameters being measured include the yield of singlet oxygen from the COIL generators, the concentration of water vapor in the flow, and small signal gain. Recent measurements have also produced preliminary temperature profiles in the flow.

We have delivered a water vapor diagnostic to the Deutsche Forschungsanstalt für Luft und Raumfahrt (DLR) Stuttgart, Germany for their COIL device. We also delivered three diagnostic systems (water vapor, oxygen, and iodine gain) to Ben Gurion University for their COIL. Delivered an order for a water diagnostic from Boeing for COIL applications. The PSI water diagnostic at Phillips Laboratory is now at TRW and is being used on the ABL program. This represents another example of technology transfer.

The water diagnostic strategy, originally developed under AFOSR support, has also had impact outside the COIL community. Under NASA support we are completed, delivered, and

flew an airborne water vapor system to study water vapor profiles from ground level to the lower stratosphere.

We have had contact with several other agencies with respect to water vapor diagnostics for manufacturing process control. For example, we are developing a high temperature water diagnostic system for wind tunnel testing at AEDC. We anticipate that these technology transfers will continue to grow.

9. NEW DISCOVERIES, INVENTIONS, OR PATENT DISCLOSURES

Patent disclosure on I* gas diagnostic being prepared.

10. HONORS/AWARDS

None.

APPENDIX 1

Optically Pumped Hydrogen Fluoride Laser

Optically pumped hydrogen fluoride laser

William J. Kessler and Steven J. Davis
Physical Sciences Incorporated, 20 New England Business Center, Andover, Massachusetts 01810

Harold C. Miller, Jr. and Gordon D. Hager
Lasers and Imaging Directorate, Air Force Phillips Laboratory, Kirtland Air Force Base, New Mexico 87117-6008

We present results from a study of an optically pumped hydrogen fluoride laser. Rotation–vibration transitions within the (2,0) band near 1.3 μm are pumped, and both amplified spontaneous emission (ASE) and laser oscillation are observed on (2,1) band transitions near 2.7 μm. Longitudinal and transverse pumping schemes are discussed. We also have pumped the (3,0) band and observed ASE on both the (3,2) and (2,1) bands. This system serves as a prototype for other mid-infrared diatomic and polyatomic lasers based upon overtone pumping. © *1998 American Institute of Physics.* [S0021-8979(98)06412-3]

I. INTRODUCTION

Optically pumped gas phase lasers have provided a fruitful avenue of research over the last two decades. Much of the early work was centered on electronic transitions within homonuclear species. Notable examples are I_2,[1-3] Na_2,[4-6] and S_2.[7] These systems produced laser oscillation that spanned the ultraviolet (UV) to near-infrared (IR) spectral regions. In these systems, a pump laser excites specific rovibronic transitions leading to population inversions between an excited rotational level within the electronically excited state and an analogous rotational level within the ground state. Typically, laser oscillation is observed on strong, Franck–Condon favored transitions terminating on relatively high (unpopulated) vibrational levels of the ground electronic state. Laser oscillation on some stable heteronuclear species as well as a few transient diatomic species have also been lased by this technique.[8-12] Electronic-transition optically pumped lasers have been used primarily as tools to study basic laser physics, spectroscopy, and chemical kinetics.

One spectral region of current interest for new laser development is the mid-IR from 3 to 5 μm. In addition to allowing detailed spectroscopic and kinetic investigations, this spectral region is of significant practical interest for several applications including environmental monitoring and some medical applications. There have been several approaches to produce lasers in this region including solid state devices, optical parametric oscillators, and diode lasers. In addition numerous optically pumped gas phase lasers have also been developed that operate in the mid-IR. These include photodissociation lasers[13-16] and directly pumped three level molecular lasers.[17-19] While some of these studies used essentially fixed frequency lasers as excitation sources and utilized coincidences with absorption features of the gas phase molecule to be pumped, there was also some early work using tunable excitation lasers. For example, Jones and Bina[20] used the rather limited tuning of the 1.3 μm line in a Nd:YAG laser to excite the hydrogen fluoride (HF) (2,0)

overtone band to determine deactivation rates. Shimoji and Djeu[21] used a Raman shifted Nd:YAG laser to produce amplified spontaneous emission in HCl. One of the most significant advantages that gas phase lasers offer is that the laser medium is self-annealing and easily replaceable.

In this article we describe the initial results of a study of a HF laser that was optically pumped on several transitions within the (3,0) and (2,0) bands. The excitation and emission scheme for overtone pumping is indicated in Fig. 1. We have excited several rotational lines in both the (2,0) and (3,0) overtone bands in HF. For some of the experiments we used no optical resonator around the HF medium. Rather, we studied amplified spontaneous emission for the overtone pumped HF. Since no wavelength dependent optical feedback elements are used, amplified spontaneous emission (ASE) provides a convenient method for assessing some of the inherent stimulated emission properties of overtone excited molecules. We also used an optical cavity to produce a true HF laser.

Although this initial study describes experiments only on the HF molecule, we are studying several other hydrogen halides at the present time including HCl, HBr, and DF. Indeed, several of the hydrogen halides and their deuterated analogs possess large absorption and stimulated emission cross sections, making them attractive candidates for this excitation strategy. Typical values for absorption cross sections on the (2,0) band are on the order of 10^{-17} cm^2 and stimulated emission cross sections for transitions on the (2,1) band are on the order of 10^{-15} cm^2. We chose HF as the first candidate because of its well-known lasing and kinetic properties, making it an ideal test system.

II. EXPERIMENT

The overtone excitation experiments on HF were performed using the apparatus shown in Fig. 2. The excitation source was a Continuum TDL 50 dye laser that was Raman shifted to produce output in the 875–1300 nm wavelength range. The dye laser was pumped by a Continuum model

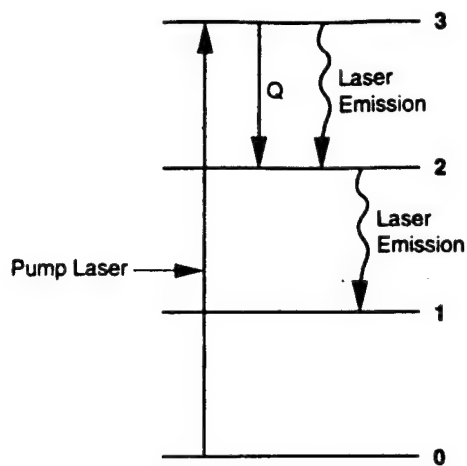FIG. 1. Energy level scheme for an overtone pumped gas phase laser.

FIG. 3. The apparatus for side pumped HF laser experiments.

481, frequency doubled Nd:YAG laser. The pulse length was approximately 8 ns, and the bandwidth of the Raman shifted output was less than 0.12 cm^{-1}.

As seen in Fig. 2, the HF cells were excited longitudinally. The excitation beam was focussed to a diameter of approximately 3 mm. Precise determination of the pump beam diameter was difficult since the output from the Raman shifter was quite divergent. We did not attempt to design a sophisticated beam focusing system. Thus, the coupling of the pump laser to the HF medium was not optimized.

We used three cells each of a different length: 112, 20, and 7.5 cm. The cells were connected to a passivated gas handling system and were pumped to less than 0.1 mTorr prior to filling. Cells were filled with neat HF or with mixtures of HF and a buffer gas such as He. Detection of both absorbed pump radiation and the HF ASE was accomplished using a liquid nitrogen cooled InAs detector. A series of long pass and short pass optical filters were used to isolate the ASE emission. For some studies, a 0.3 m McPherson model 270 monochromator was used to disperse the ASE. This not only helped assign the ASE transitions but also allowed us to study energy transfer within the excited HF.

Prior to the ASE tests a 7.5 cm long cell filled with HF was placed in a Shimadzu model 3000 spectrophotometer and we obtained absorption spectra for overtone transitions. These data helped establish the optimum excitation wavelengths.
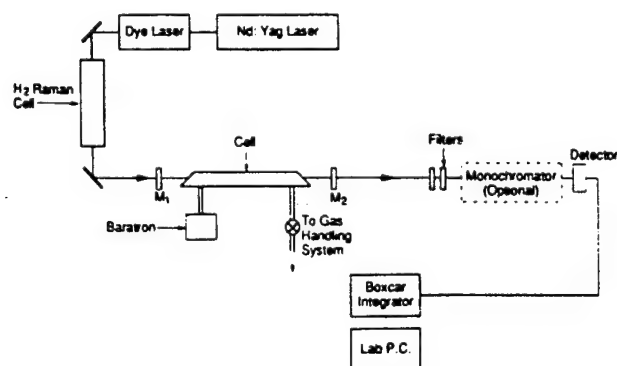

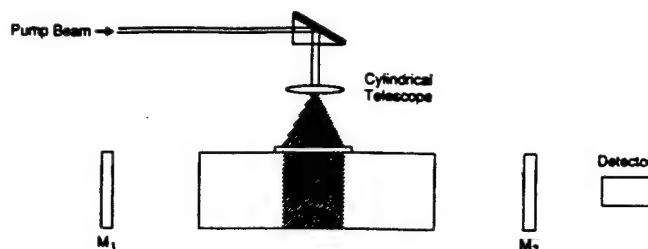FIG. 2. Block diagram of the apparatus for longitudinally pumped HF laser/ASE studies.

We performed two classes of studies. The calculated large stimulated emission cross sections for (2,1) transitions implied that single pass ASE would be observable. Thus, we initiated a series of experiments to study this phenomenon. For these experiments we used the 112 and the 7.5 cm cells. Later, we also enclosed the 20 cm HF cell in a stable optical cavity in order to investigate laser oscillation. Both of these studies are described below.

For the ASE experiments, HF in the cell was excited with the Raman shifted dye laser operating at low power. We monitored the transmitted pump power as a function of the excitation wavelength and obtained absorption spectra. Following this, the dye laser was tuned to a particular absorption line, and the dye laser power was increased and a search for stimulated emission on HF fundamental bands near 2.7 μm was initiated. For some experiments the dye laser wavelength was scanned and we monitored the broadband ASE. We confirmed the presence of ASE by observing a well defined excitation threshold. In addition, once the HF system was above threshold, a geometrically narrow beam was produced.

We also completed a series of laser tests using a stable resonator around the HF cell. The cell in these experiments was 20 cm long. The pump radiation was coupled into a HF cell through a concave (5 m radius of curvature) dichroic cavity mirror, which was highly reflective at 2.7 μm. The optimum output coupler was a CaF$_2$ flat, coated to reflect 60% at 2.7 μm. The two cavity mirrors were separated by about 45 cm, and the pump laser was focused into the optically pumped laser (OPL) cavity. As described above, although the lowest order modes of the cavity were overlapped by the pump beam, we do not feel that the coupling was optimized.

The output of the HF laser was spectrally resolved with an infrared monochromator described above. For some experiments, a high-speed Ge:Au detector (~2 ns) was used to monitor the temporal evolution of the laser pulses.

Diode lasers also are potential excitation sources for gas phase lasers in much the same way that they have been incorporated as pump sources for solid state lasers. High power diode lasers usually have a stripe or array geometry and often are incorporated in a side pump configuration for solid state lasers. Consequently, in order to investigate one additional important aspect of the optically pumped HF laser we designed a side pump configuration, shown in Fig. 3. A cylindrical beam expanding telescope was used to form the Raman shifted dye laser beam into a stripe (2.5×0.1 cm) that was used to pump a specially prepared cell. The cell was 7.5

cm long and contained a 2.5 cm side window that was used to inject the excitation beam. This geometry contained the essential features that would be used in a diode pumped system.

III. RESULTS

In Fig. 4 we present a laser absorption spectrum (top) for several rotational lines in the HF (2,0) overtone band. These data were obtained by monitoring the Raman shifted dye laser output that was transmitted through a 112 cm cell that contained 25 Torr of HF gas. Also shown in Fig. 4 (bottom) are data obtained by increasing the pump power of the Raman shifted dye laser to a value that exceeded the threshold for ASE. The strong emission features are due to the amplified spontaneous emission in the HF. These data were obtained in the 7.5 cm cell that contained 50 Torr of HF and 670 Torr of helium. The features appear sharper than the absorption lines because there is a definite threshold power level for ASE production. There is no such threshold for absorption, and the absorption features appear to be broader. This is expected since the bandwidth of the excitation source (0.1 cm^{-1}) is greater than that of the HF absorption lines $(\sim 0.03 \text{ cm}^{-1})$. We found an ASE threshold energy of less than 100 μJ.

The ASE output power was independent of the added helium bath gas for pressures up to 600 Torr of added helium. This may have some practical implications since the addition of a bath gas will broaden the overtone absorption line and this may enhance coupling of the excitation laser light into the laser media. The ASE was also quite immune to quenching by HF as seen in Fig. 5. These data were obtained pumping the $R(3)$ line with 2 mJ of excitation incident upon the cell. There is an initial rise as the concentration increased from 0 to about 100 Torr. As more HF is added, collisional vibrational deactivation of the optically pumped level begins to exceed the excitation rate and the output energy drops.

The optical gain of the optically pumped HF system can be estimated using several methods. We chose to use the measured pump energy absorbed to calculate the maximum

FIG. 5. Dependence of the HF ASE output energy/pulse as a function of the HF number density. For these data 2 mJ of pump energy was used.

initial population inversion. The initial inversion was then used with the known stimulated emission cross section to determine the gain coefficient. In the following example the HF laser cavity had been removed and ASE was observed. The cell length was 112 cm and the pump beam diameter was approximately 5 mm. For 23 Torr of HF and pumping the $R(3)$ line of the (2,0) band, 0.68 mJ was absorbed. Thus, the peak population within the $v''=2$ level, neglecting vibrational relaxation, would be $2.6 \times 10^{14} \text{ cm}^{-3}$. During the 10 ns pump pulse, rotational redistribution within $v''=2$ is rapid, and we assume rotational thermalization is complete at the termination of the pump pulse. The Boltzmann maximum occurs at $J=2$ and this level contains 29% of the population within $v=2$. Consequently, the population inversion density for the $P(3)$ emission transition is approximately 7.5×10^{13} cm^{-3}. The stimulated emission cross section for the $P(3)$ line of the (2,1) band is $1.9 \times 10^{-15} \text{ cm}^2$. The gain coefficient, g, is given by the product of the stimulated emission cross section and the inversion density, $g = N\sigma$. For the present example, $g = 0.14 \text{ cm}^{-1}$ for the $P(3)$ line of the (2,1) band, and the single pass gain coefficient for the 112 cm cell

FIG. 4. Absorption and corresponding ASE spectra for overtone pumping several R-branch lines on the HF(2,0) overtone band. The top spectrum shows the absorption of the dye laser and the bottom trace indicates the ASE. The two spectra have been offset slightly horizontally for clarity.

FIG. 6. Temporal evolution of the HF laser pulse. For these data the $R(2)$ line of the (2,0) band was pumped. The HF pressure was 5.4 Torr, and the output coupler was 60% at 2.7 μm.

FIG. 7. Spectrally resolved HF laser output for the pulse shown in Fig. 6.

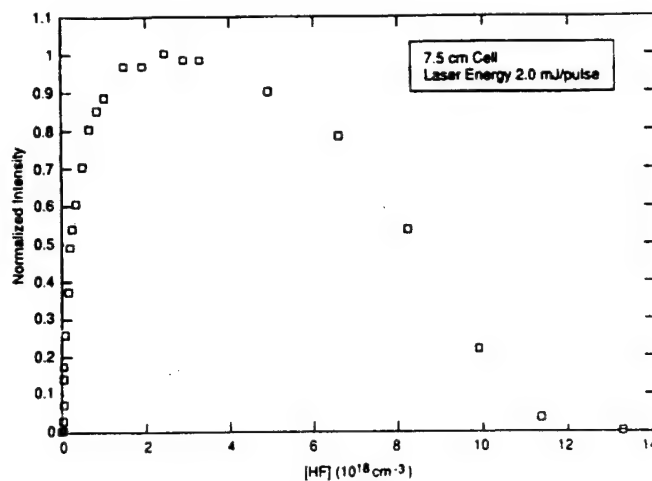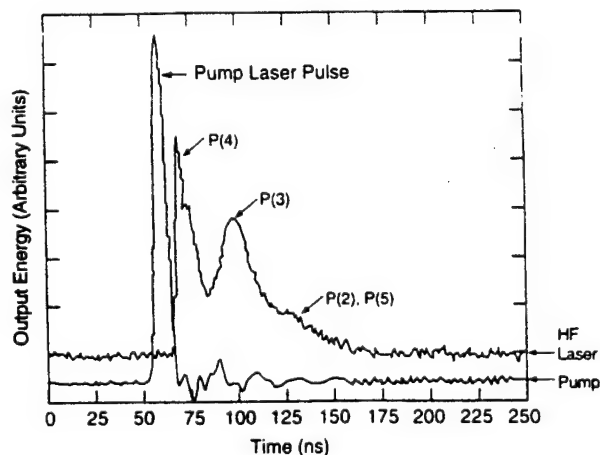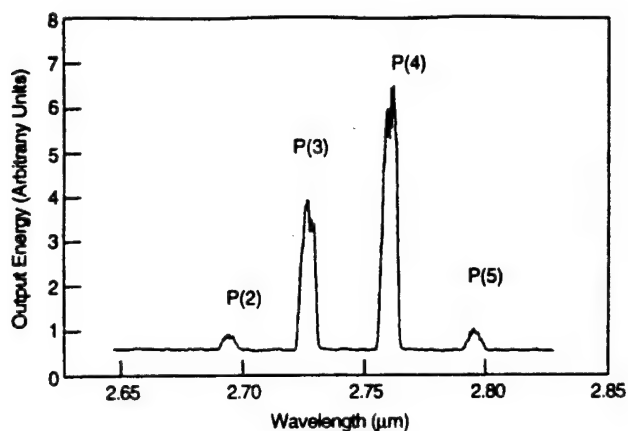is 16. This high single pass gain coefficient is consistent with the observations of strong ASE and short (10–20 ns) turn on times for the HF stimulated emission.

Rotational and vibrational energy transfer are well documented phenomena in HF (Refs. 22–27) and play a dominant kinetic role in HF chemical lasers. The temporal behavior of each HF emission line provides confirmation of the important roles of rotational energy transfer (RET) in the HF overtone pumped laser. For example, in Fig. 6, the $P(4)$ level is the first to reach laser oscillation. Note that for $P(4)$, the upper level is $J=3$, the level pumped by the excitation laser. Other P transitions ($J=2$, 1, and 5) are not directly populated by the pump laser. Rather they are collisionally populated by rotational energy transfer. Figure 7 shows a spectrally resolved output spectrum of the HF laser subse-

quent to pumping the $P(4)$ line. It is clear that extensive rotational relaxation has occurred prior to laser oscillation as indicated in Fig. 7. We note that only P lines are observed. Indeed, except at low pressure (<0.5 Torr), only P-branch laser lines are seen. This is due to the larger Einstein coefficients for P-branch lines,[28-30] and is similar to the behavior observed in HF chemical lasers. Although we have not completed a detailed kinetic analysis of these data, the rapid transfer of population from the initially excited rotational level to nearby neighbors during the time between pumping and laser onset (~20 ns) implies RET rate coefficients on the order of 10^{-10} cm^3 molecule^{-1} s^{-1}. These observations are consistent with the numerous detailed energy transfer studies that have been reported previously.[22-27]

It is relevant to note that the RET process is not a significant deactivation process for the HF laser since it only redistributes the population within the vibrational energy level originally excited. This process also will allow the laser to be spectrally tuned within a vibrational manifold.

The efficiency of the HF laser was determined using a 60% reflective output coupler. We measured output energies in the range of 20 μJ/pulse, with less than 100 μJ of pump energy absorbed. The highest energy conversion efficiency that we observed is 29% although this has not been optimized. This corresponds to a quantum efficiency of 62% and clearly indicates the inherent high efficiency of the HF device.

In the side pumped configuration shown in Fig. 3, we observed strong HF lasing on the (2,1) band. Here the optical pathlength for gain was only 2 cm. Indeed, at least 60% of the HF gas along the laser axis was unexcited, ground state
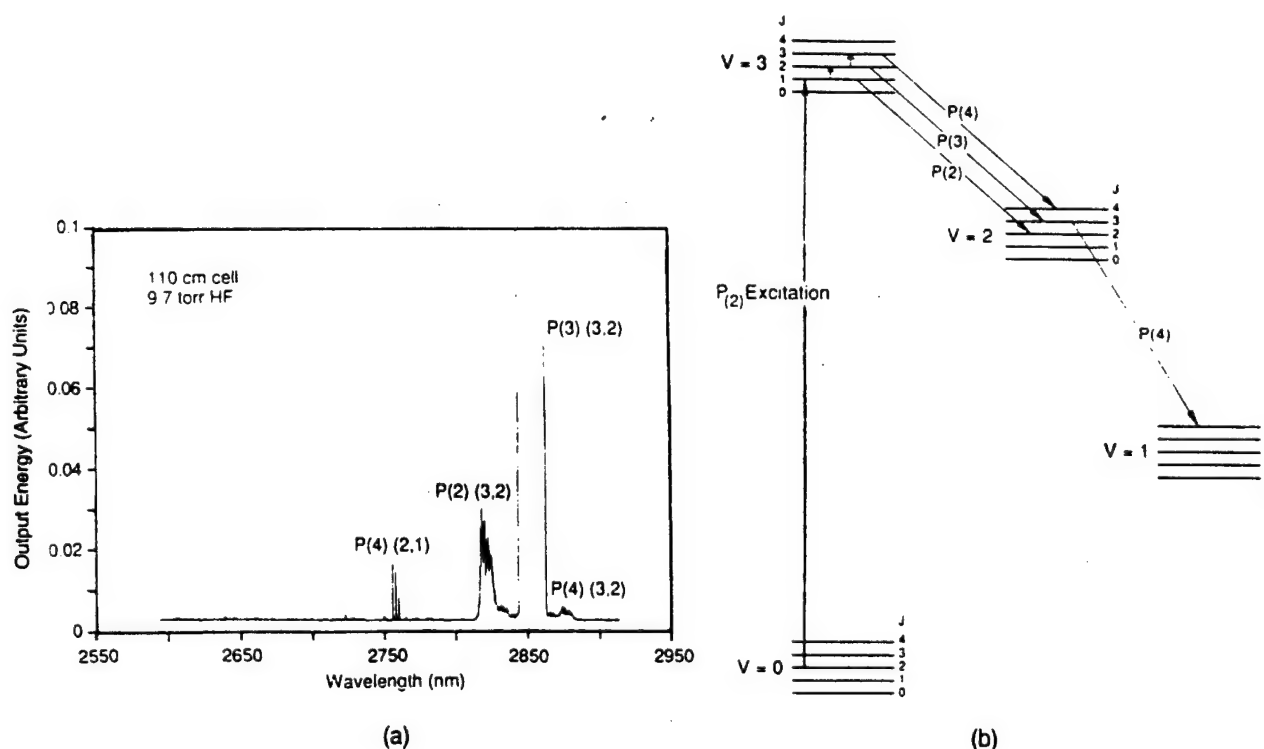

(a)   (b)

FIG. 8. (a) Spectrally resolved HF ASE output following excitation of the $v=3$, $J=2$ level. The energy levels involved are shown in (b).

Kessler *et al.*

7452   J. Appl. Phys., Vol. 83, No. 12, 15 June 1998

HF. This again indicates the high inherent gain of the HF system.

We also excited rotational levels within $v = 3$ using excitation wavelengths near 875 nm. We observed ASE from both rotational and vibrational levels distinct from that initially excited by the dye laser. These results are shown in Fig. 8. Indeed, ASE from collisionally populated rotational and vibrational levels is evident. We stress that these results were obtained with no resonator in place to help build up the HF laser flux. However, energy transfer and subsequent lasing from collisionally populated states are clearly evident. From a practical perspective our observation of ASE from both the (3,2) and (2,1) bands indicates cascading laser emission. Thus, one may be able to recover a large fraction of the initial excitation photons that were absorbed by the medium.

IV. CONCLUSIONS

The results of this study indicate that efficient gas phase mid-IR lasers can be developed. These devices will serve as convenient energy converters for several potential excitation sources including diode laser pumped solid state lasers. The strong influence of rotational and vibrational relaxation is also apparent from our initial studies. At the present time we are developing a kinetic model for these overtone pumped lasers and are extending the experimental investigations to other hydrogen halide species.

ACKNOWLEDGMENT

[1] R. L. Byer, R. C. Herbst, H. Kildal, and M. D. Levenson, Appl. Phys. Lett. **20**, 413 (1973).

[2] J. B. Koffend and R. W. Field, J. Appl. Phys. **48**, 4468 (1977).

[3] J. W. Glessner and S. J. Davis, J. Appl. Phys. **62**, 5 (1987).

[4] M. A. Henesian, R. L. Herbst, and R. L. Byer, J. Appl. Phys. **47**, 1515 (1976).

[5] H. Itoh, H. Uchiki, and M. Matsuoka, Opt. Commun. **18**, 271 (1976).

[6] B. Wellegehausen, S. Shahdin, D. Friede, and H. Welling, Appl. Phys. **13**, 97 (1977).

[7] S. R. Leone and K. G. Kosnik, Appl. Phys. Lett. **30**, 346 (1977).

[8] B. Wellegehausen, IEEE J. Quantum Electron. **QE-15**, 1108 (1979).

[9] J. B. Koffend, R. W. Field, D. R. Guyer, and S. R. Leone, *Laser Spectroscopy III*, edited by J. L. Hall and J. L. Carlsten (Springer, New York, 1977), pp. 382–393.

[10] M. D. Burrows, S. L. Baughcum, and R. Oldenberg, Appl. Phys. Lett. **46**, 22 (1985).

[11] S. G. Dinev and G. B. Hadjichristov, Chem. Phys. Lett. **175**, 216 (1990).

[12] S. J. Davis, L. Hanko, and P. J. Wolf, J. Chem. Phys. **82**, 4831 (1985).

[13] H. C. Miller, K. Yamasaki, J. E. Smedley, and S. R. Leone, Chem. Phys. Lett. **181**, 250 (1991).

[14] V. A. Zolotarev, P. G. Kryukov, Y. P. Podmarkov, M. P. Frolov, and V. A. Shcheglov, Sov. J. Quantum Electron. **18**, 643 (1988).

[15] L. E. Zapata and R. J. De Young, J. Appl. Phys. **54**, 1686 (1983).

[16] A. B. Peterson, C. Wittig, and S. R. Leone, Appl. Phys. Lett. **27**, 305 (1975).

[17] C. R. Jones, A. H. Bushnell, M. I. Buchwald, and M. A. Gunderson, IEEE J. Quantum Electron. **QE-15**, 208 (1979).

[18] C. R. Jones, R. S. McDowell, C. W. Patterson, M. I. Buchwald, and J. M. Telle, Opt. Lett. **4**, 274 (1979).

[19] C. R. Jones, L. Y. Nelson, and M. I. Buchwald, Appl. Phys. Lett. **37**, 765 (1980).

[20] C. R. Jones and M. J. Bina, Appl. Phys. Lett. **22**, 44 (1973).

[21] Y. Shimoji and N. Djeu, Appl. Phys. Lett. **49**, 1 (1986).

[22] J. C. Polanyi and K. B. Woodall, J. Chem. Phys. **56**, 1563 (1972).

[23] R. L. Wilkins and M. A. Kwok, J. Chem. Phys. **70**, 1705 (1979).

[24] R. A. Copeland, D. J. Pearson, J. M. Robinson, and F. F. Crim, J. Chem. Phys. **77**, 3974 (1982).

[25] L. S. Dzelzkalns and F. Kaufman, J. Chem. Phys. **79**, 3836 (1983).

[26] R. A. Copeland and F. F. Crim, J. Chem. Phys. **78**, 5551 (1983).

[27] S. R. Leone, J. Phys. Chem. Ref. Data **11**, 953 (1982).

[28] R. Heman and R. F. Wallis, J. Chem. Phys. **23**, 637 (1955).

[29] D. Oba, B. S. Agrawalla, and D. W. Setser, J. Quant. Spectrosc. Radiat. Transf. **34**, 283 (1985).

[30] R. E. Merideth and F. G. Smith, *Investigations of Chemical Laser Processes* (Willow Run Laboratories, University of Michigan, Ann Arbor, MI, 1971), Vol. II.

APPENDIX 2

Optical Gain on the I_2 (B→X) System Produced by a Visible Wavelength Diode Laser

51

Optical Gain on the I_2 (B-X) System Produced by a

Visible Wavelength Diode Laser

S.J. Davis and K.W. Holtzclaw

Physical Sciences Inc.

20 New England Business Center

Andover, MA 01810

ABSTRACT

We report the results of a measurement of sub-doppler gain profiles in molecular iodine produced by a low power tunable diode laser. Using a sensitive, two beam detection method, we have measured absorptions and amplifications that are only a few parts in 10^4. Amplification was observed for pump laser powers of only 200 µW, and the optical gain observed varied linearly with pump power. Comparisons with a simple, steady state model are also discussed.

INTRODUCTION

The field of optically pumped, gas phase molecular lasers has been an active area for more than two decades. In particular, argon ion and dye laser excitation of selected halogen and interhalogen molecules, e.g., I_2,[1-8] Br_2,[9] and IF[10] have resulted numerous pulsed and CW lasers with extensive, but discrete, tuning capabilities. In these prior studies, large frame argon ion and both pulsed and CW dye lasers were required as pump sources.

With the advent of visible to near IR diode lasers, there has been a rapid advance in the application of these devices as excitation sources for a variety of solid state laser materials. Perhaps the most prominent is the incorporation of diode lasers operating at 980 nm as pump lasers for fiber optic telecommunication amplifiers. These miniature diode lasers are now used routinely in long haul communications. The development of high power diode laser arrays has also led to a new class of Nd:YAG lasers that use miniature, efficient diode lasers to excite the Nd^+ ions. These compact Nd:YAG lasers can be Q-switched or operated CW and are finding many applications. Efficient non-linear conversion techniques have also allowed these systems to produce outputs over extended wavelength ranges from the UV to the mid-IR.[11,12]

While the literature is rich with reports of diode laser pumped solid state lasers,[13] there has been very little work reported concerning pumping gas phase species with diode lasers. Recently, we have been exploring the possibility of producing efficient gas phase lasers using miniature diode lasers as the excitation source. In this paper we describe results of measurements of small signal optical gain on the B-X system in molecular iodine produced by pumping rovibronic bands with a low power, visible wavelength (634 nm) diode laser. Using an ultrasensitive probe laser technique,[14,15] we have observed sub-Doppler gain profiles within selected

54

iodine absorption bands. These narrow features are attributed to the spectrally narrow, single longitudinal mode of the excitation diode laser.

EXPERIMENTAL

The experiments were performed using the apparatus shown in Figure 1. Iodine crystals were contained in an evacuated, 10 cm long, quartz cell at room temperature. No bath gas was added for these experiments. Two diode lasers were used in a pump-probe configuration. A Toshiba (9521) diode laser operating near 634 nm was used as the optical excitation source for the iodine vapor. This device produced up to 10 mW of continuous wave (CW) radiation in a single longitudinal mode. Tuning through several (B-X) transitions was accomplished by systematic variations of the temperature and the injection current in the diode laser. We monitored the wavelength of the diode laser output with a Burleigh WV 20 Wavemeter. This device displayed the frequency of the diode laser with an accuracy of 0.02 cm^{-2}.

Spectrally resolved laser induced fluorescence (LIF) from the iodine cell was monitored normal to the excitation beam using an Acton Model 270 Spectrometer with a Hamamatsu 943-02 PMT. The PMT output was amplified and recorded using a Labtech Notebook® data acquisition system. The LIF monitor was a valuable tool in assigning the transitions being excited and probed.

After completing several surveys using the 634 nm diode laser, we selected the P(38) and R(46) lines within the (8,4) band of the (B-X) system for excitation. The respective absorption line centers for these two transitions are: 15811.453 and 15811.444 cm^{-1}.[16] The hyperfine structure of the B and X states in I$_2$ results in extensive blending due to Doppler broadening. Indeed, doppler linewidths ranging from 450 to 900 MHz have been reported for individual

55

rovibronic transitions.[17,18] Thus the P(38) and R(46) lines of the (8,4), separated by 330 MHz, band can be pumped simultaneously by the excitation diode laser. With the diode laser operating near 15811.45 cm^{-1}, the pump laser produced intense visible laser induced fluorescence in the cell. The cell absorbed approximately 10% of the diode laser pump beam when the laser frequency was on resonance with these two rovibronic transitions. In modeling of this system described below, we approximated the excitation mechanism by assuming equal coupling of the pump radiation into both the P(38) and R(46) lines.

A second diode laser (Phillips CQ 806) was used as a probe for the iodine vapor. This device was scanned over a spectrally narrow region near 14783 cm^{-1} in order to probe the P(38) and R(46) lines of the (8,9) band. The pump/probe scheme is illustrated in Figure 2. The overall strategy of the experiment was to hold the pump wavelength at the center of the selected transition within the (8,4) band and then tune the probe laser wavelength through the P(38) and R(46) lines of the (8,9) band.

Each diode laser was contained in a separate ILX (4412) thermo-electric cooled mount and each was powered by an ILX (3620) current controller and an ILX (5910) temperature controller. The diode laser mounts contained focusing optics that allowed adjustment of the spot sizes of the two diode laser beams within the iodine cell. For most experiments the beam diameters of the pump and probe beams were set to approximately 0.7 mm. This was measured with a calibrated, adjustable aperture. The two beams were spatially overlapped to maximize the interaction volume of the probe beam with the excited iodine molecules.

Description of Excitation Process

We assume a steady state model to calculate $N_{v',J'}$ in the two rotational sublevels.

$$\frac{dN_{v',J'}}{dt} = R - N_{v',J'}\left(A_{v',J'-v''J''} + k_Q I_2 + K_p\right) \tag{1}$$

Solving for $N_{v',J'}$ gives:

$$N_{v'J'} = \frac{R}{I_2 k_Q + K_p + A_{v'J'-v''J''}} \tag{2}$$

where R is the excitation rate, $A_{v'J'-v''J''}$ is the radiative rate for the rovibronic pump transition, I_2 is the ground state iodine number density, k_Q is the collisional removal rate from initially excited level due to quenching and energy transfer, and K_p is the predissociation rate. Collisional quenching of the excited states dominates rotational and vibrational energy transfer with only I_2 present. The collisional, predissociative, and radiative decay rates for v',J' levels in the B state of iodine are well known from numerous previous measurements.[19-21] The sum of these rates for the relevant levels in this experiment is 1.2×10^7 s^{-1}.

In a typical experiment 4.1 mW of the pump laser was focused into the cell and 10% of this light was absorbed by the iodine. This leads to an excitation rate of 3.4×10^{16} molecules cm^{-3} s^{-1}. This value combined with the total deactivation rate discussed above provides an estimate for the steady state population of $J'=37$ and $J'=47$ within $v'=8$. We assume that the population is equally distributed between these two levels, and calculate that each has a steady state population of 1.6×10^9 cm^{-3}. The differences between these populations and those of

57

$J''=38$ and 46 within $v''=9$ will determine the population inversions and the net optical gains or absorptions of each transition.

We must also consider the linewidth of the pump laser when we estimate the gain produced by 634 nm diode laser. The gain coefficient at line center, $\gamma(v_0)$, is defined as the product of the stimulated emission cross section, $\sigma_{SE}(v_0)$, and the inversion number density $\Delta N_{v',J}$. We calculate the stimulated emission cross section from Eq. (2):

$$\sigma_{SE}(v_0) = v_0 |R_e|^2 S_{j'j'} q_{v',v''} g(v_0) \tag{3}$$

where $|R_e|^2 = 1 \ D^2$, $v_0 = 14783 \ cm^{-1}$, $S_{J'J''}$ is the rotational line strength and equals approximately 0.5, and $q_{v',v'}$ is the Frank Condon factor for the (8,9) band equals 3.21×10^{-2}. The term $g(v_0)$ is the value of the normalized emission lineshape at line center. The stimulated emission cross section is therefore $\sigma_{SE} = 9.9 \times 10^{-17} g(v_0) \ cm^{-2}$. We discuss the value for $g(v_0)$ below.

In many instances one can simply use a Doppler lineshape for $g(v)$ and calculate the expected gain. However, as we show below, the single mode diode pump laser interacts with only narrow velocity groups within the ground state $J''=38$ and 46 levels. This narrow distribution is preserved in the excited $v'=4$ level. Typical linewidths for single longitudinal mode, Fabry-Perot diode lasers are in the range of 50 to 100 MHz and are Lorentzian in shape. Thus, $g(v_0)$ is given by $0.64/\Delta v_L$ where Δv_L is the Lorentzian FWHM. This leads to an estimate for the anticipated range of the stimulated emission cross section: $1.9 \times 10^{-14} \ cm^{-2} < \sigma_{SE} < 3.8 \times 10^{-14} \ cm^{-2}$.

Absorption and Gain Measurements

The absorption or amplification of the probe beam was measured directly using a balanced ratiometric detector (BRD) originally developed by Hobbs.[14] We have described this

device in detail previously.[15] In brief, this dual beam detection system allows one to cancel coherent laser noise that resides in both the signal and reference beams. We routinely measure fractional absorptions of a few parts in 10^6 with this detector.

Prior to the introduction of the pump laser beam, we probed the iodine cell with the 676 nm diode and monitored the transmission as the diode laser frequency was scanned over a 0.6 cm^{-1} region. This scan range encompassed both the P(38) and R(46) lines in the (8,9) band. In Figure 3 we present an absorption trace that shows the two lines described above. (The third absorption line is unassigned, but irrelevant to the present experiments.) We used these absorption lines to calibrate the absorptions and gains recorded by the BRD detector as follows. The I_2 (B-X) band has been well characterized and spectroscopic and radiative constants are known to high accuracy. Thus, we can predict the absorption on assigned transitions given the path length and iodine number density. We completed such an analysis using a room temperature iodine number density (approximately 10^{16} molecules cm^{-3}). This provided a quantitative basis for the measured absorptions. The wavemeter was used to calibrate the frequency scale of the diode probe laser. From these measurements we found that the FWHM of the P(38) absorption line was 750 MHz due to hyperfine broadening. Using this in the calculation for the absorption coefficient for this line in the (8,9) band results in $k(v_0) = 3 \times 10^{-5}$ cm^{-1}. For the analogous R(46) line, $k(v_0) = 3.2 \times 10^{-5}$ cm^{-1}. It is important to note that there is no significant continuum absorption by iodine in the region of 670 nm.[22] Note that for these small absorptions (< 1%) the absorption varies linearly with the number density of the absorber. These calibration measurements were completed prior to the gain measurements described below.

When the pump laser was tuned to excite the relevant lines of the (8,4) band, bright laser induced fluorescence was observed in the iodine cell. With the pump laser frequency held fixed at the center of the spectrally blended P(38) and R(46) doublet in the (8,4) absorption band, the resolved LIF spectrum shown in Figure 4 was obtained. The Franck Condon intensity envelop of the resolved LIF also helped confirm the assignment of the pump transition band. Assignments of the rotational levels excited were completed by comparison of the actual pump wavelength with the calculations completed with previously published spectroscopic constants.[16]

Figure 5 shows the response of the BRD when the probe laser was scanned with the pump laser fixed at the center of the pump band. The narrow spikes are due to optical amplification from the narrow velocity group of population that had been pumped by the 634 nm diode laser from $J''=37$ and 46 in $v''=4$ to $v''=8$ in the B state. An expanded view of the P(38) line is shown in Figure 6. The FWHM of the narrow feature is 48 MHz which we interpret as the width of the pump laser. Note from Figure 5 that the gain peak does not appear at the same relative position on the P(38) and R(46) bands. This is because the absorption frequencies for the line centers of these two rotational lines within the (8,4) pump band are separated by 0.011 cm^{-1}, thus if the pump laser is at line center for P(38), it will be approximately 330 MHz high for the (P46) line. This is consistent with our observations in Figure 5. Indeed, we observed the position of the gain within the (8,9) band by incrementally moving the wavelength of the pump laser and then scanning the probe laser. Only when the pump laser excited some portion of the P(38) or R(46) region could the narrow amplification features be observed.

The gain transitions that we monitored both terminate in a level ($v''=9$) that has enough thermal population to produce an observable absorption in the absence of pumping. Thus the narrow pumping is directly responsible for the observation of optical gain.

The gain at line center was linearly dependent upon the power of the 634 nm pump laser as illustrated in Figure 7. Gain was observed with pump powers as small as 0.2 mW. For pump laser powers of 3.2 mW, the observed single pass gain was on the order of 0.1%. Since we did not have mirrors of sufficient reflectivity, no lasing attempts were made.

Calculation of Gain

We can compare the measured gain with that predicted based upon the observed absorption of the pump beam and knowledge of the emission transitions. Earlier we derived an expression for the expected gain on the two iodine transitions: P(38) and R(46) of the (8,9) band. For example when 0.41 mW of pump power was absorbed, we predict that the steady state number density of $J'=37$ and 47 are each 1.6×10^9 cm^{-3}. We also must consider the population within the terminal levels ($J'=38$ and $J''=46$ within $v'=9$). At a temperature of 300 K the total populations for these two levels are 8.9×10^9 cm^{-3} and 9.2×10^9 cm^{-2} respectively. Comparison with the excited state population densities would seem to preclude gain. However the population within the laser excited J' levels exist within a narrow bandwidth (50 MHz) and the population within the ground state J'' levels is spread throughout the entire Doppler width of approximately 775 MHz, thus only approximately 6% of the population within the ground J'' levels can interact with the stimulating emission field. Consequently, the respective inversion densities for $J'=37$ and $J'=47$ are: 1.4×10^9 cm^{-3} and 1.3×10^9 cm^{-3}. Inserting these values and the 50 MHz Lorentzian linewidth into equation leads to the following gain coefficients:

$$\gamma(P38) = 5.3 \times 10^{-5} \text{cm}^{-1} \text{ and } \gamma(R46) = 4.9 \times 10^{-5} \text{cm}^{-1} \tag{4}$$

61

The single pass gains for the 10 cm cell are 5.3 x 10^{-4} and 4.9 x 10^{-4} respectively. From Figure 3 we infer a single pass gain on the P(38) line of approximately 7 x 10^{-4}. Taking into account the uncertainties in the pump beam diameter and approximations used in the model, this is satisfactory agreement.

CONCLUSIONS

These results indicate the potential for using diode lasers as excitation sources for optically pumped lasers. Use of an ultra-sensitive detection system facilitated the observation of stimulated emission between two rovibronic levels that are only partially inverted due to the narrow pump source. Stimulated emission was observed for pump powers as low as 200 μW. These results imply that extension of these concepts to near IR and mid-IR diode lasers could lead to the development of optically pumped gas phase lasers operating on rovibrational levels. For example, a high power, narrow band diode laser operating at approximately 1.3 μm could be used to rotational transitions within the HF(2,0) overtone band. These experiments also further illustrate the utility of the BRD as a valuable tool not only for small absorption measurements but also for small signal gain. This is particularly valuable for potential laser systems that may have low or subthreshold gains.

REFERENCES

1. B. Wellegehausen, IEEE J. Quantum Electron. **15**, 1108 (1979).

2. R. C. Byer, R. C. Herbst, H. Kildal, and M. D. Levenson, Appl. Phys. Lett. **20**, 413 (1972).

3. J. B. Koffend, R. W. Field, D. R. Guyer, and S. R. Leone, <u>Springer Series in Optical Sciences</u>, Springer, New York, 1977, Vol 7.

4. B. Hartmann, B. Kleman, and O. Steinwall, Opt. Commun. **21**, 33 (1977).

5. B. Wellegehausen, K. H. Stephan, D. Friede, and H. Welling, Opt. Commun. **23**, 157 (1979).

6. L. Hanko, D. J. Benard, and S. J. Davis, Opt. Commun. **30**, 4468 (1979).

7. J. W. Glessner and S. J. Davis, J. Appl. Phys. **62,** 1 (1987).

8. J. W. Glessner and S. J. Davis, J. Appl. Phys. **73**, 2672 (1993).

9. G. P. Perram and S. J. Davis, J. Chem. Phys. **84**, 2526 (1986).

10. S. J. Davis and L. Hanko, Appl. Phys. Lett. **37**, 692 (1980).

11. L. Goldberg and D. A. V. Kliner, Optics Letters **20**, 1640 (1995).

12. K. P. Petrov, S. Waltman, U. Simon, R. F. Curl, F. K. Tittel, E. J. Dlugokencky, and L. Hollberg, Appl. Phys. B **61**, 553-558 (1995).

13. D. W. Hughes and J. R. M. Barr, Appl. Phys. **25**, 563-586 (1992).

14. P. Hobbs, SPIE Vol. 1376, Laser Noise, 216 (1990).

15. M. G. Allen, K. L. Carleton, S. J. Davis, W. J. Kessler, C. E. Otis, D. A. Palombo, and D. M. Sonnenfroh, App. Opt. **34**, 3240 (1995).

16. P. Luc, J. Mol. Spectrosc. **80**, 41 (1980).

17. M. Kroll and K. K. Innes, J. Mole. Spectrosc. **36**, 295 (1970).

63

18.   A. Arie, S. Schiller, E. K. Gustafson, and R. F. Byer, Opt. Lett.**17**, 1204 (1992).

19.   M. Broyer, J. Vigue, and J. C. Lehmann, J. Chem. Phys. **63**, 5428 (1975).

20.   M. Broyer, J. Vigue, and J. C. Lehmann, J. Chem. Phys. **62,** 4941 (1975).

21.   K. Sakuarai, G. Capelle, and H. P. Broida, J. Chem. Phys. **54**, 1220 (1971).

22.   J. Tellinghuisen, J. Chem. Phys. **76**, 4736 (1982).

FIGURE CAPTIONS

Figure 1.   Block diagram of apparatus.

Figure 2.   Excitation and detection scheme used in absorption and gain experiments. Note that only one of the P-R branches is shown.

Figure 3.   Absorption spectrum observed when the 676 nm diode laser was scanned across several rovibronic lines in quiescent iodine cell.

Figure 4.   Spectrally resolved laser induced fluorescence produced by diode laser excitation of the (8,4) band in I_2 (B <- X) system.

Figure 5.   Absorption and amplification spectra observed when 676 nm diode laser was scanned over features when pump laser was present.

Figure 6.   Expanded view of P(38) line showing narrow region of population inversion produced by 634 nm diode laser.

Figure 7.   Dependence of the amplification as a function of the pump laser power.
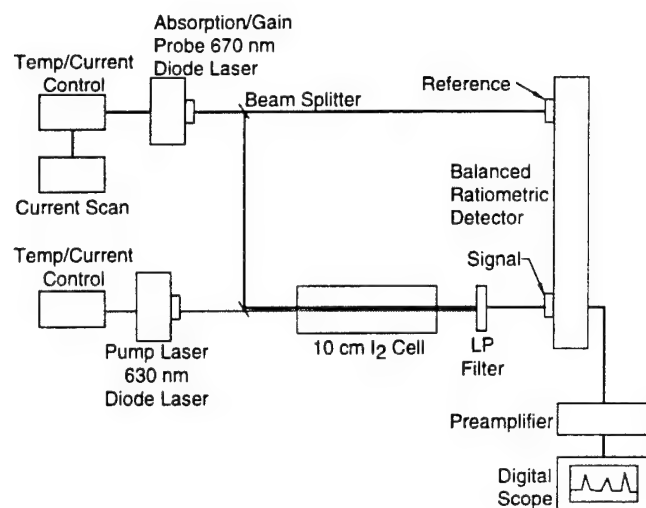
Figure 1
S. Davis
Journal of Applied Physics

Figure 2
S. Davis
Journal of Applied Physics

$B^3\Pi$ v'=8, J=37

Probe
(Probe Laser 676 nm)

Diode Laser   Pump
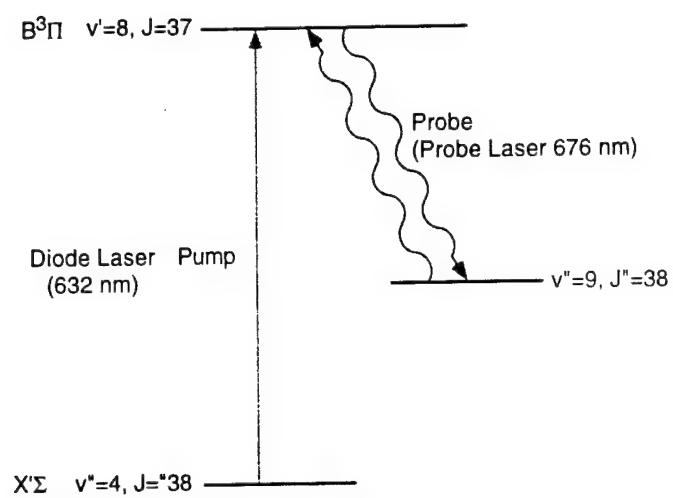(632 nm)

v"=9, J"=38

$X'\Sigma$ v"=4, J="38
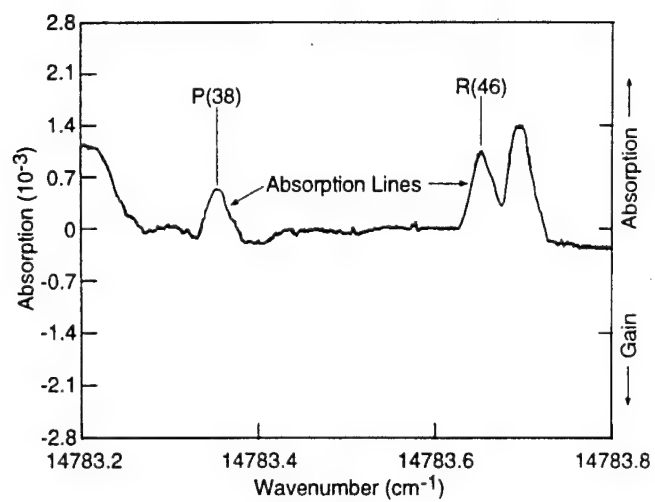
Figure 3
S. Davis
Journal of Applied Physics

Figure 4
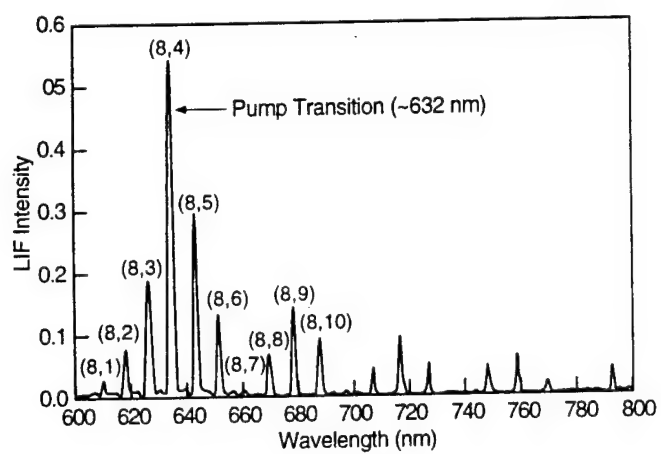S. Davis
Journal of Applied Physics

Figure 5
S. Davis
Journal of Applied Physics
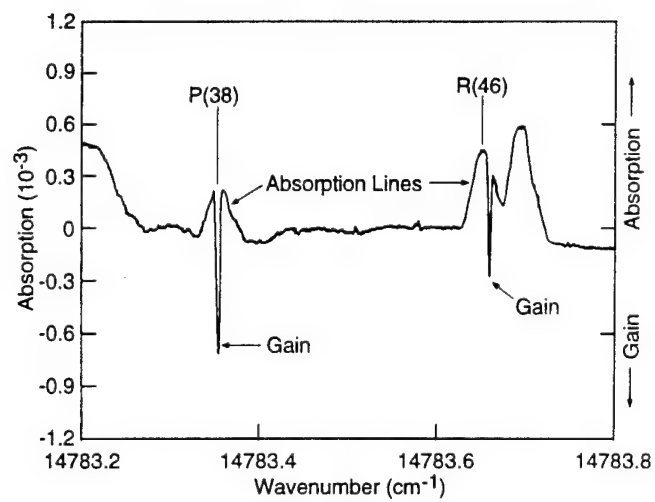
Figure 6
S. Davis
Journal of Applied Physics
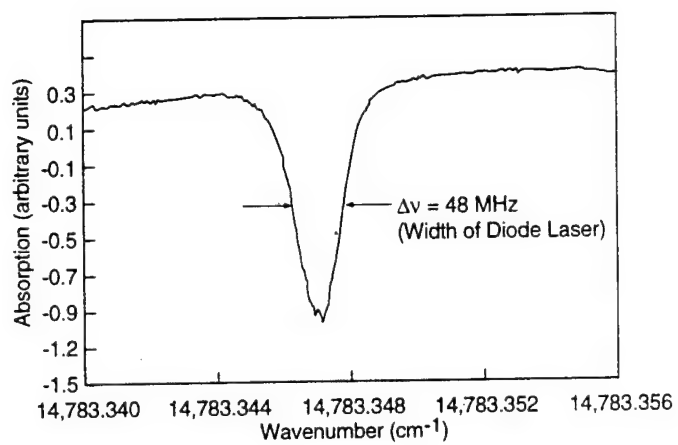
Figure 7
S. Davis
Journal of Applied Physics
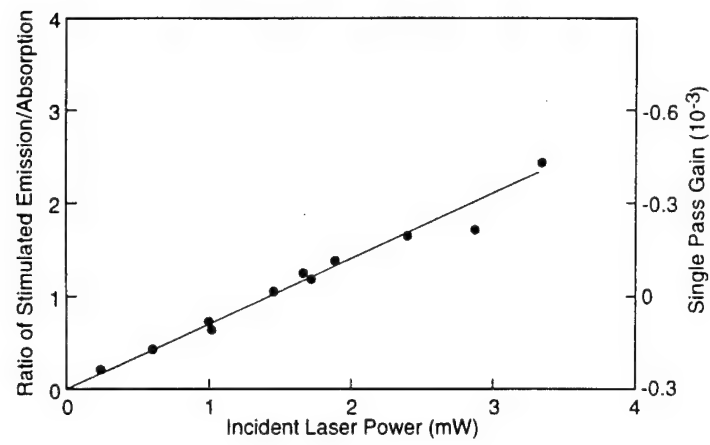
APPENDIX 3

Optically Pumped Mid-IR Vibrational Hydrogen Chloride Laser

OPTICALLY PUMPED MID-IR VIBRATIONAL

HYDROGEN CHLORIDE LASER

Harold C. Miller, John McCord, and Gordon D. Hager

Air Force Research Laboratory

Lasers and Imaging Directorate

Kirtland AFB, NM 87117-5776

and

Steven J. Davis, William J. Kessler, and David B. Oakes

Physical Sciences Inc.

20 New England Business Center

Andover, MA 01810-1077

Abstract

The results of an experimental investigation of an optically pumped vibrational laser in HCl are reported. Two different excitation sources were used: a Nd:YAG laser pumped optical parametric oscillator and a Raman shifted alexandrite laser. Overtone pumping on the (2,0) and (3,0) bands was employed to produce laser oscillation on the (3,2) and (2,1) bands near 3.8 microns. We also developed a model for the optically pumped laser and compare predictions of the model to the observed behavior of the laser. The photon efficiency of the HCl laser was found to be approximately 60%, consistent with model predictions and with previous optically pumped hydrogen halide lasers.

I. Introduction

The study of optically pumped lasers has been a fruitful area of research for many years.[1-9] Numerous atomic and molecular species have been studied using optical excitation techniques. Since many of the previous studies used visible wavelength excitation sources, a majority of the optically pumped lasers operated on electronic transitions.

The hydrogen halide molecules are well known laser species via chemical excitation. For example, the HF laser (2.7 µm) derives its energy from the reaction of $F + H_2$ that forms vibrationally inverted HF. The early successes of these chemical lasers led to detailed studies of the radiative dynamics and kinetics of this class of molecules. Consequently, there is a fairly extensive database for the hydrogen halide species.[10-17]

Optical excitation resulting in laser oscillation in selected hydrogen halide molecules has also been the subject of several studies. For example, Skribanowitz and co-workers[18-20] reported observation of laser oscillation on several rovibrational lines in HF following pumping on the (1,0) band using a discharge-initiated, pulsed HF laser as the pump source. They also observed laser oscillation on pure rotational transitions in the wavelength range 30 to 130 microns. Finally, they also reported true Dicke super-radiance on some rotational transitions in the wavelength range 50 to 250 microns. Jones and Bina[21] used the rather limited tuning of the 1.3 micron line in a Nd:YAG laser to excite the HF (2,0) overtone band to determine deactivation rates. In more recent work, a Raman-shifted Nd:YAG laser was employed by Shimoji and Djeu[22] to produce amplified spontaneous emission in HCl.

The hydrogen halide species possess strong dipole moments and since the vibrational spacings are anharmonic, overtone transitions (v>1) are strong. Consequently, the absorption

77

and emission cross sections are relatively large. The absorption and emission cross sections are perhaps the most valuable assessment tool available to evaluate the potential of a candidate laser system. They can be used to predict inversion densities and small signal gain. Often, the salient performance characteristics of an optically pumped laser can be estimated from these cross sections.

The absorption cross section is defined in Eq. (1):

$$\sigma(\nu) = (A_{ul}\lambda^2/8\pi)g(\nu)(f_u/f_l) \tag{1}$$

where λ = the wavelength of the transition,

A_{ul} is the radiative rate of the transition,

$g(\nu)$ is the lineshape factor, and

f_u/f_l is the degeneracy ratio of the two states.

The lineshape factor describes the detailed shape of the absorption or emission line. At low pressures, Doppler broadening dominates and $g(\nu)$ is described by a Gaussian, while at high pressures (typically pressures >100 Torr) the broadening is due to collisions and the lineshape is Lorentzian. While these two limiting cases are often used to describe the lineshape, in many situations, both Doppler broadening and collisional broadening are significant. Then one must use a Voigt profile that is actually a convolution of a Gaussian and a Lorentzian.

For most of the hydrogen halides, the radiative rates have been previously determined and we can accurately calculate the cross sections for both absorption and emission. In Table I we present absorption and emission cross sections calculated from published radiative rates[10] for several transitions in and HCl.

Note that for the absorption cross section we have included the relative Boltzmann population of the absorbing state in the cross section. Thus, the product of the total number

density of the hydrogen halide and the tabulated cross section is equal to the absorption coefficient, k.

Optically pumped lasers are very useful kinetic tools since selective excitation using tunable lasers allows one to form high inversion densities on time scales that are comparable to or shorter than the deactivation kinetics. Studies of the evolution of temporally and spectrally resolved laser emission can provide a wealth of information concerning energy transfer since laser oscillation often occurs not only from the particular sublevel pumped by the excitation source but also from adjacent levels that are populated by collisions. For example, in previous work on the interhalogen molecule IF, we demonstrated laser oscillation from levels that were populated via multi-level (up to five vibrational quanta) energy transfer.[5]
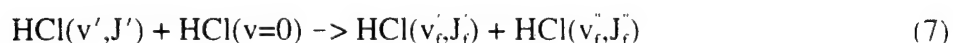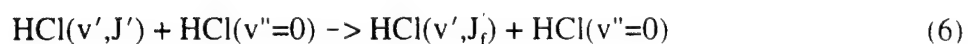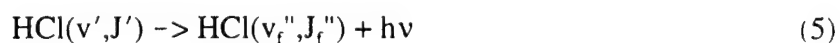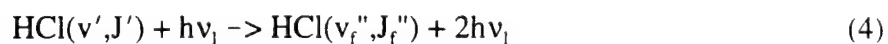
In this paper we present the results of a study in which HCl was optically pumped on overtone transitions (3,0) and (2,0). We observed strong and efficient laser oscillation. We also have determined a preliminary value for the self broadening coefficient of HCl on the (3,0) band by measuring the absorption width of the R_2 line as a function of HCl pressure. In addition, we developed a detailed kinetic model and comparisons are made between predicted and observed performance. These comparisons provide some insight into the extensive energy transfer processes that occur in the optically excited HCl energy manifold. Modeling of the energy transfer processes also allows calculation of optical gain coefficients as a function of time for each of the v,J levels expected to participate in the lasing process.

Description of Model

The major processes in the optically pumped HCl laser are indicated in Figure 1, which shows the relevant vibrational and rotational levels. A pulsed laser is used to prepare a

population inversion between two vibrational levels. Although the excitation laser connects only two rotational levels, as indicated in Figure 1, rapid rotational energy transfer (RET) redistributes the population among several rotational levels within the initially excited vibrational level. Depending upon the HCl pressure, this RET can compete on a kinetic time scale comparable to the pump pulse and laser build up time. Consequently, these processes must be included in any model to describe the optically pumped laser. This is significantly different from many previously demonstrated optically pumped electronic transition lasers such as the I_2 (B -> X) system.[23-25] In many electronic transition lasers, the pressure must be kept low, and as a result, much less RET occurs. The IF laser mentioned above is a notable exception[5] and behaves much like the HCl vibrational laser.

The important steps in our kinetic model are indicated in the following kinetic steps.

$$HCl(v'',J'') + h\nu_p \rightarrow HCl(v',J') \tag{2}$$

$$HCl(v',J') + h\nu_p \rightarrow HCl(v'',J'') + 2h\nu_p \tag{3}$$

$$HCl(v',J') + h\nu_l \rightarrow HCl(v_f'',J_f'') + 2h\nu_l \tag{4}$$

$$HCl(v',J') \rightarrow HCl(v_f'',J_f'') + h\nu \tag{5}$$

$$HCl(v',J') + HCl(v''=0) \rightarrow HCl(v',J_f') + HCl(v''=0) \tag{6}$$

$$HCl(v',J') + HCl(v=0) \rightarrow HCl(v_f',J_f') + HCl(v_f'',J_f'') \tag{7}$$
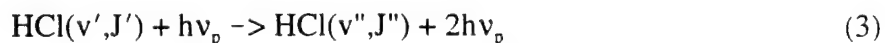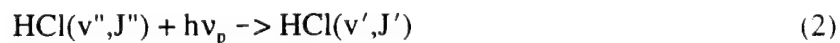
where ν_p and ν_l refer to the pump and laser emission frequencies respectively.

Equation (2) describes the optical pumping process which causes excitation of an HCl molecule from an initial level (v'',J'') to level (v',J'). The optical selection rules for rotational transitions in HCl are $J_f = J_i \pm 1$. While there are no strict selection rules for vibrational bands, the $\Delta v = 1$ transitions are much stronger than overtone ($\Delta v > 1$) transitions. In our experiments we focused on vibrational pump bands of v''=0 -> v'=2,3. The lasing transitions observed

included only $\Delta v = 1$ transitions (e.g. $v' = 2 \rightarrow v'' = 1$). We used the published radiative rates of Oba and Setser[10] for this part of the model.

Equation (3) describes stimulated emission caused by the pump laser. This term accounts for any saturation that may take place on the pump transition. Equation (5) accounts for spontaneous emission from the excited states in HCl, and Eq. (4) is the HCl laser process. Although Eqs. (4) and (5) indicate radiative emission only from the initially pumped level, the model includes many more levels and energy transfer among these levels. For example, we include vibrational levels 0 to 6 and 15 rotational levels within each of these vibrational states. Equations (6) and (7) account for vibrational and rotational energy transfer within these excited state manifolds (all rotational levels in all $v > 0$). Note that we also include rotational energy transfer within $v = 0$ in order to account for collisional redistribution within this state during the pumping pulse. This can become an important kinetic process especially at higher pressures since it tends to reduce saturation effects. For example, for strong pumping one would tend to deplete the rotational level within $v'' = 0$ during the pump pulse. However, if rotational energy transfer is significant, population from nearby levels within $v'' = 0$ will occur. This reduces pump saturation and permits a higher population inversion to occur.

In addition to strong lasing, important relaxation processes for HCl include: rotation-translation (R-T), and rotation-rotation (R-R), and vibration-vibration (V-V). Although Copeland et al.[14,16] have published an extensive set of rotational relaxation coefficients for all possible relaxation channels involving the levels $v = 2$, $J = 0$ through $v = 2$, $J = 6$ in HF, the data base is much less established for HCl. Consequently, we used the trends in the vibrational and rotational relaxation rates for HF as a guide for those in HCl. Indeed, for the model described here we used the HF rotational rate coefficients to describe the analogous process in HCl.

81

Although this is an approximation, we do not feel that this is a serious compromise since rotational energy transfer is so rapid at the pressures used in these HCl experiments. As a general statement, rotational relaxation is essentially gas kinetic and vibrational relaxation is considerably slower. Thus one expects rapid rotational redistribution in the excited vibrational level that is pumped by the pulsed excitation laser.

Vibrational relaxation in HCl has been studied by Dzelkalns and Kaufman[15] who have measured V-T,R relaxation for HF and HCl in collision with numerous gases. The model the authors used to deduce these coefficients from the data incorporated the assumption of single quantum rotational and vibrational transfer. Consequently, we modeled the relaxation process upon collision as a single quantum decrease in v and a simultaneous single quantum increase in J. An example reaction would be $HCl(v = 2, J = 3) + HCl(v = 0) -> HCl(v = 1, J = 4) + HCl(v = 0)$. It is probable that more than one rotational level is populated in the final product distribution for any one reaction. However, since rotational equilibration (the R-T,R process) occurs on a time scale of roughly 10 ns for a typical pressure (10 Torr), the anomalous rotational state distribution created by this restriction very quickly dissipates. The much slower $\Delta v = 2$ relaxation processes were neglected.

The predictions derived from this model were compared to experimental measurements of output spectra and temporal evolutions. In addition, the output power measured was compared to model predictions. One of the goals was to verify or anchor the model with direct comparisons with experimental measurements. The HCl laser is an excellent system for such comparisons since there exists a fairly extensive data base of kinetic and spectroscopic properties. Kinetic rates for the two Cl isotopes were assumed to be equal.

For single quantum transitions, we consider four possible lasing transitions; two of which populate the v,J state from the v + 1 level, and two of which depopulate the v,J state by lasing from v to v−1. This allows cascade lasing to occur. The pairs of laser lines are due to a P and R branch being allowed for each Δv transition. These processes are described by Eqs. (8) and (9).

$$N(v+1, J+M) \rightarrow N(v,J) + h\nu \tag{8}$$

$$N(v,J) \rightarrow N(v-1, J-M) + h\nu \tag{9}$$

where M = +1 for R branch transitions and M = −1 for the P branch. The small signal gain of these transitions is given by:

$$\alpha(v+1,J,M) = \sigma(v+1,J,M)\left[N(v+1,J+M) - \frac{1+2(J+M)}{1+2J} N(v,J)\right] \tag{10}$$

and

$$\alpha(v,J-M,M) = \sigma(v,J-M,M)\left[N(v,J) - \frac{1+2J}{1+2(J-M)} N(v-1,J-M)\right] \tag{11}$$

where σ is the stimulated emission cross section. We assume a plane, non-diffracting wave to obtain the average two-way intensity for each transition. The model also explicitly accounts for broadening of the optical transition lines due to pressure broadening. A voigt profile was used and the pressure broadening coefficient measured in this work was incorporated into the model. Pressure broadening has the effect of reducing the line center absorption and emission cross section values. Consequently, as more HCl is added to the cell, the predicted absorption increases at less than a linear rate once pressure broadening becomes important. For HCl this occurs when the pressure exceeds about 20 Torr. The model also included the process of saturation on the HCl laser transition.

83

II. Experiment

Introduction

Two excitation pump sources were used to excite the HCl molecules: a) a Nd:YAG pumped optical parametric oscillator (OPO) provided tunable output near 1.78 μm for (2,0) excitation and b) a Raman shifted alexandrite laser was used to pump the (3,0) band near 1.18 μm. Each of these systems is described below.

OPO Pump Source

As indicated in Table I, the strongest absorption bands in the HCl (2,0) band are near 1.78 μm. For this spectral region, we used a Spectra Technologies STI Mirage 3000 OPO that provided several mJ/pulse of tunable output with a linewidth on the order of 500 MHz.

Alexandrite Laser

A Raman shifted alexandrite laser (Light Age PAL 101) was used as the source for pumping the (3,0) band near 1.2 μm. The alexandrite laser was tuned with a bi-refringent filter to 794 nm and injection seeded using a tunable, single longitudinal mode diode laser that provided tunable output in the 792 to 797 nm wavelength range. The injection seeding was facilitated using a fiber optic to couple the diode laser into the alexandrite oscillator. Fabry-Perot interferograms provided by the laser manufacturer indicated that the linewidth of the injection seeded alexandrite laser was on the order of 500 to 600 MHz.

The output of the alexandrite laser was Raman shifted using hydrogen at 350 psi. To produce the required near IR output, we used the first Stokes shift (4155 cm^{-1}). This produced approximately 20 to 25 mJ of pulsed output at in the 1190 nm region to allow pumping of individual lines in the HCl (3,0) band. For example, studies were completed pumping the R(2) line of the H^{35}Cl isotope.

HCl Laser Apparatus

The apparatus used for the HCl laser experiments is indicated in Figure 2. Although there were some minor differences between the two setups for (2,0) and (3,0) pumping, the apparatus is adequately described by Figure 2. The HCl gas was contained in a 1 cm diameter stainless steel cell. Two cell lengths were used, 56 cm and 236 cm. While the 56 cm cell was used in both (2,0) and (3,0) pumping, the longer cell was used exclusively for the (3,0) excitation experiments since the absorption length for this overtone band is weaker than that for the (2,0) band. Regardless of cell length, CaF$_2$ windows at Brewter's angle were attached to the cell, and each cell had a CaF$_2$ window normal to the excitation laser beam axis. This window was used to view laser induced fluorescence with a HgCdTe detector. The optical cavities in each case used input mirrors that passed 80% of the pump beam and were 99.9% reflective at the 3.8 micron HCl laser wavelength. The HCl cavity output mirror was 20% transmissive at 3.8 microns.

As indicated in Figure 2, a long pass filter was used to separate unabsorbed pump light from the HCl laser output. A pyroelectric detector was used to measure HCl laser energy, and an InAs photodiode provided temporal profiles of the laser pulse. Spectral analysis of the HCl laser pulses was completed using a 0.3 meter McPherson monochromator (300 groove/mm, 3 µm blaze grating). A stainless steel gas handling system was used to purify the HCl via repeated

freeze/pump/thaw cycles. Pressures of HCl and any bath gases were measured with MKS

Baratron capacitance manometers.

In practice, a measured pressure of HCl was loaded into the HCl cell and the excitation

laser (either alexandrite laser or OPO) was scanned over an HCl absorption feature. Several sets

of experiments were completed. Excitation spectra were recorded by monitoring either the total,

spectrally unresolved HCl laser output or laser-induced fluorescence as a function of excitation

wavelength. Initial searches for laser output were completed by filling the HCl cell with

approximately 25 Torr of HCl and tuning the excitation laser through strong HCl absorption

bands. Once laser oscillation was established, kinetic and spectroscopic studies were completed.

These experiments included: the dependence of HCl laser output on HCl pressure, and

spectroscopic and kinetic investigations.

For some experiments the HCl laser output was not spectrally dispersed and the detector

monitored only broad band HCl laser output. This was a valuable diagnostic for optimizing the

HCl laser. For some subsequent experiments, the HCl laser output beam was directed to the

input of the McPherson 270 monochromator that was used to spectrally disperse the laser output.

III. Results

In Figure 3, we present excitation spectra resulting from pumping the (2.0) band. The two

chlorine isotopes (^{35}Cl and ^{37}Cl) give rise to pairs of HCl lines as indicated in the data.

Figure 4a shows spectrally resolved HCl laser spectra resulting from excitation of the R(2) line.

Laser oscillation is observed from several J' levels: J' = 2, 3, 4, and 5. The relevant energy levels

are also indicated in Figure 4b. This demonstrates the dominant role of rotational relaxation in

the optically pumped v' = 2 level. Indeed, rotational relaxation is the fastest kinetic process

within the optically pumped level. It does not necessarily degrade the performance of the laser since many of the collisionally populated levels participate in the laser output.

In Figure 5 we show an LIF trace of the R(2) line of the (3,0) band. For these data the alexandrite laser was injection tuned by scanning the output frequency of the diode laser injection seeder. By repeating this experiment for a range of HCl pressures we observed that the absorption linewidth of the HCl varied linearly with the HCl pressure as indicated in Figure 6. From these data we estimate a self-broadening coefficient of (10 ± 1.5) MHz/Torr.

In Figure 7 we show a spectrally dispersed HCl laser output spectrum resulting from pumping the R_2 line of the (3,0) band. Several P and R branch lines are obvious, and this indicates extensive rotational relaxation prior to the onset of laser oscillation. This behavior is similar to that previously observed in HF(3,0) and (2,0).[26,27] The important point is that rotational relaxation while very rapid does not remove population from the initially pumped v level and therefore is not a significant loss mechanism.

A spectrally resolved output trace of the HCl laser in the 236 cm cell is presented in Figure 8. The spectrum clearly shows the (3,2) and (2,1) lasing lines produced from one pass of the pump beam through the long gain cell. As expected from pumping of the R(2) (3,0) line, the P(4) (3,2) line has the most intensity. This in turn dictates that P(5) should be the strongest line in the (2,1) band, and this is evident in the spectrum. Intensity in the cascade band was observed to diminish with increasing pressure due to vibrational relaxation.

The HCl laser also was observed to be very immune to quenching by HCl. The data in Figure 9 show HCl laser relative output power on the P_3 branch of the (3,2) band as a function of HCl concentration. The laser output increases as the HCl pressure is increased to approximately 20 Torr and is then essentially flat until the pressure reaches approximately 90 Torr. This

87

behavior can be understood in terms of the kinetics of the optically pumped HCl laser. For example, the model described above was exercised and the results (solid line) were compared to the data in Figure 9. In the general agreement is quite good except at the lower pressures. Indeed, this suggests that the vibrational transfer rates or the self broadening coefficients used in the model need to be investigated more thoroughly.

Although the model used several hundred equations to treat the kinetic processes in the HCl energy level manifold, the overall trends in Figure 9 are due almost exclusively to the combined effects of pressure broadening of the absorption and laser transition and vibrational energy transfer that reduces the population inversion.

Often, in optically pumped lasers, there is an optimum number density of the ground state laser species with respect to output power,[1] and the data in Figure 9 emphasize this for HCl. At the low pressure end, the rather weak absorption of the HCl(3,0) band leads to a smaller population inversion. For example, the model described above predicted that 7 Torr of HCl will absorb only 7% of the pump light in a 56 cm cell. At higher pressures, larger absorptions are predicted (e.g., 28% absorption at 70 Torr), and this should result in higher inversions. However, vibrational relaxation to v=2 via HCl/HCl collisions will deplete the inversion. The self quenching rate coefficient for HCl on HCl(v=3) is $k_q = 3.6 \times 10^{-12}$ cm^3 molecule^{-1} s^{-1}.[15] The kinetics code indicated that the laser threshold buildup time for HCl laser oscillation on (3,2) transitions would be about 50 ns for a variety of conditions. When the pressure of HCl is 7 Torr, the vibrational relaxation rate is only 8×10^5 s^{-1} and can be neglected with respect to laser turn on time. In contrast at 70 Torr, the vibrational relaxation rate is 8×10^6 s^{-1} and in 50 ns only 70% of the initially prepared state will remain. The predicted ratio of the expected initial inversions (during pump pulse) for these two cases is approximately four. Thus, we expect the

88

ratio of the output energies at 70 and 7 Torr to be approximately 4 x 0.7 = 2.8. Inspection of Figure 9 indicates qualitative agreement with these estimates.

At intermediate pressures there is a balance between absorption and quenching. In other words, as the number density is increased, the initial inversion density will be higher, but quenching will be more pronounced. At the intermediate pressures these two effects essentially "balance", and the available inversion for laser oscillation is nearly constant. At the highest pressures quenching will dominate. A similar comparison was made for (2,0) excitation, and the agreement was comparable.

We also measured the conversion efficiency of the HCl laser. For (2,0) pumping we observed an energy conversion efficiency of 30% or a 60% photon efficiency. For comparison, for (2,0) pumping the model predicted a photon efficiency of 62%. These efficiencies compare favorably with previous measurements in HF for (2,0) pumping that observed photon conversion efficiencies of greater than 50%.[26,27] The earlier results of Djeu[22] also reported high conversion efficiencies (10%) for HCl amplified spontaneous emission following excitation on the (2,0) band by a Raman shifted Nd:YAG laser[22]. Indeed, the conversion efficiencies for the optically pumped hydrogen halide lasers appear to be much greater than those for optically pumped, electronic transition diatomic lasers. This is due to the fact that in the vibrational hydrogen halide lasers, rotational energy transfer is the dominant kinetic process and it only repartitions population to neighboring rotational levels. This does not significantly reduce the laser performance since these collisionally populated levels also contribute to the laser process. In contrast, in the $I_2(B \rightarrow X)$ optically pumped laser, the efficiency is less than 1% efficient due to rapid collisional and collisionless deactivation processes such as predissociation.[23-25]

IV. Conclusions

An optically pumped HCl laser has been demonstrated using two excitation schemes: (2,0) and (3,0) pumping. For (2,0) pumping the laser was observed to be very efficient. Extensive rotational relaxation was observed within the originally pumped vibrational level. The HCl laser can be considered to be a prototype system for other hydrogen halide molecules.

Acknowledgements

References

1. B. Wellegehausen, *IEEE J. Quant. Electron.*, QE-15, 1108 (1979).

2. J.B. Koffend, R.W. Field, D.R. Guyer, and S.R. Leone, Laser Spectroscopy III, (Springer-Verlag, New York), ed. by J.L. Hall and J.L. Carlsten, 382 (1977).

3. M.D. Burrows, S.L. Baughcum, and R. Oldenberg, *Appl. Phys. Lett.*, 46, 22, (1985).

4. S.G. Dinev and G.B. Hadjichristov, *Chem. Phys. Lett.*, 175, 216 (1990).

5. S.J. Davis, L. Hanko, and P.J. Wolf, *J. Chem. Phys.*, 82, 4831 (1985).

6. H.C. Miller and K. Yamasaki, J.E. Smedley, and S.R. Leone. *Chem. Phys. Lett.*, 181, 250 (1991).

7. V.A. Zolotarev, P.G. Kryukov, Y.P. Podmarkov, M.P. Frolov, and V.A. Shcheglov, *Sov. J. Quantum. Electron.*, 18, 643 (1988).

8. L.E. Zapata and R.J. De Young, *J. Appl. Phys.*, 54, 1686 (1983).

9. Alan B. Peterson, Curt Wittig, and Stephen R. Leone, *Appl. Phys. Lett.*, 27, 305 (1975)

10. D. Oba, B.S. Agrawalla, and D.W. Setser, *J. Quant. Spectrosc. Radiat. Transfer*, 34, 283 (1985).

11. R.E. Meredith and F.G. Smith. "Investigations of Chemical Laser Processes. Vol II". Willow Run Laboratories, University of Michigan. Ann Arbor, MI (1971).

12. J.C. Polanyi and K.B. Woodall. *J. Chem. Phys.*, 56, 1563 (1972).

13. R.L. Wilkins and M.A. Kwok, *J. Chem. Phys.*, 70, 1705 (1979).

14. R.A. Copeland, D.J. Pearson, J.M. Robinson, and F.F. Crim, *J. Chem. Phys.*, 77, 3974 (1982).

15. L.S. Dzelzkalns and F. Kaufman. *J. Chem. Phys.*, 79, 3836 (1983).

16. R.A. Copeland and F.F. Crim, *J. Chem. Phys.*, 78, 5551 (1983).

17. S.R. Leone, *J. Phys. Chem.*, Ref. Data 11, 953 (1982).

18. N. Skribanowitz, I.P. Herman, J.C. MacGillivray, and M.S. Feld, *Phys. Rev. Lett.*, 30, 309 (1973).

19. N. Skribanowitz, I.P. Herman, R.M. Osgood, Jr., M.S. Feld, and A. Javan, *Appl. Phys. Lett.*, 20, 428 (1972).

20. N. Skribanowitz, I.P. Herman, and M.S. Feld, *Appl. Phys. Lett.*, 21, 456 (1972).

21. C.R. Jones and M.J. Bina, *Appl. Phys. Lett.*, 22, 44 (1973).

22. Y. Shimoji and N. Djeu, *Appl. Phys. Lett.*, 49, 1 (1986).

23. R.L. Byer, R.L. Herbst, H. Kildal, and M.D. Levenson, *Appl. Phys. Lett.*, 20, 463 (1972).

24. J.B. Koffend and R.W. Feild, *J. Appl. Phys.*, 48, 4468 (1977).

25. J.W. Glessner and S.J. Davis, *J. Appl. Phys.*, 73, 2676 (1993).

26. S.J. Davis, W.J. Kessler, G.D. Hager, and H.C. Miller, "Lasers '92," STS Press, McLean, VA (1993).

27. H.C. Miller, D.T. Radzykewycz, G.D. Hager, W.J. Kessler, and S.J. Davis, *SPIE*, 1871, 2 (1993).

Table I. Calculated Cross Sections for Absorption and Emission for HCl.

Transition (v',v"):P or R	Wavelength (μm)	Cross Section (cm²)
(2,0); R_2	1.73	1.0×10^{-18}
(3,0); R_2	1.18	4.9×10^{-21}
(2,1); P_2	3.8	1.6×10^{-15}
(3,2); P_2	3.8	2.1×10^{-15}

List of Figures

Energy

Interatomic (H-Cℓ) Distance

v = 4
v = 3
v = 2
v = 1
v = 0

Figure 1
Miller et al.
Journal of Applied Physics

Figure 2
Miller et al.
Journal of Applied Physics

Figure 3
Miller et al.
Journal of Applied Physics

(a)

(b)

Figure 5
Miller et al.
Journal of Applied Physics
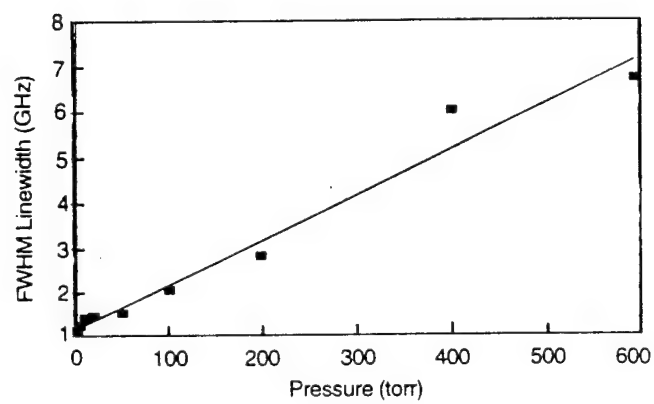
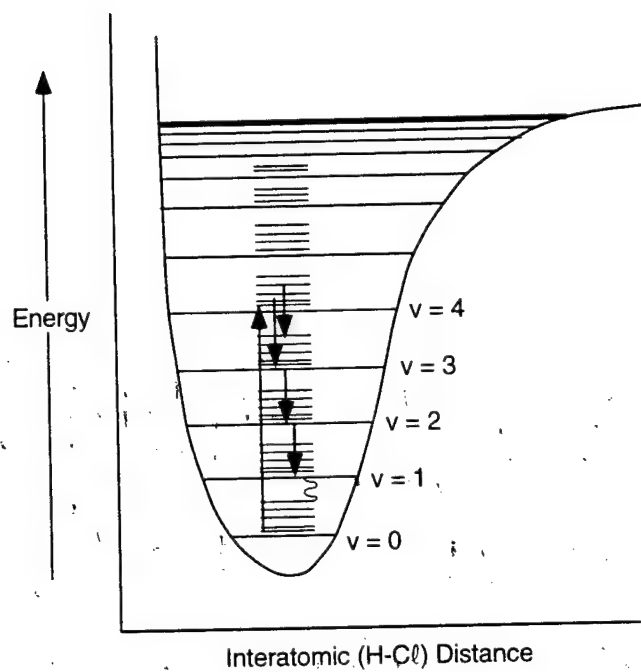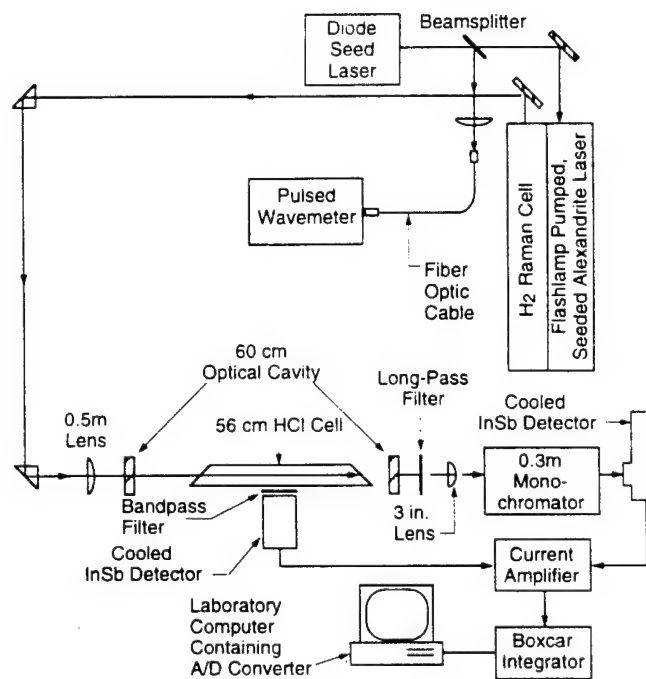Figure 6
Miller et al.
Journal of Applied Physics
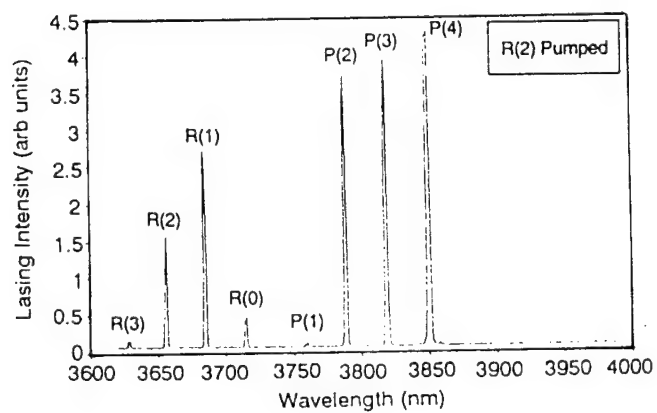
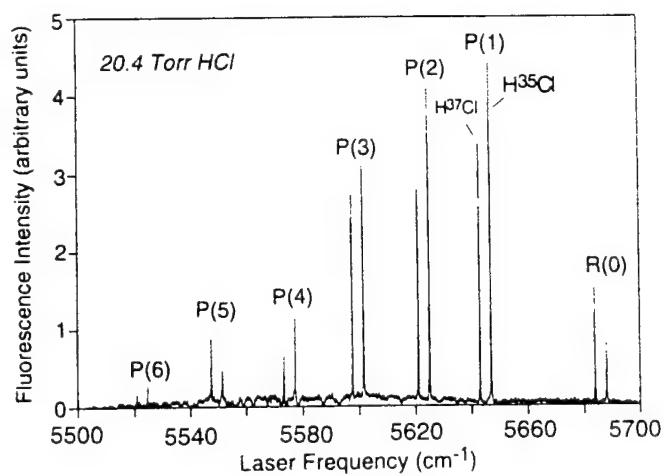Figure 7
Miller et al.
Journal of Applied Physics
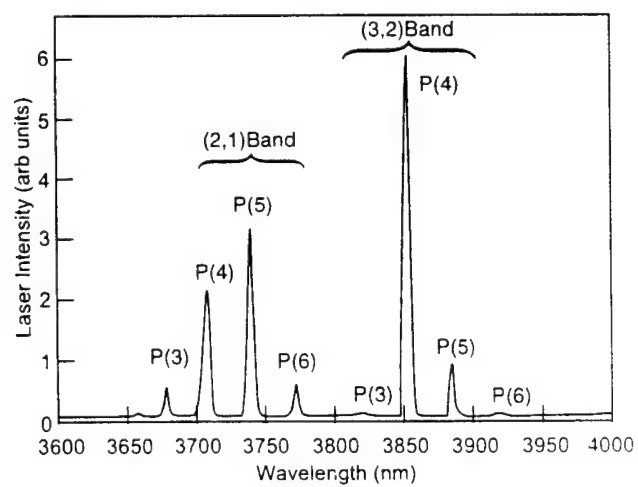
Figure 8
Miller et al.
Journal of Applied Physics
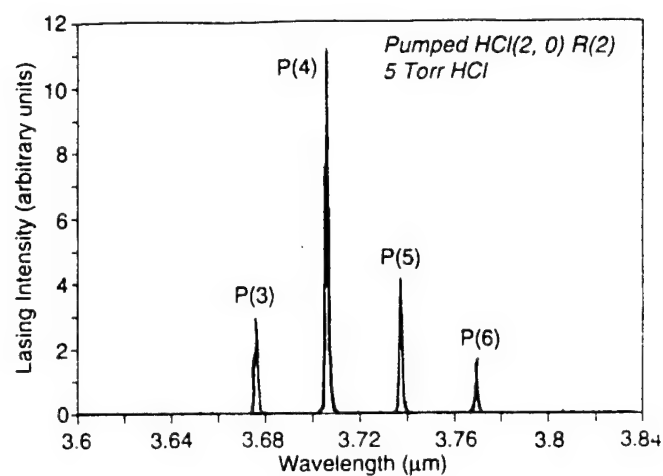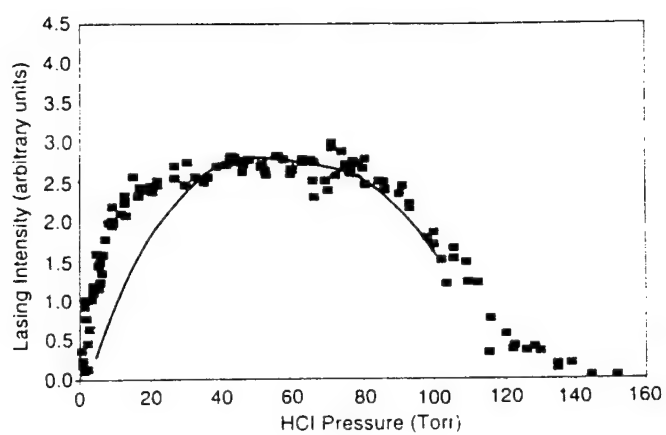
Figure 9
Miller et al.
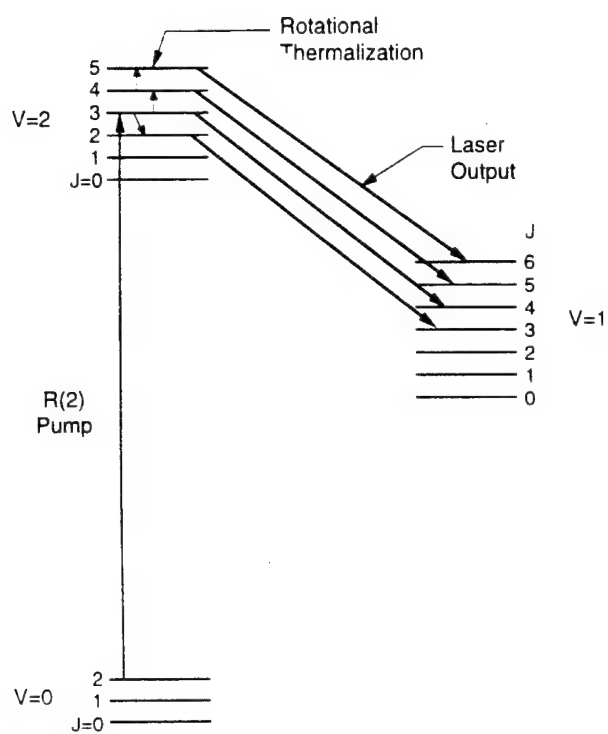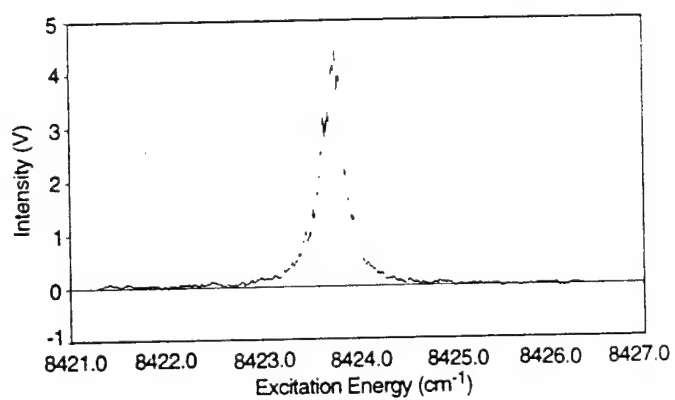Journal of Applied Physics

APPENDIX 4

State-Resolved Rotational Energy Transfer in ICℓ(B), v'=1 in Collisions with ICℓ

State-Resolved Rotational Energy Transfer in ICl(B) v'=1

in Collisions with ICl

Karl W. Holtzclaw, William J. Kessler, and Steven J. Davis[*]

Physical Sciences Inc.

20 New England Business Center

Andover, MA 01810

Abstract

We discuss detailed measurements of rotational energy transfer in ICl(B;v=1) with ICl(X) as the collision partner. Over 200 state-to-state rate coefficients are reported from three initially prepared levels: J=35,57, and 61. We also discuss comparisons of our data to the predictions of several fitting laws for rotational energy transfer.

[*]Corresponding Author; e-mail: davis@psicorp.com; Ph: (978) 689-0003; Fax: (978) 689-3232

1. Introduction

Rotationally inelastic collisions are among the most probable of energy transfer processes involving charge neutral molecules due, in large part, to the relatively small amounts of energy being exchanged. However, the energy differences between the initial and final states are only one of several factors that influence transfer. The importance of the collision partner is evident in several studies of the $B^3\Pi$ states of the halogens and interhalogens, many of which are good candidates for the study of rotational energy transfer (RET) due to their ready excitation with visible laser sources. For example, Davis and Holtzclaw[1] used a series of noble gases as collision partners in investigating state-resolved rotational energy transfer (RET) in IF(B). An increase in the propensity for large ΔJ transfers was observed in the rate coefficients for the heavier noble gases. This trend is qualitatively consistent with a simple classical model[2] describing the angular momentum the colliding atom brings into the encounter. A similar trend was observed in the pioneering work of Steinfeld and Klemperer[2] for I_2(B) in collisions with the noble gases and by Dexheimer et al. for I_2(B) in collisions with helium and xenon.[3] Notably, this trend is not observed in the more recent work of Perram, Massman, and Davis[4] who observe that the propensity for large ΔJ changing collisions in Br_2(B) with He, Ar, and Xe, decreases with increasing collision-partner mass. This seemingly contradictory trend may be a consequence of the predissociative nature of Br_2(B).

In this paper we report the results of an extension of the approach described in paper I (IF(B) collisions with several bath gases) to RET collisions between selected v',J' states in ICl(B) ground state ICl(X). These data are, to our knowledge, the first published for the interhalogens where both species in the collision have permanent dipole moments. We present state-resolved rate coefficients for ICl(B, v'=1) for transfer out of three different rotational states.

These data offered an opportunity to test several fitting laws[7] on a fundamentally different system. We have therefore applied one version of each of the exponential gap, statistical power gap, energy corrected sudden, and infinite order sudden fitting laws to these data in an attempt to deduce closed form expressions for the R-T transfer rate coefficients of these systems.

2.   The Experiment

A block diagram of the apparatus is shown in Figure 1. The heart of this experiment was a Coherent ring dye laser (Model 699-05) that was used to prepare ICl molecules in a selected, single rovibrational level within the electronically excited B state. The dye laser not actively stabilized, but its stability was sufficient for the experiments performed. The linewidth of the dye laser was measured with a large frame scanning Fabry-Perot interferometer (Burleigh Model 140). The measured linewidth was less than 70 MHz which is much less than the room temperature Doppler width (600 MHz) for the IC1 absorption lines. The wavelength of the dye laser output beam was measured with a Burleigh Model WV-20 wavemeter.

The fluorescence observation chamber was constructed from a teflon coated brass block that contained observation windows and sidearms to transmit the dye laser beam. An f/0.65 aspheric lens was used to collimate the LIF radiation and a single element lens was used to match the f/8, 1.26 m Spex monochromator. The monochromator was coupled to a Princeton Instruments intensified diode array (750 active element) was used to disperse and record the laser induced fluorescence. This instrument provided spectral resolution of 0.06 nm which was sufficient to resolve a substantial fraction of the rotational structure in the B-X (1,7) band monitored in these experiments. A second window in the fluorescence chamber was viewed by a Hamamatsu PMT (R955) that detected the total Icl fluorescence intensity. The PMT anode current was displayed on a Keithley picoammeter that provided a continuous monitor of the ICl

(B → X) LIF. This diagnostic confirmed that the frequency of the ring dye laser did not drift during data collection. In general, the frequency of the dye laser could be set at the center of an ICl absorption line and the LIF intensity would be stable to 10% for at least 10 min. This was five times longer than the longest data acquisition times for the LIF measurements. Any runs in which the LIF intensity drifted by more that this value were discarded. It is important to note that this was a conservative approach for assess possible biased data since our measurements were essentially independent of variations in the laser intensity.

With the OMA we could record an entire LIF rotationally resolved ICl spectra in only 16 ms. In practice summed and averaged up to 1000 such scans to increase the signal to noise to useful levels.

The ICl vapor was produced in a pyrex flask that contained ICl_3 crystals. The ICl pressures ranged from 5 to 59 mTorr in these experiments. The vapor above this solid is predominately ICl and Cl_2. The Cl_2 reactively removes any I_2 vapor. This is an important advantage since the strong and spectrally dense iodine B-X absorption system overlaps and interferes with the weaker ICl system. Using this approach, we observed no significant interferences arising from $I_2(B → X)$ emission.

We introduced the ICl vapor into the fluorescence chamber through a 500 micron diameter pinhole. The overall pressure in the fluorescence chamber was measured with a temperature controlled Baratron capacitance manometer.

3. Data Analysis

The Determination of R-T Rate Coefficients

The R-T rate coefficients were derived in a simple steady state kinetic analysis. In dilute conditions where a fluorescing molecule experiences on average only a single R-T collision during its lifetime, the steady state expression for the population of the final state is given by Eq. (1):

$$\frac{d[J_f]}{dt} = [J_i][ICl]k(i\to f) - \frac{[J_f]}{\tau} = 0 \quad . \tag{1}$$

This equation can be rearranged to give an expression to derive the R-T rate coefficients.

$$\frac{[J_f]}{[J_i]} = [ICl]k(i\to f)\ \tau \tag{2}$$

where $[J_i]$ and $[J_f]$ are the relative populations of the initial and final states, $k(i\text{-}f)$ is the rate coefficient for the transfer from J_i to J_f, and τ is the effective lifetime of J_f. When the single collision assumption is valid, a Stern-Volmer plot of $[J_f]/[J_i]$ versus $[ICl]$ will be linear in $[ICl]$ and the slope will be proportional to the R-T rate coefficient. In our experiments, care was taken to avoid bath gas pressures that resulted in a significant fraction of the ICl(B) molecules undergoing multiple collisions. This was facilitated by the large electronic self quenching cross-section for ICl(B)-ICl collisions.[8]

The effective lifetime in Eq. (2) is given by:

$$\tau = \frac{1}{k_R + \left(k_q + k_v\right)[ICl] + k_p} \tag{3}$$

where k_q, k_p, k_v, and k_R are the respective rate coefficients for electronic state quenching by

ICl(X), predissociation, vibrational energy transfer, and radiative decay. All of these rate

coefficients are known, can be estimated, or are negligible for ICl(B). It has been shown[8,9,10] that

the v'=1 rotational manifold is stable with respect to predissociation, consequently k_p is

negligible. We employed the value of 2.1×10^{-10} cm^3 molecule^{-1} s^{-1} for k_q as determined by

Kitimura et al.[8] We assumed that k_v was negligible based on the results for the low v' levels of

BrCl(B) measured by Clyne and Zai.[11] They measured vibrational self relaxation rate

coefficients for v'=1 and v'=3 that are about 1.5% of the ICl(B)-ICl electronic quenching rates.

If we assume that vibrational self relaxation in ICl(B) and BrCl(B) are comparable, then we can

neglect this process. We saw no evidence of vibrational relaxation under our experimental

conditions.

The determination of state-resolved R-T rate coefficients requires measurement of the

relative populations of the initial and final states involved in the transfer and defined in Eqs. (2)

and (5). These populations were determined from measurements of the intensities of the

respective P and R branch transitions from these levels (there are no Q branch transitions due to

symmetry restrictions). The relationship between the relative intensities and relative populations

is given in Eq. (6):

$$I_{J',J''}^{v',v''} = N_{J'}^{v'} \; v^3 \cdot |Re|^2 q_{v',v''} \left(\frac{S_{J',J''}}{2J'+1} \right)$$ (4)

where $S_{J',J''}$ is the rotational linestrength, v is the transition frequency, R_e is the electronic

transition moment, and $q_{v',v''}$ is the Franck-Condon factor. Since the spectral resolution available

to us was insufficient to completely resolve all the observed transitions, we used a spectral fitting

program that allows the determination of populations from dispersed fluorescence spectra even

when substantial overlap occurs. The spectral fitting procedure requires the calculation of ICl(B-X) spectra; the constants of Brand and Hoy[12] were used in for ICl(X) and those of Clyne and McDermid[13] were used for ICl(B). The spectral fitting procedure has been described in detail previously.[1]

The Fitting Laws

We have tested one variant of each of the four laws that describe rotationally inelastic energy transfer in an attempt to determine simple closed form expressions for the rate coefficient matrix describing RET in these systems. The exponential gap law (EGL) and the statistical power gap law (SPG) scale the calculated rate coefficients with the rotational energy change resulting from the collision. The energy corrected sudden law (ECS) and the infinite order sudden law (IOS) scale the rate coefficients with the angular momentum exchanged during the collision. These fitting laws are described in greater detail in References 7 and 14 to 18.

The exponential gap law (EGL) was originally proposed by Polanyi and Woodall[14] to account for RET resulting from HF-HF collisions and is given by:

$$k^{EGL}_{(i \to f)} = a \cdot e^{-(\Theta|\Delta E_{ROT}|)} \cdot R(\Delta E) \cdot (2J_f+1) \qquad (5)$$

where a and Θ are the fitted parameters, ΔE is the difference in rotational energy between J_i and J_f, and $R(\Delta E)$ is the ratio of final to initial translational state densities. Inclusion of the term $2J_f+1$ corresponds to the assumption that all final m_J states are accessible in the collision.

The statistical power gap law (SPG) was originally proposed by Brunner et al.[15] to account for RET in collisions between Na_2 and Xe and has since been applied with some success to data from Na_2 in collision with additional bath gases[16] and I_2 in collisions with He and Xe.[3] This law

113

differs from the exponential gap law in that rate coefficients scale as a power of the energy difference and is given by:

$$k^{SPG}_{(i \to f)} = a \cdot \left| \frac{\Delta E_{ROT}}{B_v} \right|^\alpha \cdot N_\lambda(J_{i,J_f}) \cdot (R(\Delta E) \tag{6}$$

where a, α, and λ are the fitted parameters, and B_v is the rotational constant. We have employed a version of this law that allows restrictions to be placed on Δm_J.[7] These restrictions are contained in the factor N_λ and are determined by the parameter λ. This provision allows limits to be placed on relative spatial orientation of the rotating molecule before and after a collision. When lambda exceeds $J_i + J_f$, N_λ reaches a limiting value of $2J_f + 1$ and there is no longer a restriction in Δm_J.

The energy-corrected sudden law was originally proposed by DePristo et al.[17] and arises from the sudden approximation of inelastic scattering theory. It has been applied with success to RET in several systems[3,7,16,18]. This law is given by:

$$K^{ECS}(J_i \to J_f) = (2j_f + 1) \exp\left[\left(E_{J_i} - E_{J_>}\right)/kT\right]$$

$$\times \left[\sum \begin{pmatrix} j_i & j_f \\ 0 & 0 & 0 \end{pmatrix}^2 (2\ell + 1) \begin{bmatrix} j_> \\ A \\ \ell \end{bmatrix} k(\ell \to 0) \right] \tag{7}$$

where the term in brackets is a 3-j symbol, J> is the larger of J_i and J_f, and the sum over ℓ ranges from $|J_i - J_f|$ to $|J_i + J_f|$.[7] The k(1→0) are referred to as basis rate coefficients and describe transfer out of $J_i = 0$. In principle these quantities can be measured, however such measurements would be challenging (e.g., isolating a transition populating J=0 and resolving the resulting fluorescence). Consequently, like other investigators, we employ an analytic form given by Eq. (10):

$$K(\ell \to 0) = \alpha[\ell(\ell+1)]^{-\gamma} \qquad (8)$$

where α and γ are the variable parameters. This form for the basis rate coefficients has been successfully used to fit rate coefficients from the $I_2(B)+Xe,He^3$ system, $Na_2(A)$ in collisions with several gases.[13] The term $A_{J>}$ is an adiabatic correction allowing for molecular rotation during the collision and is given by:

$$A_\ell^{J>} = \frac{1 + \tau_\ell^2/6}{1 + \tau_{J>}^2/6} \qquad (9)$$

The factor of 6 is appropriate for long-range molecular interaction potentials that scale as r^{-6}.[17] τ is a reduced collision duration given by given by :

$$\tau_J = 4\pi l_c cB_v(J + 1/2)/\bar{v} \qquad (10)$$

where B_v is the rotational constant, vbar is the mean closing velocity of the collision pair, and l_c is a velocity-averaged impact parameter or characteristic length for the R-T transfer. Along with the terms in the basis rate coefficients, l_c was varied in order to best fit the data.

The infinite order sudden (IOS) law is a simplification of the energy corrected sudden law where the effective collision length is assumed to be zero and the collision duration to be infinitely short.[7,18] The expression for the infinite order sudden law is given by Eq. (9) where the adiabatic correction term $A_{J>}$ is now unity. This law is expected to be most appropriate for collisions with light, fast moving collision partners which are more likely to produce short impulsive collisions. Examples of systems to which the infinite order sudden law has been applied with success include $I_2(B) + He,[3]$ $Na_2(A) + He,[16]$ and $Li_2(A) + He.[18]$

115

The fitting of data was performed using a non-linear least squares program based on the Levinburg-Marquardt algorithm as found in Bevington.[19] This is a rapidly converging algorithm which attempts to produce a best fit by minimizing the reduced chi square function given by:

$$\chi^2 = \sum_{J_f} + \frac{[(k_{fit}(i \rightarrow f) - k_{expt}(i \rightarrow f))]^2}{\sigma^2(i \rightarrow f)\nu} \tag{11}$$

where ν is the number of independent degrees of freedom in the fit (number of experimental data points minus the number of fitted parameters) and σ are the individual errors associated with the rate coefficients. For the σ we used the standard deviations calculated in performing the least squares analysis used to determine the rate coefficients. Data from all J_i for a given collision partner were used simultaneously in a global fit. We present two figures of merit to judge the quality of the fit: the reduced chi-square, and the average percent deviation between the calculated and experimental rate coefficients.

4.   Results

ICl(B-X) Spectra and Corresponding Rate Coefficients

In Figure 2 we present sample spectra from the 1-7 transition for four different pressures of ICl. The effects of R-T transfer are quite apparent in these spectra as fluorescence from collisionally populated rotational levels becomes more prominent with increasing ICl concentration. A distinct propensity for small ΔJ transfer is indicated by the presence of relatively intense P- and R- branch transitions arising from rotational levels adjacent the initially pumped state. Figure 3 shows a portion of a spectrum arising from $J_i = 57$ along with the calculated spectrum arising from the spectral fit. The light line represents the data and the bold line is the spectral fit. In most regions of the spectrum they are indistinguishable.

116

A representative Stern-Volmer plot is shown in Figure 4 for ΔJ transfer ($J_f - J_i$) of -13 ($J_i=57$). We have tested for the presence of multiple collisions in these data by summing the populations for the 20 lowest J_f levels for $J_i = 57$ and 61 and performing a Stern-Volmer analysis with these summed populations. Summing the populations significantly reduces the scatter in the Stern-Volmer plot and allows greater sensitivity to the presence of multiple collisions. Furthermore these lowest J_f levels should be most sensitive to the presence of multiple collision transfer. The Stern-Volmer plot for $J_i = 57$ and J_f 11-31 is shown in Figure 5, a similar plot was generated for $J_i = 61$. We note that a somewhat smaller (10-15 %) rate coefficient for transfer to these levels can be generated by omitting the higher pressure data. Consequently, multiple collisions may not be entirely absent in the higher pressure data. However it does not appear that multiple collisions are present in our data in sufficient magnitude to inflate the large negative ΔJ coefficients by the factor of 2 needed to make the data consistent with rate coefficients predicted with the energy corrected sudden fitting law. In Tables 1 through 3 we present the rate coefficients for ICl(B, v=1) J'=35, 57, and 61. The quoted uncertainties represent one standard deviation in the slopes of the Stern-Volmer plots. The initially populated levels (J_i) are indicated in the tables as are rate coefficients (k (J_i, J_f)) and the standard deviations (σ).

Inspection of the state-resolved, velocity-averaged cross-sections (Figure 5) clearly shows the strong propensity for small ΔJ transfer that is apparent in the spectra. The absolute magnitude of the ΔJ +1 and -1 cross-sections are quite large at roughly one third of the gas kinetic value assuming an ICl-ICl gas kinetic cross-section of 7×10^{-15} cm^2 as estimated from Lennard Jones data for I_2 and Cl_2.[22] Also apparent in the $J_i = 57$ and 61 data is a propensity for large ΔJ transfers that do not diminish rapidly with increasing negative ΔJ. This trend is similar to that observed in

117

IF(B)[1] and I_2(B)[12] in collisions with the heavier noble gases and in IF(B) in collision with N_2 and CF_4.[1]

The cross-sections for $J_i = 57$ and 61 exhibit considerable scatter for $\Delta J < -20$ to -25. These data originate from the region in the spectra where the individual rotational transitions are no longer resolved. The corresponding Stern-Volmer plots for the J_f in these regions are nonetheless linear and indicate well-determined rate coefficients. Consequently, the populations determined in the spectral fitting procedure are consistent on a relative basis from spectrum to spectrum. For this reason we believe that while the scatter is large for these cross-sections, their general magnitude, as would be indicated by an appropriate running average of these data, is nonetheless significant.

We were not able to measure all relevant rate coefficients for a given J_i primarily due to inadequate spectral resolution at and near the bandheads in the corresponding spectra. In these regions, the separation between transitions becomes comparable to and sometimes smaller than the point spacing in the spectra themselves at which point our spectral fitting code fails. Nonetheless, the extraordinary efficiency of R-T transfer in the ICl(B)-ICl system is indicated in the sums of the measured rate coefficients and cross-sections presented in Table 4 for each of the J_i investigated. These partial cross-sections are 4 to 5 times larger than the corresponding velocity-averaged cross-sections we measured for transfer out of $J_i = 72$ in the IF(B) + Xe system[1] and are roughly 3 to 5 times the gas kinetic value.

Fitting Law Results

In fitting the data, we included only those rate coefficients from each J_i which described a reasonably smooth trend. Those coefficients for large negative ΔJ transfer out of $J_i = 57$ and 61

were not included except when exploring the energy corrected sudden fitting law where we wished to explore the use of this law in describing large negative ΔJ transfer.

We nonetheless applied each fitting law to an extensive data set encompassing three initial rotational levels and a total of 201 rate coefficients. Comparisons of the data with rate coefficients computed from the fits are shown for the energy corrected sudden law and the statistical power gap law in Figures 6 and 7 respectively.

The fits are summarized in Table 4. It is clear from this work that the exponential gap fitting law is the least appropriate for these data as shown in Table 4 in which a summary of the resulting fitted parameters and merit figures are presented. Of the remaining laws, the two angular-momentum-based laws fit the data somewhat better than the statistical power gap law with the energy corrected sudden law giving a somewhat better fit than the infinite order sudden law.

In performing the nonlinear least squares fitting procedure, a set of initial fitting parameters is introduced to begin the fit. Many fits were performed for each law, each with different initial fitting parameters, in order to establish the parameters given in Table 5. We found the energy corrected sudden, infinite order sudden, and the exponential gap laws to be insensitive to reasonable but different values of the initial fitting parameters. This was not the case for the statistical power gap law where significantly different fitted parameters were produced that, nonetheless, reproduced the data with near equivalent quality. The two parameters a and λ were most sensitive to the values of the initial parameters introduced into the fit. For example, λ values ranging from 0.4 to 37 were produced with χ^2 and $\Delta\%$ figures very similar to those given in Table 5. For this reason we are uncertain of the physical significance of the fitted values using the statistical power gap law when applied to the ICl(B)-ICl system.

119

5. Discussion

The results presented above show that R-T transfer in the ICl(B)-ICl system is characterized by efficient transfer out of the initially prepared level as well as a propensity for very efficient small ΔJ ($J_f - J_i$) transfer. The latter is combined with a propensity for transfer that persists for large values of ΔJ and which is particularly apparent in transfer to $J_f \ll J_i$. The data most amenable to comparison are those presented in paper (I) for IF(B) $v' = 6$, $J_i = 72$ in collision with the noble gases, N_2, and CF_4 since these data span a comparable range of ΔJ and involve a species that is polar and of similar mass. The most striking comparison lies in the overall efficiency of R-T transfer out of an initially pumped level: the partial cross-sections presented in Table 4 are roughly 5 to 15 times larger than the total cross-sections for any collision partner listed in paper (I) for IF(B). The energy spacings between rotational levels in IF(B) are somewhat larger than for comparable levels in ICl(B) which, in turn, would tend to reduce the overall efficiency of R-T transfer. However, it is unreasonable for such large discrepancies being accounted for by this fact alone. Instead, it is probable that the bulk of the increased efficiency for R-T transfer in the ICl(B)-ICl system arises from the fact that both collision partners possess permanent dipole moments.

A distinct propensity for small ΔJ transfer is present in IF(B) in collision with He, Ne, and N_2[1] that has also been observed in $I_2(B)$ in collision with light gases.[12] This is readily explained with a simple classical model[1,x] describing the limited angular momentum these light gases bring into the collision which limits on the angular momentum that can be exchanged. In light of the dipole-dipole interactions in the ICl(B)-ICl system as well as the large mass of the collision partner, it is clear that the propensity for small ΔJ transfer in this system has a fundamentally

120

different origin than that observed in the IF(B) data. We suggest that much of the propensity for small ΔJ transfer in the ICl data arises from grazing collisions where the interaction distance relatively long and thus the extent to which angular momentum or energy can be exchanged limited. We postulate that these long-range collisions contribute disproportionately to the small ΔJ transfer. It is probable that such collisions would not induce significant R-T transfer, in the absence of dipole-dipole interactions that allow torque to be exerted over a long range. A test of this postulate would involve the study of R-T transfer in ICl(B) in collision with the homonuclear halogens since these species would possess similar properties in terms of mass and polarizability to ICl but would not possess a permanent dipole moment.

The propensity for R-T transfer involving large changes in J observed in the present data is also characteristic of transfer in IF(B) in collision with the heavier noble gases. This propensity is also consistent with the simple classical model mentioned above in that the heavier collision partners carry more angular momentum into the collision, or, equivalently, exert more torque on the target diatomic. We note however that the velocity averaged cross-sections for R-T transfer of comparable ΔJ in IF(B) in collision with Xe or CF_4[1] are only about 1/5 those for ICl(B)-ICl system. Consequently this simple picture is not adequate Nor is it likely that the rotational degrees of freedom of ICl, which introduce new channels, can account for this enhancement since CF_4 does not produce markedly larger cross-sections than the heavier noble gases for transfer in IF(B). Therefore, the attractive dipole-dipole interactions must also enhance the cross-sections for large ΔJ transfer by increasing the range over which the angular momentum can be exchanged. An investigation of R-T transfer in ICl(B) in collision with polar species of differing mass would be instructive since insight into the role collision partner mass plays in a polar collision system might be gained.

121

We have shown that, of the laws tested here, the energy corrected sudden law best reproduces the experimental data. The characteristic interaction lengths resulting from applications of this law varied from system varied from 1.9 A to 1.2 A depending on the range in ΔJ of the rate coefficients included in the fit. Data extending to only $\Delta J \pm 5$ for each J_i produced the smaller value and a better reproduction of the small ΔJ rate coefficients. Equations 9 and 10 indicate that l_c is dependent on the assumed long-range interaction potential. If one assumes that dipole-dipole forces dominate and thus that the interaction potential scales as r^{-3}, then l_c should be adjusted since the adiabaticity parameter is now given by:[17]

$$A_{j>} = \frac{1 + \tau_1^2 / 13.5}{1 + \tau_{j>}^2 / 13.5} \tag{12}$$

Consequently, l_c can be adjusted after the fact to reflect a dipole-dipole interaction by multiplying by the ratio $(13.5)^{1/2}/(6)^{1/2}$ which results in somewhat larger l_c values of ranging from 1.8 to 2.9 A.

Regardless of the assumed interaction potential, the l_c values for the ICl(B)-ICl system are smaller than those derived in applying the energy corrected sudden law to other systems. For example, values for l_c of 3.2 A and 5.3 A have been deduced for data from the $I_2(B) + Xe^3$ and $Na_2(A) + Xe^{16}$ systems respectively (where a long range potential scaling as r^{-6} was assumed). We note that the I_2 and Na_2 data were fit with the same form of the energy corrected sudden law used here. The smaller l_c for ICl(B)-ICl is also inconsistent with the larger total cross-sections for R-T transfer for the ICl(B)-ICl system than for $I_2(B)$ in collision with the heavier noble gases[5] (e.g., roughly 3 to 4 $\times$ 10^{-14} cm^2 for ICl(B) + ICl as opposed to 1.1 $\times$ 10^{-14} cm^2 for $I_2(B) + Xe^{5,1}$). Indeed, one might expect l_c to be larger for the ICl(B)-ICl system since dipole-dipole forces are effective

122

over longer distances than forces involving polarizabilities which would likely operate in these other systems.

Since the energy corrected sudden law as applied in this work does not reproduce all the data adequately, it is not clear that the law as applied to these data is appropriate and thus that the parameter l_c should be attributed significant physical meaning. For example, the basis rate coefficients ($\{k(1,0)\}$) deduced in the fit may not reflect the corresponding measured coefficients if the assumed form (Equation 8) is not adequate. (An interesting experiment would involve measuring these quantities.) Nonetheless, the good agreement between the fitted and measured rate coefficients within a restricted range of ΔJ range suggests that this fitting law is adequate for a large fraction of the rate matrix.

7. References

(1) Davis, S.J.; Holtzclaw, K.W. *J. Chem. Phys.* **1990**, *92*, 1661.

(2) Steinfeld, J.I.; Klemperer, W. *J. Chem. Phys.* **1965**, *42*, 3475.

(3) Dexheimer, S.L.; Durand, M.; Brunner, T.A.; Pritchard, D.E. *J. Chem. Phys.* **1982**, *76*, 4996.

(4) Perram, G.P.; Massman, D.A.; Davis, S.J. *J. Chem. Phys.* **1993**, *99*, 6634.

(5) Steinfeld, J.I.; Ruttenberg, P. *Scaling Laws for Inelastic Collision Processes in Diatomic Halogens*, JILA Information Center Report No. 23; JILA: **City**, 1983.

(6) Kurzel, R.B.; Steinfeld, J.I.; Hatzenbuhler, D.A.; Leroi, G.E. *J. Chem. Phys.* **1971**, *55*, 4822.

(7) Brunner, T.A.; Pritchard, D.E. "Fitting Laws for Rotationally Inelastic Collisions," *Dynamics of the Excited State*, ed. K.P. Lawley; John Wiley & Sons. Ltd.: New York, 1982, 589-641.

(8) Kitimura, M.; Kondow, T.; Kuchitsu, K.; Munakata, T.; Kasuya, T. *J. Chem. Phys.* **1985**, *82*, 4986.

(9) Clyne, M.A.A.; McDermid, I.S. *J. Chem. Soc. Faraday Trans. II* **1977**, *73*, 1094.

(10) Gordon, R.D.; Innes, K.K. J. Chem. Phys. **1979**, *71*, 2824.

(11) Clyne, M.A.A.; Zai, L.C.; *J. Chem. Soc. Faraday Trans. II* **1982**, *78*, 1221.

(12) Brand, J.C.D.; Hoy, A.R. *J. Mol. Spectry.* **1985**, *114*, 197.

(13) Clyne, M.A.A.; McDermid, I.S. *J. Chem. Soc. Faraday Trans II* **1976**, *72*, 2252.

(14) Polanyi, J.E.; Woodall, K.B.; *J. Chem. Phys.* **1972**, *56*, 1563.

(15) Brunner, T.A.; Driver, R.D.; Smith, N.; Pritchard, D.E. *Phys. Rev. Lett.* **1978**, *41*, 856.

(16) Brunner, T.A.; Smith, N.; Karp, A.W.; Pritchard, D.E. *J. Chem. Phys.* **1980**, *74*, 3324.

(17) DePristo, A.E.; Augustin, S.D.; Ramaswamy, R.; Rabitz, H. *J. Chem. Phys.* **1979**, *71*, 850.

(18) Scott, T.P.; Smith, N.; Pritchard, D.E. *J. Chem. Phys.* **1984**, *80*, 4841.

(19) Bevington, P.R. *Data Reduction and Error Analysis for the Physical Sciences*; McGraw-Hill: New York, 1969.

Table 1. A Summary of the Rate Coefficients Measured for ICl(B) in Collision with ICl(X); $J_i = 35$

J_f	$k(J_i,J_f)$	σ	J_f	$k(J_i,J_f)$	σ
	ICl + ICl ($J_i = 35$, $v_i' = 1$)			ICl + ICl ($J_i = 35$, $v_i' = 1$)	
	(10^{-12} cm^3 molecule^{-1} s^{-1})			(10^{-12} cm^3 molecule^{-1} s^{-1})	
27	14.7	3.4	67	3.8	0.3
28	20.3	0.9	68	3.8	0.3
29	23.7	1.3	69	3.1	0.3
30	23.8	1.0	70	3.0	0.2
31	27.4	1.7	71	2.5	0.1
32	34.1	1.2	72	2.2	0.2
33	45.9	1.2	73	1.4	0.3
34	70.7	2.5	74	1.2	0.2
35	0.0	0.0	75	1.2	0.2
36	71.1	2.7	76	1.5	0.2
37	37.7	1.0	77	1.4	0.1
38	28.5	0.8	78	1.4	0.2
39	20.8	0.9	79	1.3	0.1
40	17.5	0.9	80	1.4	0.2
41	15.2	0.9	81	1.0	0.1
42	10.5	1.0	82	1.0	0.2
43	12.9	0.5	83	1.3	0.2
44	12.3	0.5	84	1.1	0.2
45	11.9	0.5			
46	11.3	0.4			
47	12.0	0.5			
48	9.2	0.5			
49	8.3	0.6			
50	10.0	0.4			
51	10.2	0.4			
52	8.3	0.2			
53	7.8	0.2			
54	7.5	0.2			
55	7.0	0.2			
56	6.1	0.2			
57	6.2	0.4			
58	5.2	0.4			
59	3.1	0.6			
60	4.6	0.4			
61	4.8	0.4			
62	5.0	0.3			
63	4.5	0.2			
64	3.5	0.4			
65	3.9	0.3			
66	3.8	0.2			

Table 2. A Summary of the Rate Coefficients Measured for ICl(B)
in Collision with ICl(X); $J_i = 57$

	ICl + ICl ($J_i = 57$, $v_i' = 1$)			ICl + ICl ($J_i = 57$, $v_i' = 1$)	
	(10^{-12} cm^3 molecule^{-1} s^{-1})			(10^{-12} cm^3 molecule^{-1} s^{-1})	
J_f	$k(J_i, J_f)$	σ	J_f	$k(J_i, J_f)$	σ
11	6.9	1.0	54	31.8	0.7
12	8.0	1.3	55	39.5	1.3
13	4.8	1.0	56	61.7	2.6
14	5.3	1.6	57	0.0	0.0
15	6.5	1.1	58	64.2	2.5
16	6.5	0.7	59	40.2	1.4
17	10.2	0.8	60	28.1	1.0
18	11.9	0.9	61	21.5	0.8
19	7.2	0.7	62	19.2	0.8
20	4.6	0.6	63	15.5	0.4
21	5.0	0.9	64	15.5	0.5
22	8.1	0.7	65	13.9	0.5
23	10.1	0.6	66	12.2	0.5
24	9.0	0.7	67	10.0	1.1
25	7.7	0.4	68	8.4	0.5
26	6.6	0.5	69	8.6	0.4
27	8.2	0.4	70	7.5	0.4
28	12.0	0.5	71	7.0	0.4
29	14.1	0.4	72	6.3	0.4
30	13.9	0.7	73	5.6	0.3
31	9.8	0.8	74	5.2	0.3
32	10.4	0.8	75	4.5	0.4
33	12.3	0.6	76	3.8	0.4
34	13.7	0.6	77	3.4	0.5
35	14.8	0.6	78	3.4	0.4
36	12.6	0.6	79	2.8	0.4
37	10.6	0.6	80	3.3	0.2
38	12.9	0.4	81	2.9	0.2
39	12.8	0.3	82	2.6	0.3
40	12.8	0.3	83	1.9	0.3
41	12.8	0.3	84	2.1	0.3
42	12.4	0.7	85	2.3	0.3
43	11.5	0.4	86	2.3	0.4
44	12.4	0.7	87	2.1	0.3
45	14.5	0.6	88	0.6	0.2
46	16.0	0.7	89	0.9	0.1
47	16.1	0.5	90	0.8	0.2
48	17.1	0.6	91	0.6	0.1
49	18.0	0.6	92	1.2	0.3
50	16.8	0.9	93	2.6	0.4
51	19.6	0.9	94	2.1	0.3
52	23.1	0.8	95	1.9	0.4
53	26.7	0.7			

Table 3. A Summary of the Rate Coefficients Measured for ICl(B) in Collision with ICl(X); $J_i = 61$

J_f	ICl + ICl ($J_i = 61$, $v_i' = 1$) $(10^{-12}$ cm^3 molecule^{-1} s^{-1}) $k(J_i,J_f)$	σ	J_f	ICl + ICl ($J_i = 61$, $v_i' = 1$) $(10^{-12}$ cm^3 molecule^{-1} s^{-1}) $k(J_i,J_f)$	σ
18	7.8	1.5	59	44.0	1.4
19	6.9	1.0	60	60.3	1.4
20	7.4	1.4	61	0.0	0.0
21	6.6	1.0	62	53.1	2.0
22	4.3	1.0	63	37.3	1.0
23	6.7	0.6	64	28.9	2.3
24	9.5	1.0	65	21.4	0.8
25	14.6	1.0	66	17.1	1.1
26	11.6	1.2	67	16.1	1.9
27	9.1	1.7	68	15.9	1.0
28	9.9	1.9	69	13.7	0.9
29	10.6	0.7	70	14.2	1.8
30	13.1	1.1	71	11.3	0.9
31	14.2	1.4	72	10.0	0.7
32	12.6	1.2	73	8.2	0.4
33	9.5	1.2	74	6.5	0.8
34	8.5	0.8	75	6.7	0.5
35	12.1	1.1	76	6.4	0.4
36	11.4	1.0	77	5.9	0.4
37	10.5	1.2	78	5.2	0.4
38	10.7	0.9	79	4.6	0.4
39	10.6	0.7	80	4.5	0.5
40	8.6	0.5	81	4.8	0.4
41	11.8	0.8	82	4.0	0.5
42	14.3	1.0	83	3.9	0.4
43	12.1	0.6	84	3.1	0.5
44	12.7	0.6	85	4.5	0.5
45	12.1	1.3	86	4.5	0.4
46	14.0	0.7	87	3.9	0.3
47	13.8	0.8	88	1.7	0.4
48	15.0	0.8	89	1.7	0.2
49	14.7	1.0	90	1.4	0.2
50	13.5	0.9	91	0.9	0.4
51	12.4	0.9	92	2.6	0.4
52	15.5	0.7	93	4.7	0.5
53	17.5	0.6	94	4.6	0.6
54	17.5	0.9	95	4.8	0.7
55	19.2	0.8			
56	21.9	0.6			
57	25.3	0.7			
58	32.2	1.1			

Table 4. Summary of Fitting Law Results

Fitting Law	Fitted Parameters[‡]	Figures of Merit	
		ψ^2	$\Delta\%$
ECS	$a = 5.02 \times 10^{-11}$, $\gamma = 0.763$, $\ell_c = 1.83 \times 10^{-8}$	11.31	13.07
10S	$a = 3.46 \times 10^{-11}$, $\gamma = 0.226$	13.82	14,82
SP6	$a = 3.28 \times 10^{-11}$, $\gamma = 0.682$, $\lambda = 25.33$	20.75	18.23
E6	$a = 3.38 \times 10^{-11}$, $\theta = 8.80 \times 10^{-3}$	59.99	29.97

[‡]$J_i = 35$, $J_F = 27 - 71$

$J_i = 57$, $J_F = 35 - 87$

$J_i = 61$, $J_F = 35-87$

Table 5. Total RET Rate Coefficients and Cross Sections

J_i	$\Sigma \, \sigma \, (J_F, J_i)$ (cm^{-2})	$\Sigma \, k \, (J_F, J_i)$ (molecule cm^{-3} s^{-1})	ΔJ Range $(J_F - J_i)$
35	2.35×10^{-14}	6.56×10^{-10}	-8, + 36
57	3.45×10^{-14}	9.65×10^{-10}	-46, +30
61	3.37×10^{-14}	9.43×10^{-10}	-43, +26

[FIGURE CAPTIONS]

Figure 1.   A block diagram of the experimental apparatus.

Figure 2.   ICl(B-X) fluorescence from the 1-7 transition recorded in the presence of several

pressures of ICl while pumping the 1-0 R(56) transition in absorption.

Figure 3.   ICl(B-X) fluorescence from the 1-7 transition recorded in the presence of

53.9 mtorr of ICl while pumping the 1-0 R(56) transition. The light line is the data

and the dark line is the spectral fit.

Figure 4.   Stern Volmer plots for collisions resulting in $\Delta J = -13$ transfer.

Figure 5.   State-resolved, velocity averaged cross-sections for ICl(B, v=1), $J_i = 35, 57$, and 61

in collision with ICl(X).

Figure 6.   A Stern-Volmer plot for $J^i = 57$, and a sum of populations for $J_f = 11$-31. The

resulting composite rate coefficient is 1.76×10^{-10} cm^3 molecule^{-1} s^{-1}.

Figure 7.   Comparisons of measured rate coefficients with ECS law using parameter from

Table 5.

Figure 8.   Comparisons of measured rate coefficients with SPG law using parameters from

Table 3.
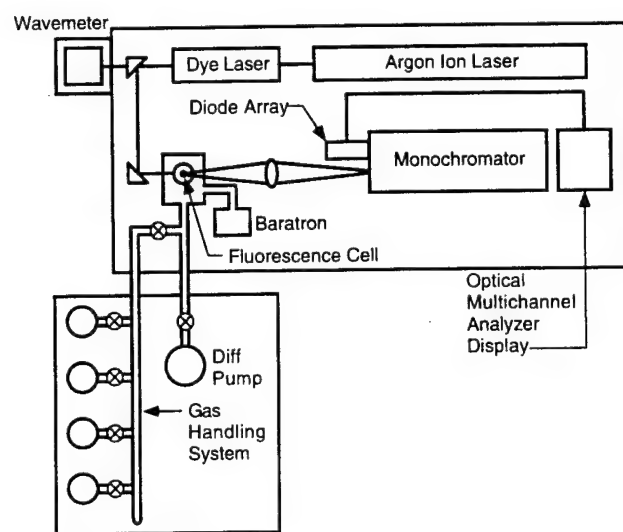
Figure 1
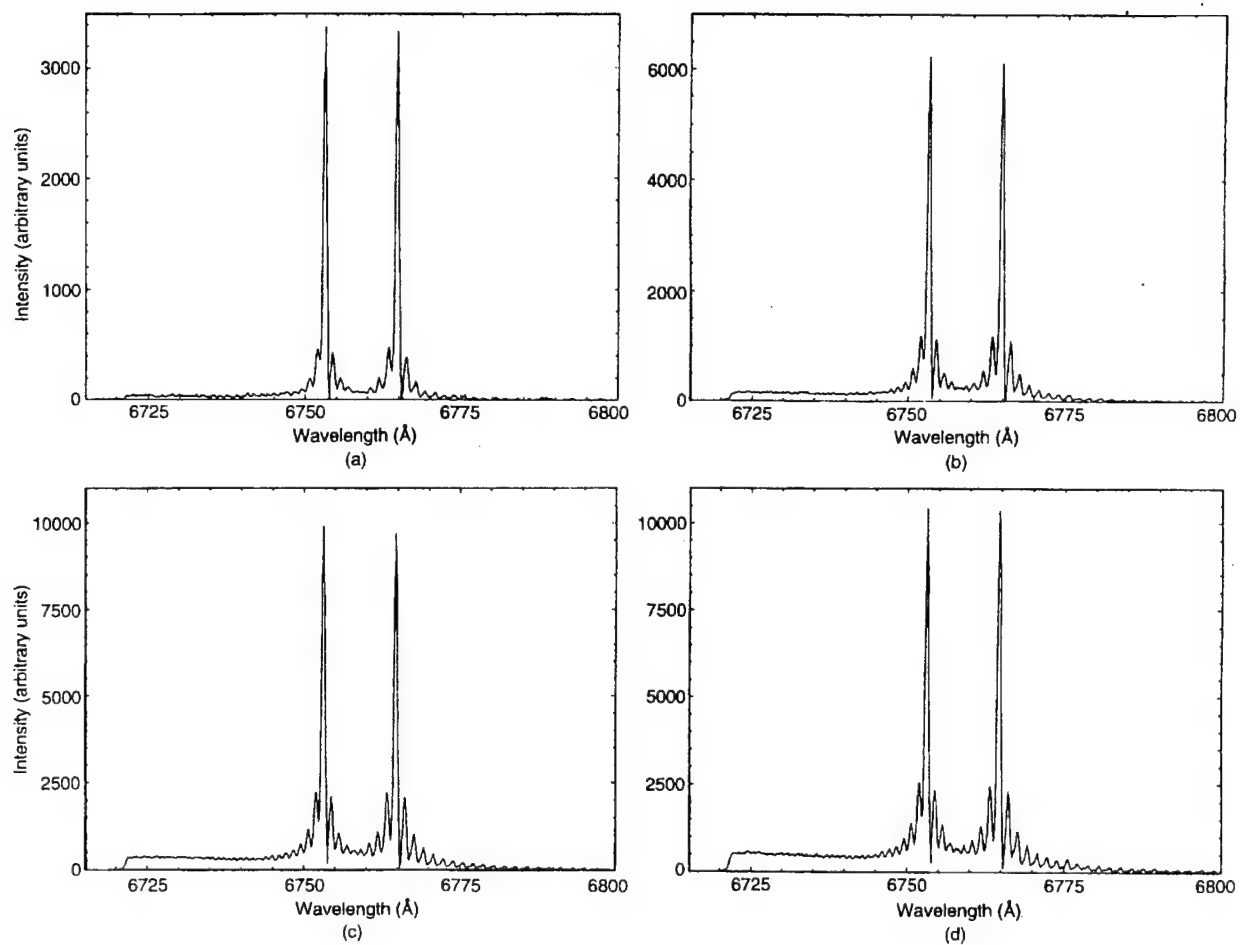
Figure 2
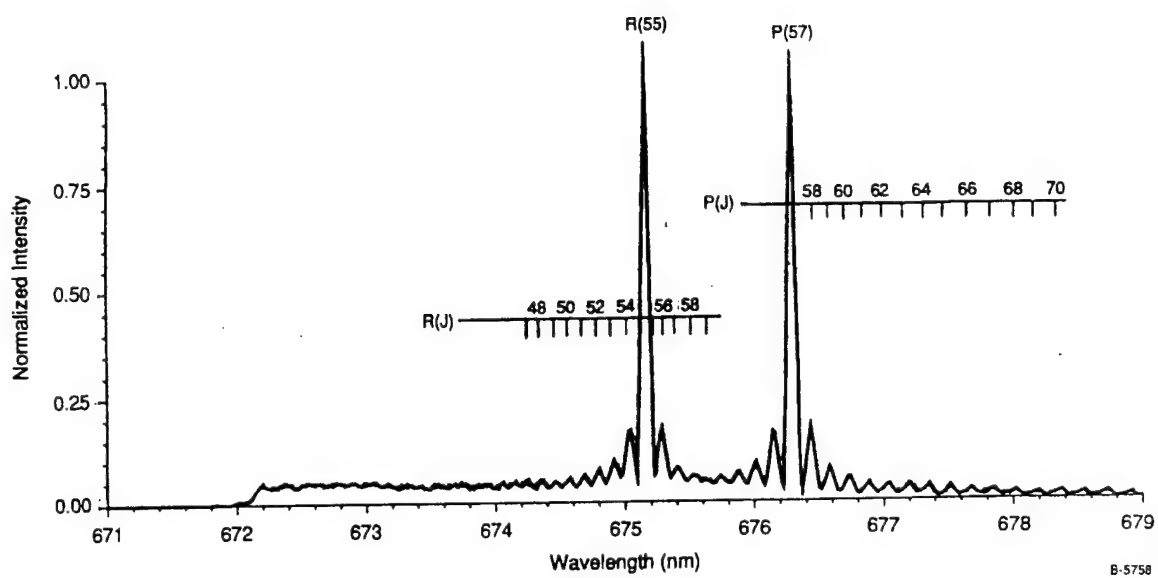
Figure 3
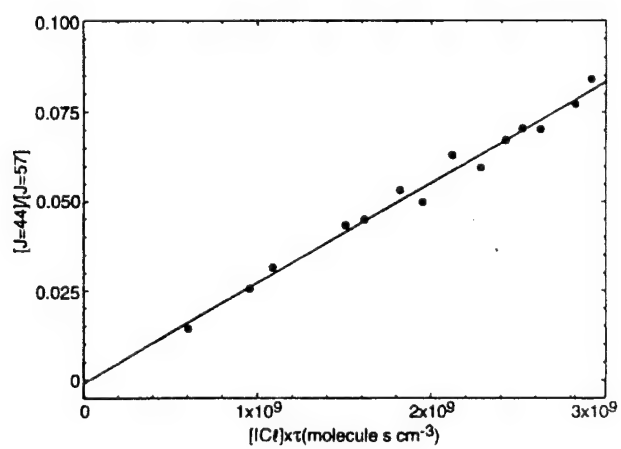
Figure 4
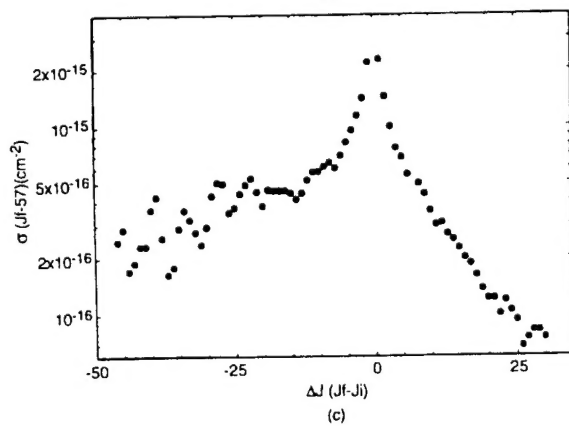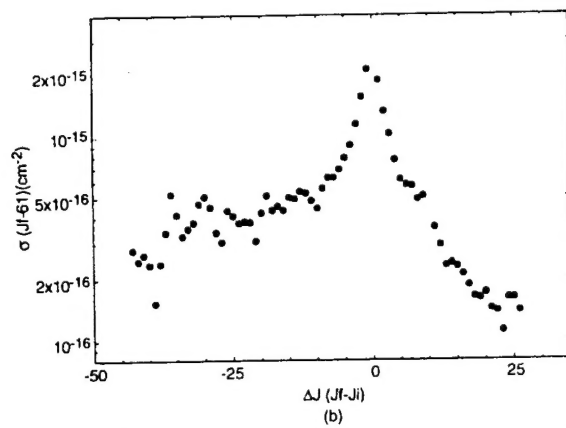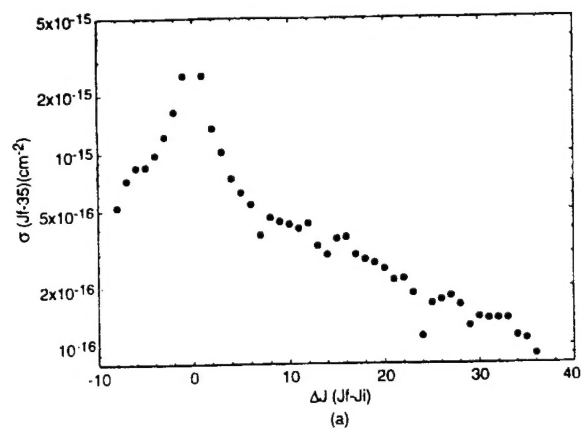
Figure 5

Figure 6

Figure 7

137

Figure 8

138